ISSN: 1977-5296

ESARDA

European Safeguards Research & Development Association

The International Journal of Nuclear Safeguards and Non-Proliferation

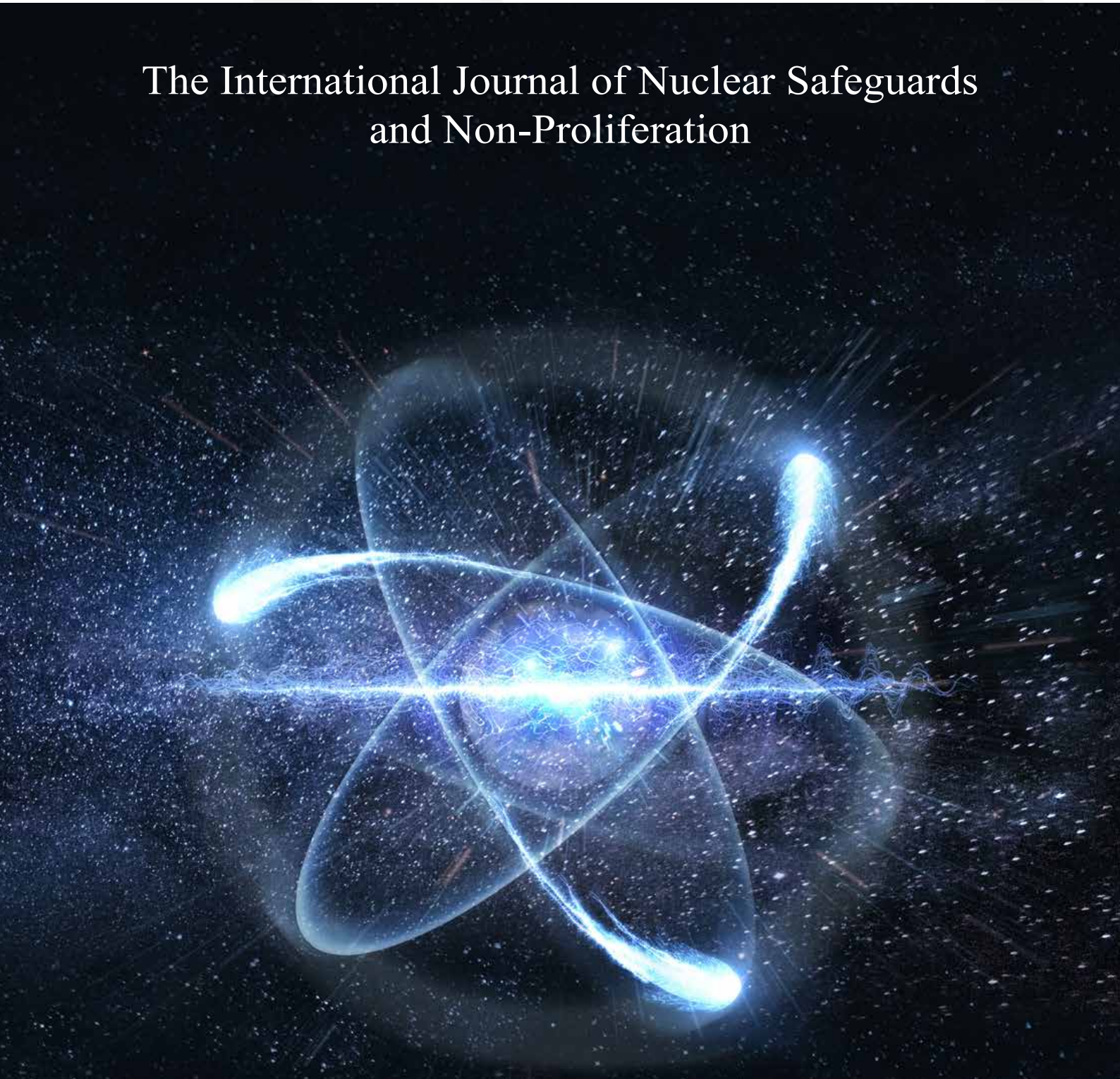

June 2021 Bulletin No.62

ISSN 1977-5296
KJ-BB-21-001-EN-N

Number 62
June 2021

European Commission, Joint Research Centre,
Directorate G - Nuclear Safety and Security
Nuclear Security Unit G.II.7
T.P. 800, I-21027 Ispra (VA), Italy
Tel. +39 0332-786182
EC-ESARDA-BULLETIN@ec.europa.eu

ESARDA is an association formed to advance and harmonize research and development for safeguards. More information can be found at the following address:

https://esarda.jrc.ec.europa.eu/

Papers submitted for publication are reviewed by independent authors including members of the Editorial Board.

Manuscripts have to be sent to the Editor (EC-ESARDA-BULLETIN@ec.europa.eu) following the paper guidelines available in the ESARDA Bulletin section of the ESARDA website (https://esarda.jrc.ec.europa.eu/) where the bulletins can also be viewed and downloaded.

Accepted manuscripts are published free of charge.

ESARDA Bulletin is published jointly by ESARDA and the Joint Research Centre of the European Commission and distributed free of charge to over 700 registered members, libraries and institutions worldwide.

The publication is authorised by ESARDA.

Cover designed by Christopher Craig Havenga, (consultant at EC, JRC, G.II.7, Italy)

ESARDA
European Safeguards Research & Development Association

Bulletin

Contents Issue n° 62

Editorial

Peer Reviewed Articles

Editorial

Elena Stringa

Dear Readers,

I am very pleased to present you the Issue 62 of the ESARDA Bulletin – The international Journal for Nuclear Safeguards and Non-proliferation. In this issue we have very interesting contributions on the following topics:

- techniques and standards for non-destructive analysis of nuclear material
- nuclear security, forensics and archaeology
- data analytics for strategic trade control and non-proliferation
- distributed ledger technologies applied to nuclear safeguards.

As I mentioned in the previous Bulletin issue, the journal has been accepted by SCOPUS. The first articles can be found in Scopus (www.scopus.com). In order to maintain the ESARDA Bulletin presence in Scopus I encourage researchers to continue to submit valuable contributions to the journal and to disseminate the work already published in the past issues.

Issue 63 of the Bulletin, expected for December 2021, will be a special one: it will collect academic contributions on the topic of "Data Analytics for Safeguards and Non-Proliferation". A presentation of the issue together with instructions on how to submit contributions can be found at: https://esarda.jrc.ec.europa.eu/news/esarda-bulletin-n63-special-issue-call-manuscripts-2021-05-17_en.

Technical contributions, i.e. articles relevant for the ESARDA community with a content more technical than academic, can be considered for publication in the Connector newsletter by sending them to EC-ESARDA-CONNECTOR@ec.europa.eu.

In the Connector newsletter n.4, edited while I am writing this editorial, you can find updated news from the various ESARDA working groups.

Before concluding I would like to thank authors who contributed to the current Issue of the ESARDA Bulletin – The International Journal of Nuclear Safeguards and Non-proliferation. Moreover, I would like to express my gratitude to our reviewers that anonymously engaged to assess and comment the content of the received manuscripts, often dedicating their free time to this task: thank you very much.

I also would like to thank my colleagues Andrea De Luca, Guido Renda and Simone Cagno for the fruitful exchanges and for the support they provided in the preparation of the current Issue of the Bulletin. Thanks also to the Editorial Committee colleagues who contributed in the selection of reviewers.

Finally, thanks to Chris Havenga, author of the Bulletin cover, who prepared the layout of the journal.

Take care and have a pleasant read.

Errata corrige

The printed version of the ESARDA Bulletin No.61 contained some errors in equation 1, pag. 11. Moreover, some symbols referring to the equation were reported in the text at pag. 12 in a wrong way. Readers interested to have the correct version of the article are invited to read it from the online version, that reports all the symbols correctly.

We sincerely apologize with the authors and with the readers for the inconvenience.

Investigating the sensitivity to irradiation history when predicting fuel parameters using random forest regression

Erik Branger, Zsolt Elter, Sophie Grape and Markus Preston,
Division of Applied nuclear physics,
Department of Physics and Astronomy
Uppsala University, Sweden
E-mail: erik.branger@physics.uu.se

Abstract

Safeguards verification of spent nuclear fuel assemblies is frequently done by performing non-destructive measurements, which are used to verify the completeness and correctness of operator declarations such as initial enrichment (IE), burnup (BU) and cooling time (CT) of the fuel. However, different irradiation histories may result in the same combination of CT, BU and IE, and such fuels may behave differently despite identically declared values. The goal of this work is to investigate what effect the irradiation history has on the ability to predict the fuel parameters using random forest regression.

Random forest regression models were trained to predict the fuel parameters IE, BU and CT based on combinations of radiation signatures calculated from a previously modelled Pressurised Water Reactor (PWR) spent nuclear fuel library. The radiation signatures studied were the relative gamma-ray activities of Cs137, Cs134 and Eu154, their total gamma-ray activity, the total neutron emission rate and the parametrised early die-away time τ from the Differential Die-away Self Interrogation (DDSI) instrument. The performance of the models were tested on simulations of 2192 PWR fuel assemblies from the Ringhals 3 and 4 nuclear power plants in Sweden, which were simulated based on their documented irradiation histories.

Despite significant differences in irradiation history between the training and testing data sets, the Ringhals assembly parameters could be predicted with similar accuracy as for assemblies in the training set. The relative gamma-ray activities were sufficient to predict the CT with an RMSE of 2 years, and adding a total gamma or total neutron signature allowed the BU to be predicted with an RMSE of 1.4 MWd/kgU. The DDSI early die-away time τ enabled an accurate IE prediction, with an RMSE of 0.16 w%. The differences between irradiation histories introduced a systematic bias where CT was overestimated by about 1 year and the BU by about 1.5 MWd/kgU.

Keywords: Nuclear safeguards, fuel parameter prediction, machine learning, random forest regression, irradiation history

1. Introduction

One of the many tasks undertaken by international nuclear safeguards inspectors is the verification of spent nuclear fuel (SNF) assemblies. Such verifications are done both to verify that the assemblies do indeed contain nuclear material (gross defect verification) and that parts of the fuel assembly have not been diverted (partial defect verification). However, due to the intense radiation emission from fission products and minor actinides, a direct determination of the fissile content is challenging. As a pragmatic solution, most verifications are done using non-destructive assay, aimed at verifying that operator-declared fuel parameters, such as cooling time (CT), burnup (BU) and initial enrichment (IE) are consistent with the measured radiation emissions. Computer codes are then used to estimate the fissile material inventories of the fuel assemblies using CT, BU and IE. These results are combined with other safeguards relevant information to evaluate the completeness and correctness of declarations and compliance with international non-proliferation treaties.

Before SNF assemblies are placed in difficult-to-access storage, such as dry storage or deep geological repository, the completeness and correctness of the operator declarations must be verified to high accuracy and precision, since it may not be possible to re-verify the data after storage. Traditionally, inspectors select an instrument that can measure the fuel assembly inventory at sufficient accuracy and precision, and bring the instrument to the fuel storage to perform a verification campaign. However, for a more thorough analysis, such as before encapsulation, it may be necessary to combine data from multiple instruments that are sensitive to different physical properties, in order to verify fuel parameters and correctness of declarations to the best possible accuracy and precision. Although potential measurement systems which could be used for safeguards measurements have been investigated previously [1], these investigations often focused on what information a single system can provide. This work aims at investigating how to combine different

measurements using machine learning to extract more information from the measurements.

Due to the complex interplay between fuel usage in a reactor and the fission product and minor actinide abundance, machine learning has been investigated in the past few years for interpreting the data in a systematic way, and to extract safeguards-relevant information. Machine learning has been applied to gamma spectroscopy data from spent nuclear fuel [2,3,4], and for predicting fuel parameters based on several types of measurements [5,6]. It has also been used for partial defect detection purposes in spent fuel [7,8,9], for process monitoring at reprocessing facilities [10] and to classify uranium oxide fuels and mixed uranium oxide fuels [11].

This work builds upon the work of [5] and investigates the capability of a random forest (RF) regression model to predict CT, BU and IE for the complete modelled fuel inventory of the Ringhals 3 and 4 PWR reactors in Sweden. The objective is to investigate if a RF regression model trained on SNF having a simplified irradiation history (as done in [5]) generalizes to a realistically modelled SNF inventory, representing a fuel inventory to be placed in a final repository. In order for a regression model to be useful in safeguards, it must be able to reliably predict the CT, BU and IE for a real inventory.

The motivation behind investigating the impact of the irradiation history is that although the radionuclide composition of a SNF is predominantly coupled to the CT, BU and IE of the assembly, the irradiation history may also influence the fission product and minor actinide abundance [12,13]. For fuel assemblies with more than a few years CT, which is the topic of this work, the gamma emission is dominated by Cs134, Cs137 and Eu154 [12]. Due to its half-life of 30.2 years, which is typically longer than the time the fuel assembly is in the reactor, Cs137 is often considered to build up linearly with BU. However, for very long gaps in irradiation, on the order of decades, Cs137 created in the cycles before the gap will have had noticeable time to decay during the gap. Cs134 is created through neutron capture by the direct fission product Cs133, hence its production depends strongly on the neutron flux in the reactor core, and thus the reactor power. Due to its shorter half-life of 2.1 years, even a one-year gap in irradiation will allow Cs134 produced in earlier cycles to decay noticeably. For Eu154, its production path is more complicated, and a fuel depletion calculation using the irradiation history is required for accurate results. With respect to neutron emission, the build-up of the principal neutron-emitting radionuclides depends strongly on the total neutron fluence but is relatively insensitive to the power level. However, the rate of build-up is significantly affected by the initial U235 content and any gaps in the irradiation, though the effect is the most significant at short CTs [12].

2. Methodology

To investigate what effect the irradiation history has on the fuel parameter predictions when using RF regression models, the spent fuel inventories of the Ringhals 3 and 4 PWR reactors were modelled. Section 2.1 explains how the spent fuel modelling was done, section 2.2 describes the non-destructive assay signatures considered, and section 2.3 provides an overview to the RF method that was used to predict the fuel parameters.

Due to the optimized usage of the nuclear fuel at nuclear power plants, many fuel assemblies experience a similar irradiation history. The achievable discharge BU strongly depends on the IE, where an increasing IE enables a higher discharge BU, and possibly more cycles spent in the reactor. Modern fuel assemblies, i.e. those with a short CT, tend to have a higher IE compared to older ones, and thus a higher discharge BU [14]. Since a fully-burned fuel inventory from a commercial nuclear power plant represents a limited set of combinations of CT, BU and IE values, it cannot be used to train a model that should be able to predict all practically achievable fuel parameter values. Furthermore, although the majority of fuel assemblies reach their intended terminal BU upon discharge, some assemblies are discharged earlier, and have values of CT, BU and IE that significantly differ from the majority of the other assemblies. A reliable and robust model should be able to predict the parameters also in such cases.

The RF regression models in this work were trained on the simulated spent fuel library of [15], which covers fuel assemblies with CTs between 0 and 70 years, BUs between 5 and 70 MWd/kgU, and IEs between 1.5% and 6%. Different RF regression models were trained to predict CT, BU and IE. The performances of these models were evaluated on two different test data sets: one test data set from the same fuel library, with fuel assemblies having the same irradiation history as in the training data, and one data set comprising the modelled Ringhals fuel assemblies. By comparing the performance of the RF regression models on these two test sets, it is possible to identify what uncertainties are due to the models themselves and assumptions underlying the fuel depletion calculations, and what additional uncertainty is added in the predictions due to the irradiation history in the Ringhals case. The values of CT, BU and IE from the Ringhals fuel assemblies all fall within the ranges of the parameters in the fuel library used for training, hence the RF models are trained on data that covers all Ringhals combinations of CT, BU and IE. The regression and evaluation strategy used in this work is summarized in Figure 1.

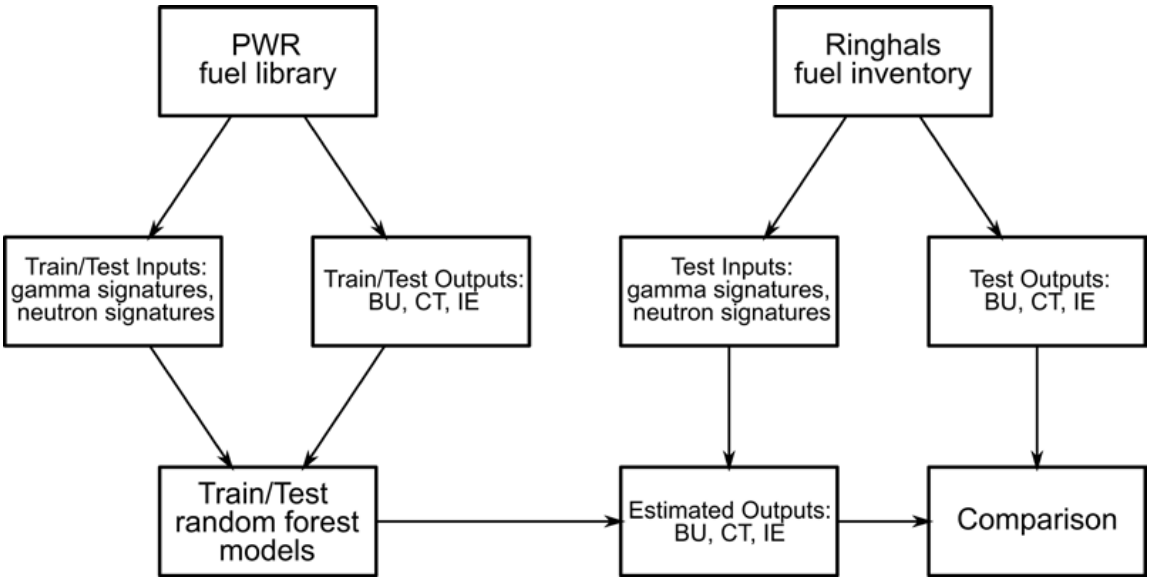

Figure 1: The training of the RF regression models was done using 80% of the fuel library of [15]. The remaining 20% was used to test the performance of the models and investigate what uncertainties are inherent due to the models and underlying assumptions. The trained model performance was also tested on the Ringhals fuel inventory, to assess the performance for fuel assemblies with real irradiation histories.

2.1 Spent fuel modelling

The spent fuel library of [15] contains in total 789 406 uranium dioxide (UO2) fuel samples, and was created using Serpent2 [16]. In the creation of the library, a generic irradiation history was assumed. The fuel was simulated to experience a constant power level, and the desired BU was obtained by increasing the number of irradiation cycles, and adjusting the length of the last irradiation cycle to obtain the desired burnup. The irradiation history in the library also assumed that after a period of 365 days of irradiation, a 30-day cooling period followed. This approximately corresponds to the revision period at the Swedish nuclear power plants.

For the Ringhals 3 and 4 fuel assemblies, the fuel assembly information provided by the operator Vattenfall includes the IE, the start and end dates of each irradiation cycle, and the BU of each cycle. Using this data, the fuel depletion of each fuel assembly was simulated in ORIGEN [17], due to its efficiency since all assemblies had to be simulated individually. The result of the ORIGEN simulations is an estimate of the material composition and neutron emission of each SNF assembly. The radionuclide content was then converted to a corresponding gamma-ray activity using the nuclide half-lives. For this work, it is assumed that the radionuclide gamma-ray activities can be assessed from a gamma-spectroscopic measurement, hence that the RF regression models can be trained using the gamma-ray activities as input features.

The Ringhals data includes the complete SNF inventory of the two reactors from the start of the reactors in 1980 and 1983 until the year 2012, and the fuel radionuclide abundances were calculated to correspond to 1st of July 2020. In this way, the modelled assemblies have a minimum of 8 years of cooling, enabling an investigation of the fuel parameter prediction capability for medium- and long-cooled fuel, which were shown in [5] to be more challenging than fuels with shorter CTs. Additionally, in the context of verification before encapsulation and final storage, many of the fuel assemblies are expected to have relatively long CT to ensure a sufficiently low residual heat. The Ringhals 3 fuel assembly data set contains 1083 assemblies, and the Ringhals 4 set contains 1109 assemblies, for a total set of 2192 assemblies. Due to the potentially sensitive nature of this data set, it cannot be published, and we focus on general results and trends that may be of relevance to PWR reactors in general, while keeping the specifics at a minimum.

Investigating the Ringhals fuel assembly irradiation histories, a few general remarks can be made:

- The PWR fuel library assumes a constant power level, whereas most Ringhals fuel assemblies experienced a roughly 20-40% higher power level in the first one or two cycles, as compared to the remaining cycles. As a consequence, we expect that for the Ringhals assemblies the modelled activity of short-lived radionuclides such as Cs134 is lower at discharge as compared to the fuel

library for the same CT, BU and IE values, since they were produced earlier in the Ringhals case and have had more time to decay before discharge.

- The majority of the Ringhals assemblies experienced a very regular irradiation, without spending cycles outside the reactor. However, a significant fraction of the Ringhals assemblies were reinserted into the reactor for a final low-power irradiation cycle, typically after having spent one or two cycles outside the reactor. For the assemblies that were part of the first core loading, the gap to the final cycle could be significantly longer, up to ten years, and the final cycle could be of comparatively high power. A smaller fraction of the fuel also had a gap in the irradiation after the first or second cycle. This is a noticeable difference to the fuel library, which has no gaps in the irradiation, and this affects the abundance of short-lived fission products at discharge.
- In some of the Ringhals assemblies, burnable absorbers were initially present. Such absorbers are not included in the PWR fuel library. Since the provided operator data on burnable absorbers is incomplete, and the absorbers mainly affects the beginning of the first cycle, they were not modelled. Note also that for depletion calculations, the neutron flux is set to yield the desired power level, which in part compensates for the effect of the burnable absorbers.

A summary of the CT, BU and IE of the Ringhals fuel assemblies is shown in Figure 2.

2.2 Non-destructive assay signals considered

This work considers several of the non-destructive assay signatures used in [5], such as the relative gamma-ray activity of selected abundant radionuclides, the total gamma-ray activity of the selected radionuclides, and the parameterised early differential die-away time τ. Since [5] found that the total Cherenkov light emission carries the same information as the total gamma-ray signature, we use only the total gamma-ray activity, since it does not require an additional measurement instrument. In addition, we include the total neutron emission rate of the fuel as a new signature, to investigate what impact it has on the model capability of predicting the fuel parameters.

Since the fuel assemblies considered here have a minimum CT of eight years, and a maximum CT of almost 40 years, the gamma-ray activity is predominantly caused by Cs134, Cs137 and Eu154, which therefore are the radionuclides considered in this work. These radionuclides are all abundant in SNF and have a long enough half-life to be measurable after more than eight years. For the Ringhals assemblies, these three radionuclides account for more than 99% of the total gamma-ray activity, and other radionuclides can therefore be neglected with a minimal loss of accuracy. For the relative gamma-ray activity, the sum of these three gamma-emitting radionuclide activities were scaled to 1. This corresponds to a measurement where an absolute calibration has not been made, and only the relative intensities of the gamma-ray emissions can be determined. The total gamma activity is the sum of the three gamma-ray activities, and although it does not correspond to the absolute intensity for the fuel assembly, it is proportional to it. This in turn, enables a comparison of the total gamma-ray activities between fuel assemblies.

As in [5], a minimum threshold activity was included, at 0.1 % of the lowest Cs137 activity in the training dataset. The activities of radionuclides below the threshold were set to 0. The value of 0.1% is arbitrary, but reflects the fact that radionuclides with low activities may fall below the threshold of detectability. Based on [5], it is expected that Cs134 (with half-life 2.1 years) is only measurable for a short while after eight years of cooling using this threshold, and Eu154 (with half-life 8.6 years) may be below the threshold for long-cooled, low-BU assemblies. Note however that the real threshold of a measurement depends on both the fuel assembly and the measurement

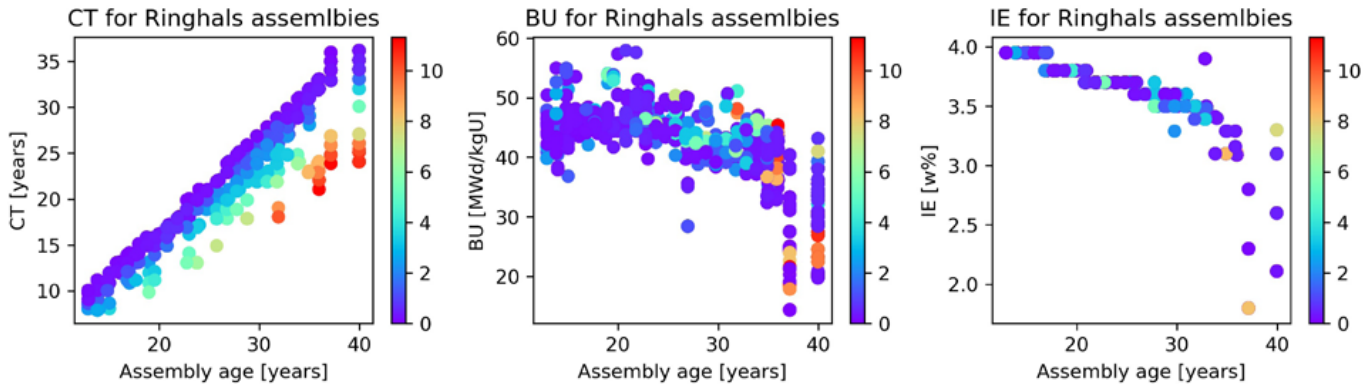

Figure 2: The distribution of CT, BU and IE for the Ringhals 3 and 4 spent fuel assemblies. The colour of the markers indicates the cumulative number of years an assembly spent outside the reactor between consecutive irradiation cycles. The assembly age is the number of years since first irradiation.

setup. Since this work does not consider the measurement setup at all, a global threshold is a simple way to include the main effect of a detectability limit on the subsequent analysis. For shorter CTs, additional radionuclides are expected to contribute and their activity will depend even more strongly on the power level of the final irradiation cycle and hence the irradiation history [12], but such investigations are outside the scope of this work, and such low-CT assemblies are not part of the Ringhals test set.

The total neutron emission rate of the Ringhals assemblies were provided by the ORIGEN simulations, which includes spontaneous fission and (α, n)-reactions. For the fuel database of [15] which was generated using Serpent2, the total neutron emission rate is not provided. The SF neutron emission rate was instead calculated based on the abundance of fissile radionuclides and minor actinides, and neutron emission data for these radionuclides from [12]. The (α, n) neutron contribution was calculated based on the abundance of fissile radionuclides and minor actinides and data from [18]. The total neutron emission rate was calculated as the sum of these two contributions. In general, for most Ringhals fuels the (α, n)-reactions contribute with about 1-5% of the total neutron rate, however for certain long-CT, low-BU assemblies the contribution could reach 20%. In the fuel library, the (α, n) contribution can exceed 50% for very low-BU and long-CT assemblies.

Since the neutron emission rates were calculated using different methods for the two fuel sets, and since the burnup calculations and underlying cross-sections also differ, additional errors and uncertainties arise when comparing the two data sets. A thorough benchmark of the two methods is outside the scope of this paper, but eight Ringhals assemblies with varying irradiation histories were selected and depleted with the real irradiation history using Serpent. The results indicate that the Serpent neutron emission rates were 2-12% higher than the ORIGEN emission rates, primarily due to a higher Cm244 production, which may introduce a bias in the results. However, since the neutron emission rates from the Ringhals fuel assemblies span more than two orders of magnitude, the bias is expected to be modest in the RF regression models.

To assay the fissile content of a SNF assembly, this work includes the signature from the DDSI instrument, which measures neutrons in coincidence to determine a so-called early die-away time τ. This feature is sensitive to the fissile content, making it useful for IE determination using machine learning [5]. To predict the early die-away time for a large number of fuel assemblies, the parameterization function of [19] was used, using an updated set of fit coefficients valid for a larger range of fuel parameters. For fuel assemblies with more than a few years cooling, the updated parameters give comparable results to the original parameters, thus either sets of parameters can be used. To verify the accuracy of the parameterization function, MCNP simulations were run for eight selected Ringhals fuel assemblies with irradiation histories that differ significantly from the one assumed in the parameterization function. The results show that the simulated and the parameterized τ values are within 1.5% of each other, with the exception of one fuel assembly for which τ differs by almost 4%. Hence, we judge the parameterized τ values to be sufficiently accurate for the purpose of this work.

Each signature in the training set, the fuel library test set and the Ringhals test set had a 1% Gaussian noise added to it, to account for measurement uncertainty. It is noted in [5] that such a low uncertainty is not unfeasible for gamma spectroscopy or the DDSI signal τ, however the actual measurement uncertainties will depend on the selected measurement setup, which is not considered in this work. The effect of higher levels of noise is presented in section 3.4.

2.3 Random Forest Regression

The RF method [20] is a further development of the decision tree method, and can be used either for classification or regression, i.e. predicting the value of a continuous variable. The RF method is a supervised learning algorithm, where the model is trained on known input-output pairs. The key improvement of RF over decision trees is that the RF predictor is made up of a number of trees, each being trained on a unique randomly sampled subset of the total training data. The output of the RF regression model is the mean value of the output of all decision trees. By using multiple trees, the RF method becomes less prone to overfitting compared to decision trees, where overfitting means a poor capability to generalize beyond the training data. The RF regression model implementation used in this work is the one from scikit-learn [21].

To control how the RF regression model is trained, two hyper-parameters were in [5] found to have an impact on the model performance. The first is the number of decision trees, and [5] notes that a wide range could be used with similar results. Here, we chose 250 trees as the default number if nothing else is specified. The second parameter is the number of features used in each node of the decision trees to make a decision about which leaf the input data belongs to. Again, [5] notes that several values give similar results, and this work use a default value of 3 in the analysis. This is large enough to be within the previously found minima, and additionally the models trained in this work always contains at least three input features.

Three data sets are typically used in machine learning regression: a training set, a validation set, and a testing set.

The training set is used to provide known input-output pairs to train the model, where the input here is some combination of the gamma-ray activities, the neutron emission rate and τ, and the output is the predicted values of CT, BU and IE. The validation set is used to tune the performance of the model when using different hyper-parameters. The testing set is used to assess the performance of the trained model on new data. Since it was found in [5] that the hyper-parameter optimum is rather broad, tuning the model using the validation set was omitted in this work. However, this work instead considers two test sets: one test set comprising data from the same fuel library used to train the model, and another test set comprising the modelled Ringhals fuels. These two test sets are used to assess what uncertainties arise from the RF regression model itself and assumptions made in the depletion calculations, and what additional uncertainty is introduced by the actual irradiation history introduced in the Ringhals test set. The training set consists of 631 525 unique samples from the fuel library, the fuel library test set consists of the remaining 157 881 fuel library samples, and the Ringhals test set consists of the 2192 samples from both reactors.

As was done in [5], all input features in the training set were rescaled to have a mean value of 0 and a variance of 1 before the analysis. The same scaling was applied to the training set and both test sets, to ensure that all values after rescaling were directly comparable to each other. Since the fuel library and the modelled Ringhals assemblies were modelled using different depletion codes, the ORIGEN data for the Ringhals assemblies were converted from emissions per ton uranium to emissions per cm^3 to match the Serpent data in the fuel library, before the standard scaler was applied.

3. Results

In this section we present prediction results for the two test sets. For a given set of input signatures, three RF regression models were trained: one for predicting CT, one for BU and one for IE. Each model used the same training data and hyper-parameters. Following the work of [5], we first considered different combinations of gamma-ray signatures, and then added neutron signatures to the analysis.

3.1 Analysis using gamma-ray signatures

RF regression models were trained to predict IE, BU and CT for two scenarios: i) using the relative gamma-ray activities of Cs134, Cs137 and Eu154 as input, and ii) using in addition the total gamma-ray activity as input.

Table 1 reports the average and root mean square error (RMSE) of the difference between the predicted and true values of the CT, BU, and IE for the two test sets. The average difference (or error) indicates if there is a systematic bias in the predictions and reflects the accuracy of the models. The RMSE provides an indication of the precision. Figure 3 shows the predicted parameter values versus the true values for scenario ii). The marker colour shows the cumulative outage time between consecutive irradiation cycles, to highlight assemblies that spent cycles outside the reactor before reinsertion. Figure 3 also shows a histogram of the errors in the predicted CT, BU and IE for the fuel library test set and the Ringhals test set.

The overall results in Table 1 match those found in [5]. Using only the relative activities of the selected radionuclides, CT can be predicted with good accuracy and precision. However, fuel assemblies with a gap in their irradiation history are systematically over-predicted, as shown in Figure 3. Table 1 also shows that the RMSE for the CT prediction of the fuel library test set is higher than the RMSE for the Ringhals test set, which can also be seen in the histogram in Figure 3. The cause is that the training data includes low-BU high-CT fuels, where both the Cs134 and Eu154 activities are below the detectability threshold, and only Cs137 remains. Almost all Ringhals assemblies have reached a high BU at discharge, and are more likely to include these two radionuclides with activities above the detection threshold. There are however some long-CT, high-BU assemblies in the Ringhals test set, which are under-predicted, as shown in the CT plot in Figure 3.

The large bias and RMSE in the BU reported in Table 1 reveal that the BU of the Ringhals assemblies cannot be

Features	Data set	CT [days]		BU [MWd/kgU]		IE [w%]	
		Avg. error	RMSE	Avg. error	RMSE	Avg. error	RMSE
Relative radio- nuclide activities	Fuel library	3.3	2159	0.03	12.4	0.03	1.2
	Ringhals	425	608	8.88	12.1	0.35	1.13
Relative radio- nuclide activities and total gamma	Fuel library	1.2	683	0.001	0.90	0.001	0.92
	Ringhals	227	448	0.66	1.39	0.42	0.94

Table 1.Average error and RMSE in the fuel predictions for the fuel library test set and the Ringhals test set, with different input features considered in the analysis. The uncertainties in the values due to randomness in the training of the regression models is around 1% of each value.

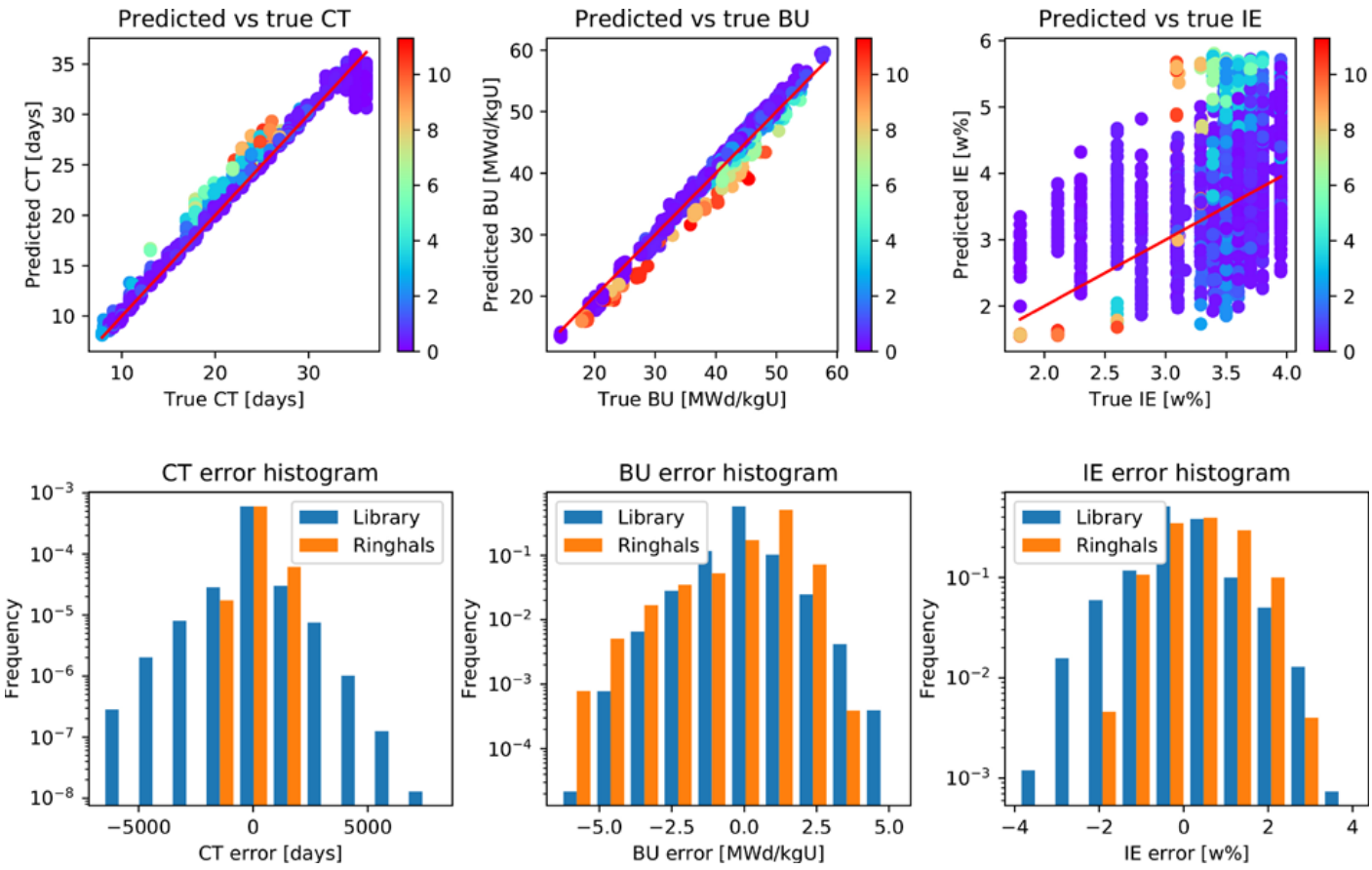

Figure 3. Performance of the RF regression models trained on the relative activities of selected radionuclides, and the total gamma-ray activity. Top row: the true and predicted values of CT (left), BU (centre) and IE (right), for the models. The red line is a guide for the eye, indicating where the regression matches the real values. The colour of the markers shows the cumulative number of years of cooling between consecutive irradiation cycles. Bottom row: Histograms of the errors in predictions of CT (left), BU (centre) and IE (right). The training errors were calculated based on the fuel library test set (labelled "Library"), and the Ringhals test set (labelled "Ringhals").

predicted by only considering relative gamma-ray activities. When the total gamma feature is included, this bias and spread is largely eliminated. The BU plot in Figure 3 shows that some assemblies are under-predicted by around 2-4 MWd/kgU, and these are the ones with a significant gap in their irradiation history. This group of fuels also causes the skewed error distribution seen in the error histogram plot.

Finally, the IE predictions fail since none of the gamma-ray activities depend strongly on it. Additional input features are needed to predict IE, such as neutron-based features, described in the next section.

3.2 Analysis using gamma-ray and neutron signatures

Two different neutron signatures were considered: the gross total neutron emission rate and the parameterized early die-away time τ from the DDSI instrument. RF regression models were trained for two sets of input features: i) using relative radionuclide gamma-ray activities, the total gamma-ray activity and total neutron rate, and ii) using in addition τ.

Table 2 shows the average error and the RMSE for the predictions of CT, BU and IE as a function of input features for the two test data sets. Figure 4 shows plots of the predicted and true parameter values. The colour of the markers shows the cumulative outage time in between irradiation cycles. Figure 4 also shows histograms of the errors in the predictions.

As can be seen when comparing Table 1 and Table 2, including the total neutron emission rate as an input feature improves the CT prediction slightly, the BU prediction remains unchanged, and the IE prediction is significantly improved. For the fuel library test set, the IE predictions are not significantly improved by adding τ when the total neutron emission rate is available. However for the Ringhals test set the precision of the IE predictions are noticeably improved by adding τ, although the accuracy is somewhat worsened due to adding a systematic deviation in the predictions. Hence, for the more realistic

Features	Data set	CT [days]		BU [MWd/kgU]		IE [w%]	
		Avg. error	RMSE	Avg. error	RMSE	Avg. error	RMSE
Relative radio-nuclide activities, total gamma and total neutron	Fuel Library	-0.18	157	0.001	0.53	0.001	0.12
	Ringhals	271	380	0.74	1.40	0.05	0.23
Relative radio-nuclide activities, total gamma, total neutron and τ	Fuel Library	0.16	79	0.001	0.52	0.001	0.11
	Ringhals	270	378	0.72	1.33	0.08	0.16

Table 2. Average error and RMSE in the fuel predictions for the fuel library test set and the Ringhals test set, with different input features considered in the analysis. The uncertainty in the values due to randomness in the training of the regression models is around 1% of each value.

Ringhals test set, τ provides valuable information useful in determining IE.

The plots in Figure 4 show that the bias in the predicted CT for long-cooled Ringhals fuel assemblies, caused by a lack of data at long CT, is removed when additional input features are used. However, the over-prediction of CT and under-prediction of BU for Ringhals assemblies having a gap in their irradiation history remain. This group of assemblies also causes the error histogram plots in Figure 4 to be skewed, where a symmetric distribution would be expected if the errors were random. Additionally, Table 2 shows that the RMSE values for the predictions of the Ringhals test set tend to be a factor 2-5 higher compared to the predictions of the fuel library test set, and this additional uncertainty is also introduced by the irradiation history. Furthermore, the histograms in Figure 4 show that the most likely error in CT is around 1 year, and the most likely error in BU is around 1.5 MWd/kgU. This bias is caused by the differing irradiation histories, and that the final low-power cycles in the Ringhals case resulted in a different abundance of radionuclides at discharge, as compared to a fuel assembly from the library with identical values of CT, BU and IE. Hence, the irradiation history introduces both a bias and an uncertainty in the predictions, when the models are trained on a simplified irradiation history.

3.3 Hyper-parameter selection considerations

Since there are differences in irradiation history as well as in the software used to produce the data sets, it must be verified that the RF regression models are not fitting to features in the training data set that do not generalize to the Ringhals test set. Such a lack of generalization could be due to the choice of hyper-parameters. For the hyper-parameter study, we used all six features (three relative radionuclide activities, their total gamma-ray activity, total neutron emission rate and τ) to predict the fuel assembly parameters. The two hyper-parameters that were investigated here were the number of decision trees used by the RF regression models and the number of features used in each node to make the decision. The default values used in the previous section was 250 trees per RF, and splitting on three features.

For the number of trees, values in the range 50 to 300 in steps of 50 were evaluated. The results show that just as in [5], changing the number of trees has little impact on the performance of the RF regression models. Considering the uncertainty introduced by the randomness in the data sampling, different values of the hyper-parameters do not result in significant differences in fuel parameter prediction capability.

For the number of features used to split each node in the decision tree, values between 1 and 6 were evaluated. For BU and IE, the results are again similar to [5], with little change in performance as a function of the number of features. For CT however, the results improves slightly for the fuel library test set with increasing number of features, but the corresponding performance for the Ringhals test set is a worsened performance with an increasing number of features. This suggests that the RF regression model predicting CT may be fitting to structures in the fuel library that do not generalize to the Ringhals test set, and that splitting using fewer features may be preferred. However this needs to be verified using other test sets before the choice of splitting on one feature can be selected as default.

3.4 Noise considerations

In the previous analysis, a default 1% Gaussian noise was added to all input features in both the training and two test sets, to include the effect of counting statistics and measurement uncertainties. However, depending on the measurement situation, the level of noise may vary. To investigate the impact of also other levels of noise, RF models were trained and then tested when 1%, 5% and 10% noise was applied to all data, with all features used for training. The results are shown in Table 3.

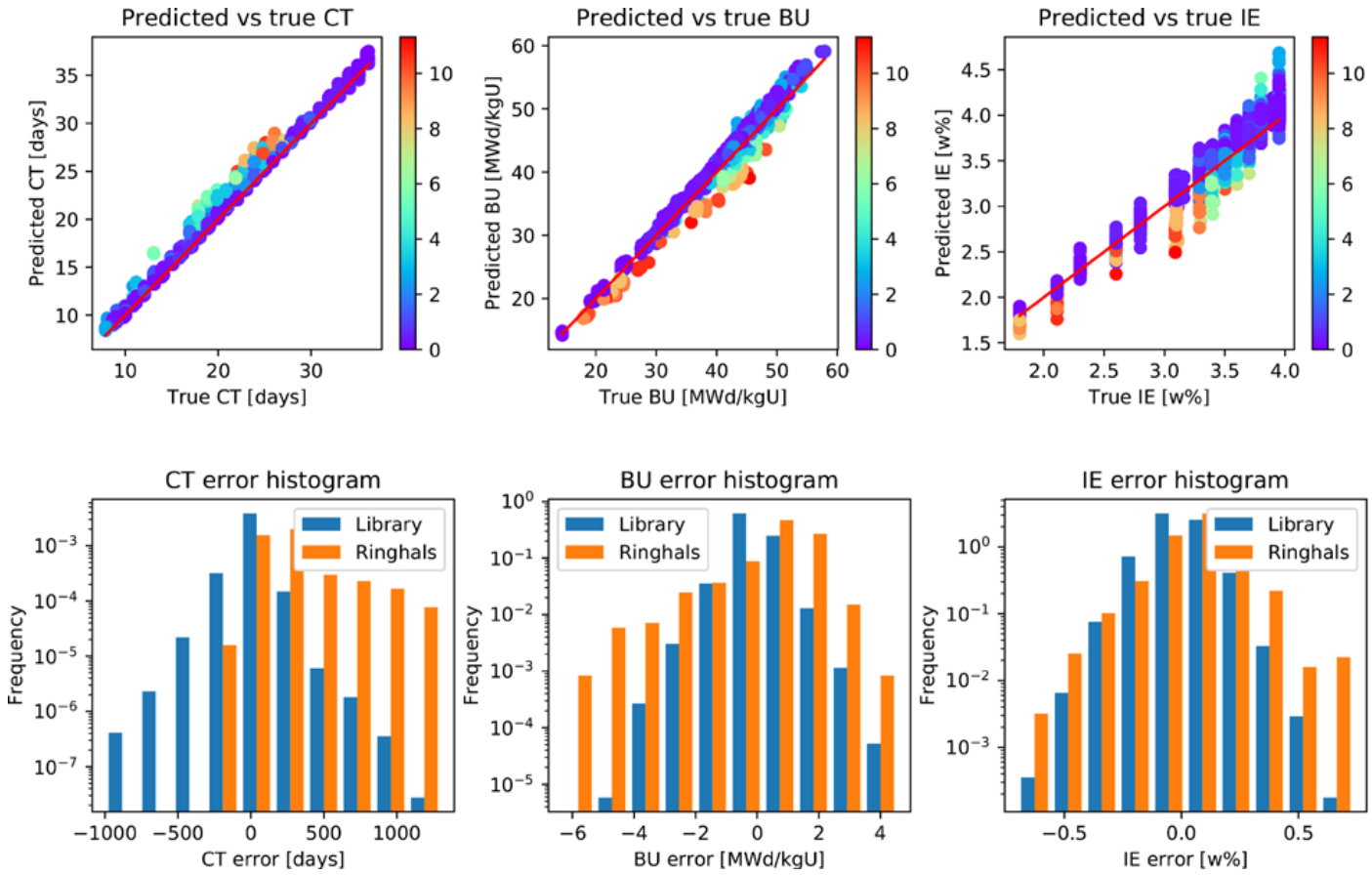

Figure 4. Performance of the RF regression models trained on the relative activities of selected radionuclides, the total gamma-ray activity, the total neutron emission rate and τ. Top row: the true and predicted values of CT (left), BU (centre) and IE (right), for the models. The red line is a guide for the eye, indicating where the regression matches the real values. The colour of the markers shows the cumulative number of years of cooling in between irradiation cycles. Bottom row: Histograms of the errors in predictions of CT (left), BU (centre) and IE (right). The training errors were calculated based on the fuel library test set (labelled "Library"), and the Ringhals test set (labelled "Ringhals").

Overall, the behaviour of the fuel library test set with increasing levels of noise is similar to [5], where the average error changes little, and the RMSE increases with increasing noise. For the Ringhals test set, the RMSE values are higher at lower noise, but the increase as a function of noise is similar to the fuel library test set. Thus, the noise appear to have comparable effects to the precision of the predictions for both test sets. For the Ringhals test set, the average error however increases somewhat with noise. In general, as in [5], the CT prediction is not too sensitive to increased noise, the BU prediction is a bit more sensitive but is manageable also at higher noise levels, but the IE predictions are highly sensitive to the addition of noise. Hence for accurate fuel parameter predictions, effort should be made to have a well-characterized and low-noise DDSI measurement, or a total neutron emission measurement if the DDSI is not used.

4. Conclusions

In this work, we have trained RF regression models to predict the fuel parameters CT, BU and IE of modelled PWR fuel assemblies, based on non-destructive data that could be obtained through gamma and neutron measurements. The models were trained on modelled PWR assemblies from a fuel library with a wide range of CT, BU and IE values, which was created assuming a standardized, simplified irradiation history. The RF regression models were tested on both data from this library, as well as modelled PWR fuels from the Swedish commercial nuclear power reactors Ringhals 3 and 4, to investigate what impact a realistic fuel irradiation history has on the prediction capabilities of RF regression models. In the analyses, input features corresponding to relative radionuclide activities, total gamma-ray activity, total neutron emission rate and the parametrised early die-away time τ from the DDSI instrument were considered.

Based on the results, a gamma-spectroscopic measurement should be sufficient to allow a RF regression model

Noise level	Data set	CT [days]		BU [MWd/kgU]		IE [w%]	
		Avg. error	RMSE	Avg. error	RMSE	Avg. error	RMSE
1%	Fuel Library	0.16	79	0.001	0.52	0.001	0.11
	Ringhals	270	378	0.72	1.33	0.08	0.16
5%	Fuel Library	-0.56	298	-0.001	1.94	0.001	0.36
	Ringhals	311	442	1.40	2.36	0.17	0.39
10%	Fuel Library	-1.32	509	-0.002	3.16	0.001	0.59
	Ringhals	359	541	2.04	3.84	0.30	0.66

Table 3. Average error and RMSE in the fuel predictions for the fuel library test set and the Ringhals test set, with different input features considered in the analysis. The uncertainty in the values due to randomness in the training of the regression models is around 1% of each value

to predict CT well, and a well-calibrated setup that also provides enough information to allow a comparison between fuel assemblies of the absolute total gamma-ray activity will improve the results further. For a good BU prediction, both the relative radionuclide activities and the total gamma-ray activity are required, whereas the total neutron emission rate signature can be added to slightly improve the predictions. For the IE predictions, τ is the input feature considered of highest importance, since it is the only one which probes the fissile content, and hence IE. While the total neutron was sufficient for IE predictions of the fuel library test set, the more realistic Ringhals test set showed that τ provides more information as compared to the total neutron feature. Using the total neutron emission rate instead of τ worsens the results, since the RMSE of the predictions increase. This is because the abundance of neutron-emitting radionuclides does not only depend on the IE but also on the irradiation history, which differs for the training and Ringhals test set.

Due to the differences in irradiation history, the simulated Ringhals fuel assemblies have comparatively lower abundance of radionuclides such as Cs134 at discharge, compared to fuel assemblies from the fuel library with equivalent values of CT, BU and IE. As a consequence, the RF regression models systematically overestimate CT and underestimate BU for the Ringhals assemblies. However, the systematic deviation is rather modest, typically around 2-5% of the values. Fuel assemblies that were outside the reactor for some time before a final low-power cycle are in general predicted to have a CT that is 1-3 years too long, even if the time spent outside the reactor before the final irradiation cycle could be up to ten years. Overall, the predicted fuel parameter values are rather similar to the true values and may therefore be of use to a safeguards inspector despite the fact that fuel irradiation histories may differ from what is assumed in the predictions. As in the previous work, the choice of hyper-parameters has a negligible impact on the performance of the predictions, though the CT predictions do seem to benefit from choosing a low number of features to split nodes on.

5. Acknowledgements

This work was supported by the Swedish Radiation Safety Authority (SSM) under contract SSM2017-5979 and SSM2020-996. The authors are grateful to Klaes-Håkan Bejmer and Andreas Lidén at Vattenfall for providing the irradiation history of the fuel assemblies for the Ringhals 3 and 4 reactors.

6. References

[1] S. Tobin, P. Jansson, Nondestructive assay options for spent fuel encapsulation. SKB technical report, TR-13-30. ISSN 1404-0344. March 2013. https://skb.se/publication/2697744/TR-13-30.pdf

[2] J. Coble, C. Orton, J. Schwantes, Multivariate analysis of gamma spectra to characterize used nuclear fuel, Nucl. Instrum. Methods Phys. Res. A 850, pages 18–24. 2017

[3] C. Hellesen, S. Grape, P. Jansson, S. Jacobsson Svärd, M. Åberg Lindell, P. Andersson, Nuclear spent fuel parameter determination using multivariate analysis of fission product gamma spectra. Annals of Nuclear Energy, volume 110, Pages 886-895. December 2017.

[4] Zs. Elter, L. Caldeira Balkeståhl, S. Grape, C. Hellesen, Nuclear safeguards verification of modelled BWR fuel using a multivariate analysis approach, in: IAEA Safeguards Symposium: Building Future Safeguards Capabilities, Nov 5–8, Vienna, 2018.

[5] S. Grape, E. Branger, Zs. Elter, L. Pöder Balkeståhl. Determination of spent nuclear fuel parameters using modelled signatures from non-destructive assay and Random Forest regression. Nuclear Instruments and Methods in Physics Research Section A: Accelerators, Spectrometers, Detectors and Associated Equipment, Volume 969, July 2020. DOI: 10.1016/j.nima.2020.163979

[6] A. M. Bachmann, J. B. Coble, S. E. Skutnik, Comparison and uncertainty of multivariate modelling techniques to characterize used nuclear fuel, Nucl. Instrum. Methods Phys. Res. A 991 (2021) 164994.

[7] R. Rossa, A. Borella, Use of machine learning models for the detection of fuel pin replacement in spent fuel assemblies. The ESARDA Bulletin No.58. 2019.

[8] R. Rossa, A. Borella and N. Giani, Comparison of machine learning models for the detection of partial defects in spent nuclear fuel. Annals of Nuclear Energy, volume 147 page 107680. 2020.

[9] Zs. Elter, S. Grape, A methodology to identify partial defects in spent nuclear fuel using gamma spectroscopy data. The ESARDA Bulletin No. 61, 2020.

[10] C.R. Orton, C.G. Fraga, R.N. Christensen, J.M. Schwantes, Proof of concept simulations of the multi-isotope process monitor: An online, nondestructive, near-real-time safeguards monitor for nuclear fuel reprocessing facilities, Nucl. Instrum. Methods Phys. Res. A 629 (1) 209–219. 2011

[11] M. Åberg Lindell, Safeguards Evaluation and Analysis Techniques for Nuclear Material In Generation IV Fuel Cycles (PhD Thesis). Uppsala University, 2018.

[12] D. Reilly, N. Esslin, H. Smith, S. Kreiner. Passive Nondestructive Assay of Nuclear Materials. Technical report. LA-UR-90-732, Los Alamos National Laboratory, Los Alamos, NM, U.S.A. March 1991.

[13] A. Bolind, The use of the BIC set in the characterization of used nuclear fuel assemblies by nondestructive assay. Annals of Nuclear Energy, Volume 66, pages 31-50. 2014. https://doi.org/10.1016/j.anucene.2013.11.010.

[14] U.S. Energy Information Administration, Annual commercial spent fuel discharges and burnup, 1968 - June 30, 2013. Available at https://www.eia.gov/nuclear/spent_fuel/ussnftab3.php Retrieved February 9:th, 2021.

[15] Zs. Elter, L. Pöder Balkeståhl, E. Branger, S. Grape. Pressurized water reactor spent nuclear fuel data library produced with the Serpent2 code. Data in Brief, Volume 33, December 2020. DOI: 10.1016/j.dib.2020.106429

[16] J. Leppänen et. al. The Serpent Monte Carlo code: Status, development and applications in 2013. Annals of Nuclear Energy, volume 82 pages 142-150. 2015.

[17] S. M. Bowman, L. C. Leal, O. W. Hermann, C. V. Parks. ORIGEN-ARP, A Fast and Easy-to-Use Source Term Generation Tool. Journal of Nuclear Science and Technology, vol. 37, no. sup1, pp. 575-579, 2000. DOI: 10.1080/00223131.2000.10874953

[18] Update of the α – n Yields for Reactor Fuel Materials for the Interest of Nuclear Safeguards. S. Simakov, Q. van den Berg, Nuclear data sheets, volume 139, January 2017. https://doi.org/10.1016/j.nds.2017.01.005

[19] L. Caldeira Balkeståhl, Zs. Elter, S. Grape. Parametrization of the differential die-away self-interrogation early die-away time for PWR spent fuel assemblies. Presented at the 41st ESARDA Annual Meeting in Stresa, Italy, May 2019. Published in the ESARDA bulletin, no. 58, June 2019.

[20] L. Breiman, Random forests, Mach. Learn. 45 pages 5–32. 2001

[21] F. Pedregosa et al. Scikit-learn: Machine Learning in Python. Journal of Machine learning Research, volume 12, pages 2825-2830. 2011.

Sensitivity analysis of the Rossi-Alpha Distribution and the early die-away time τ from the DDSI instrument due to modelling assumptions

Sophie Grape, Zsolt Elter, Erik Branger, Li Pöder Balkeståhl,

Division of Applied nuclear physics,
Department of Physics and Astronomy
Uppsala University, Sweden
E-mail: sophie.grape@physics.uu.se

Abstract

Under the Next Generation Safeguards Initiative, several different nuclear safeguards measurement techniques were studied. One of them was the Differential Die-Away Self-Interrogation technique, and the research showed that its early die-away time τ was proportional to the fuel assembly multiplication and thus sensitive to the fissile content of the fuel assembly under assay. A prototype instrument was later built and tested in the field, and the measurements showed that the instrument could be used successfully in the field.

This work builds on previous efforts, and systematically studies the effects of assumptions about the fuel properties (such as its dimensions) and its irradiation conditions in the reactor, on the Rossi-Alpha Distribution (RAD) and τ. The motivation is twofold, firstly to better understand if and what impacts such assumptions have on the RAD and τ, and secondly to investigate how well the simulation model used to estimate the RAD and τ is able to generalize to other fuel types and irradiation conditions than those modelled.

20 spent nuclear fuel assemblies currently residing in the Swedish interim storage for spent nuclear fuel were measured by the prototype DDSI instrument. The assemblies were modelled using Serpent2 and MCNP6 in this work. Fuel depletion calculations were performed assuming both a standard irradiation cycle and the actual irradiation history as provided by the operator. Fuel properties and irradiation conditions were also modified and their effect studied.

Based on the simulated DDSI instrument response in MCNP6, the RADs were created and τ determined. The analysis shows that each modelling assumption on its own affects both the RAD and the τ value. However, some of the individual effects work in opposite direction and cancel out when considered at the same time. For this reason, the default model is considered to be a good and valid approximation of the more complex one and results are expected to generalize well.

Keywords: Nuclear safeguards, DDSI, neutron coincidence, *tau (τ)*, modelling

1. Introduction

The DDSI instrument detects neutrons emitted from spent nuclear fuel. The detected neutrons originate from spontaneously fissioning radionuclides which act as a neutron source, interrogating the fissile content of the spent nuclear fuel. Depending on the nuclide inventory of the spent nuclear fuel, fission chains of various lengths develop and give rise to a distribution which describes the time evolution of the neutron population and is known as the Rossi-Alpha Distribution (RAD) [1]. That distribution is then used to determine the die-away time, τ, of the neutron population inside the nuclear fuel.

The DDSI technique was studied in detail under the Next Generation Safeguards Initiative, a project aiming to develop non-destructive assay instrumentation to verify operator declarations and fuel parameters, detect diversion of fuel material, estimate plutonium mass and decay heat, and to determine the reactivity of spent fuel assemblies [2]. Simulated responses were analysed to investigate the capability of the DDSI instrument to reach these goals (see for instance [3, 4]). A prototype DDSI instrument was also built and tested in the field, and it was shown that several algorithms developed to determine fuel assembly characteristics worked successfully on measured data [5,6].

The parameter τ is sensitive to the balance of fissile material and neutron absorbing isotopes, and has a high relevance in safeguards evaluations. The nuclide inventory of a spent nuclear fuel (and thus τ) depends on several things such as the fuel assembly's initial enrichment, burnup and cooling time. This work aims at investigating if and to what extent the RAD and τ are also affected by parameters which are often not (well)known to a nuclear inspector in the field, such as the fuel geometry, the irradiation history, and irradiation conditions. It does not aim at confirming previous results or predict safeguards-relevant properties.

Although results on the sensitivity of τ to modelling assumptions have not been published before, the sensitivity in calculated nuclide inventories due to approximations or uncertainties in the input (such as key design features and operating conditions) has been investigated extensively, see e.g. [7] and references therein. The power history has been found to be of minor importance for most actinides and fission products at the time of discharge, but the

moderator temperature (and its density) has been identified as important in the physics calculations. The boron concentration has also been found to be important as it influences the neutron spectrum in the fuel. The impact of the fuel temperature is more difficult to assess as it is not measured directly, and it is associated with major uncertainties. Other works, such as [8], have also studied the effects of the UO_2 mass density, power levels and irradiation history on uranium and plutonium concentrations and found them to be of little importance. Actinide inventories, and particularly short-lived nuclides, were however found to be the most sensitive to irradiation history variations. Reference [9] reported on small effects on a number of calculated isotopic concentrations due to changes in fuel temperature, and [10] showed that for BWR burnup credit calculations, the control blade position is important because it affects the ^{239}Pu concentration in the fuel.

In safeguards assessments, it is rare to have access to detailed information about the fuels under assay and it may be necessary to make assumptions similar to those made in the simulations here. In the event that an inspector has access to detailed information about the fuel, an accurate model can be created, but at the expense that the model probably does not generalize well to fuels with other properties. In this work we investigate how systematic uncertainties from various modelling assumptions affect the RAD and the predictions of τ. We do this by studying the implications of various modelling assumptions on the Rossi-Alpha Distribution (RAD) and τ, for 20 spent nuclear fuel assemblies of Pressurized Water Reactor (PWR) type. The scope of this work does not cover investigations on if and how the modelling assumptions impact the DDSI capbility to detect diversion of fuel material, estimate plutonium mass, decay heat, or determine the reactivity of spent fuel assemblies.

2. The DDSI principle and instrument design

The DDSI technique is a passive non-destructive assay technique, relying on neutron coincidence counting, that has been developed to study nuclear material such as spent nuclear fuel. In such fuel, radionuclides such as ^{244}Cm undergo spontaneous fission and act as an internal neutron source that interrogates the fissile content of the fuel. Some of the neutrons emitted by e.g. ^{244}Cm thermalize in the water surrounding the fuel rods, and induce fissions in primarily ^{235}U, ^{239}Pu, and ^{241}Pu. Depending on the nuclide inventory of the spent nuclear fuel (and thus the fuel assembly multiplication), fission chains with various lengths will develop. This affects the possible detection of the correlated neutrons, and therefore of the RAD and its decrease over time as quantified by the early die-away time τ.

The value of τ can be determined from the RAD, which is a histogram describing the number of subsequent neutrons detected within a certain time window after the trigger neutron. The distribution can be described by a single exponential function in a limited time span, although the underlying physics can be explained by two different physical processes, each of which can be described by an exponential function. One process concerns neutrons coming from the same fission event, or from fast fission processes where the neutron has not thermalized before inducing fission. These neutrons typically have a fast die-away time (or a fast time component) which is determined mainly by the time needed for the neutron to reach the DDSI detectors and thermalize in the polyethylene around them (the die-away time of the detectors is approximately 19 μs). The second process concerns time-correlated neutrons coming from fission reactions in the same fission chain, where at least one second fission was induced by a thermal neutron. The second process may take much longer time than the first process, and its die-away time may extend up to hundreds of μs. The so-called early die-away time τ is a function of both processes and can be determined in a specific time range of the RAD, where properties of the spent nuclear fuel (such as abundance of fissile and neutron absorbing material) as well as properties of the DDSI instrument design, play a role. Reference [4] showed that in the time window of 4-52 μs, τ was found to be quadratically related to the SFA multiplication, which makes τ interesting in the context of spent nuclear fuel verification for nuclear safeguards purposes.

A model of the DDSI prototype instrument design is shown in Figure 1. There are four detector pods, symmetrically located around the FA. Each of them contains 14 ^{3}He-detectors, surrounded by polyethylene and encased in steel containers filled with air. Between the detector pods and the FA, there is a lead shield and a funnel which guides the fuel assembly into position, as it is inserted into the instrument from above.

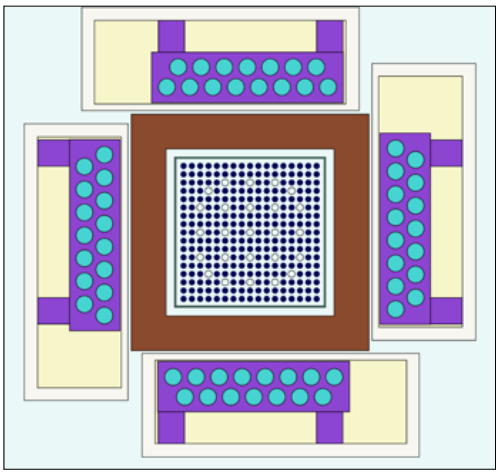

Figure 1. The DDSI instrument as implemented in MCNP. The fuel assembly is shown in the centre, surrounded by a lead shield (brown) and four detector pods. The ^{3}He detectors are shown in blue inside the pods, and the polyethylene surrounding them is shown in purple.

3. Modelling spent nuclear fuel and the DDSI instrument response

The 20 studied spent nuclear fuel assemblies are all PWR 17x17 fuel assemblies irradiated at the Ringhals nuclear plant in Sweden. They are produced by five different fuel manufacturers, but according to the fuel information in [11], 17 out of the 20 fuel assemblies are very similar with respect to fuel dimensions, while the remaining three have fuel rod dimensions which deviate from the other 17 fuel assemblies by less than 10%. The initial enrichment of all 20 fuel assemblies ranges between 2.1-3.9 %, the burnup ranges between 20-48 GWd/tU and the cooling times are approximately 10-35 years. The information provided to the authors at the time of this work does not include any information on whether or not there are Gd rods present in any of the fuel assemblies, and thus Gd rods were not modelled. Should additional information indicate that there are indeed such rods present, their impact would need to be studied using a different model since the burnup calculations in this work are made with a single-pin model, and thus assumes that all fuel rods are identical in the subsequent steps.

The Serpent2 code [12] was used to define a fuel pin model, deplete it and estimate its material composition. The fuel pin was placed in an infinite 2D lattice in Serpent2, and run in criticality source mode.

MCNP6 [13,14] was then used to construct a model of the DDSI instrument in water, sample spontaneous fission neutrons emitted by the spent nuclear fuel, transport the neutrons from the source to the DDSI instrument and estimate its response. A full fuel assembly was assumed, consisting of identical fuel rods where the material composition was taken from the output of the Serpent2 calculations. A spontaneous fission source was evenly distributed across all fuel pins, but restricted in the axial direction to 145 cm centred on the DDSI, because it was found that regions farther from the instrument do not contribute to the detector signal. It can be pointed out that the simulations do not include background contributions from e.g. (α, n)-reactions, which are randomly distributed in time and thus neutrons from such reactions do not contribute to the rate of time-correlated neutrons. The neutron detection was simulated with neutron coincidence capture tallies (F8 CAP in MCNP6) in the ^{3}He tubes. One hundred F8 tallies, each with 2 μs gates were used to make the RAD of true neutron coincidences. 5 million neutron histories were simulated, which was sufficient for most of the tallies to pass the ten statistical checks performed by MCNP6 (in a few tallies there were not enough hits to reliably estimate the slope of the probability density function). In order to determine τ, the RAD was created, showing the time difference between detected neutrons. A single exponential function was fitted to the RAD in the time window of 4-52 μs, as indicated in [4].

3.1 Modelling the fuel irradiation and DDSI instrument response

For the 20 studied fuel assemblies, two types of irradiation histories were considered in this work: a default irradiation and its actual irradiation. The default irradiation scheme was defined as 365 days of irradiation in the reactor, followed by 30 days of downtime. The reactor power was set so that a burnup of 10 GWd/tU per full cycle was achieved. The duration of the last cycle was adjusted to result in the desired discharge burnup value. The burnup step used was 0.5 GWd/tU. With respect to the actual irradiation scheme, this information was provided by the operator. It showed that the fuels had indeed undergone varying irradiation histories, ranging from some fuel assemblies having resided in the reactor only for two cycles, to others having been irradiated for up to five cycles. The burnup per cycle also varied both between fuel assemblies and between cycles. In the burnup calculations, the accurate irradiation histories as provided by the operator were used together with information on the average power level in each cycle, and 50-day burnup steps were used.

In order to systematically study the impact of also other changes than the fuel irradiation, the impact of the other parameters were studied in isolation. In Serpent2, the boron concentration in the water during irradiation was changed from 0 in the default case to 200 ppm, 630 ppm and 1100 ppm in three different simulations. The fuel temperature was 1500 K in the default case and 900 K in the realistic case; the fuel pellet density was 10.5 g/cm^3 in the default case and 10.41 g/cm^3 in the realistic case; the water density was 0.75 g/cm^3 in the default case and 0.723 g/cm^3 in the realistic case, and the fuel pellet radius was adjusted according to the values in [15]. With respect to the fuel pellet and fuel rod dimensions, either a default geometry representative of PWR fuel in general, or geometry and irradiation conditions based on the Westinghouse 17x17 Standard fuel in the Scale 6.1 manual [15], was used. Reference [11] conveys that dimensions for fuels from the other manufacturers are similar to those of Westinghouse 17x17 Standard fuel.

Also in MCNP6, changes were done to the model used to investigate the impact of the individual changes as well as their total effect. The effect of having guide tubes and a central instrumentation tube present (or not) was studied, and the fuel density and pellet radius were adjusted to match the values used in the corresponding Serpent2 calculations. In the final case, the total effect of all assumptions in both Serpent2 as well as MCNP6 was investigated.

The identified cases and details on model properties in Serpent2 and MCNP6 are shown in Table 1.

Modelling property	Software	Default properties	Realistic properties
1. Default irradiation history	Serpent2	Ideal irradiation history with 10 GWd/tU per 365-day irradiation cycle, followed by a 30-day outage.	-
2. Actual irradiation history	Serpent2	-	Actual irradiation history and power density as provided by the operator.
3. Boron concentration during irradiation	Serpent2	0 ppm	200 ppm 630 ppm 1100 ppm In case 9, 630 ppm was used.
4. UO_2 fuel temperature	Serpent2	1500 K	900 K
5. H20 density	Serpent2	0.75 g/cm^3	0.723 g/cm^3
6. Guide tubes and central instrumentation tube	MCNP6	No tubes	24 water-filled guide tubes and one central instrumentation tube
7. UO_2 fuel density	Serpent2/ MCNP6	10.50 g/cm^3	10.41 g/cm^3
8. UO_2 fuel dimension	Serpent2/ MCNP6	0.41 cm fuel pellet radius. 0.1 mm gap (void). Cladding outer radius equal to 0.48 mm. Pitch 1.26 cm.	0.4025 cm fuel pellet radius. 0.085 mm gap (void). Cladding outer radius equal to 0.475 mm. Pitch 1.26 cm.
9. All of the above assumptions	Serpent2/ MCNP6	All of the above default settings in Serpent and MCNP	All of the above realistic settings in Serpent2 and MCNP6.

Table 1. Default as well as more realistic properties used in the Serpent2 and MCNP6 modelling. The realistic values are taken from the Scale manual [15]).

4. Results

For three of the 20 fuel assemblies, representing fuels with both regular and irregular irradiation history, the impact of the modelling assumptions were studied in greater detail by implementing them one at a time to see their individual effects. These results can be found in section 4.1. For the remaining 17 fuel assemblies, three of the nine cases were investigated: the default case (case 1), the actual irradiation history (case 2) and when all assumptions are changed at once (case 9, denoted as “change all”). These results can be found in section 4.2.

4.1 Results from detailed investigations

This section presents separately the results on the RAD and τ from the studies of the three selected fuel assemblies.

4.1.1 Results on the RAD

Figure 2 shows the RADs and the fits to determine τ for the three fuel assemblies denoted fuel 1, 2 and 3.

One thing to immediately notice is the difference in RAD amplitudes between the fuels. The fuel with the highest RAD amplitude has an initial enrichment almost twice as large as of the other two fuel assemblies, but also a discharge burnup which is approximately twice as high. The fuel with the highest initial enrichment experienced an irradiation history similar to what was assumed in the default case, while the fuel with the lowest RAD amplitude experienced a very long first irradiation cycle and then a short period outside the reactor before being re-irradiated a second time. The authors acknowledge that this irradiation scheme seems out of the ordinary and could possibly be due to a reporting error by the operator; nevertheless, it is the information made available and it was therefore assumed to be true in this work. The fuel with a RAD amplitude between the other two fuel assemblies, experienced the same irradiation history as the fuel with the lowest RAD amplitude during the first two cycles and then resided outside the reactor for approximately ten years before being re-irradiated for two more cycles. Figure 2 also shows that the RAD for the default case (shown with black triangles) it is found roughly in the middle of all RADs, meaning that the various modelling assumptions separately result in both increased and decreased RAD amplitudes. However, for all three fuel assemblies:

- Increased boron content results in a higher RAD amplitude, as compared to the default case,

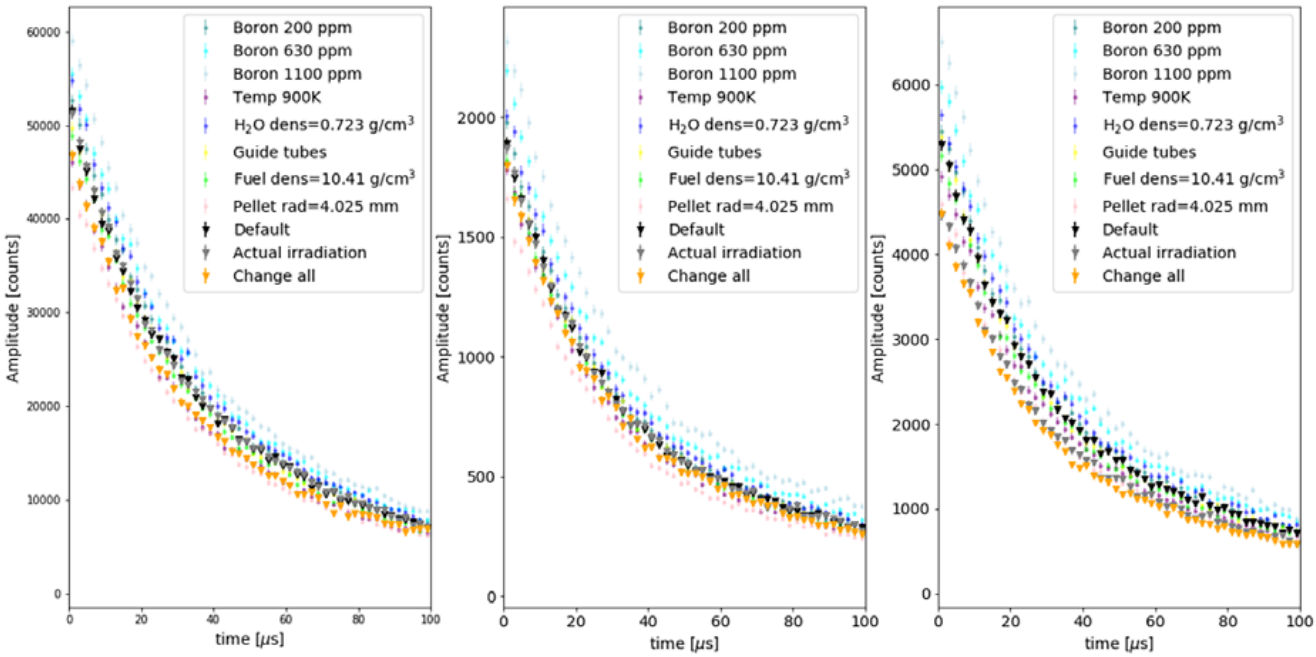

Figure 2. Resulting RAD distributions for the three fuel assemblies studied in greater detail: fuel 1 (left), fuel 2 (centre) and fuel 3 (right).

- Lower water density leads to a higher RAD amplitude, as compared to the default case,
- Decreasing the pin radius to more realistic values results in a lower RAD amplitude likely because this implies less material to assay, and
- Lowering the fuel temperature from 1500 K to 900 K changes the cross sections in the depletion calculations, which in turn results in a lower RAD amplitude.

The impact of the guide tubes is negligible, as is slightly lowering the UO_2 density to a more realistic value. The impact of the actual irradiation history is different in all three cases, probably because the default irradiation history is varying to different degrees from the actual irradiation history.

Interestingly enough, Figure 2 shows that for fuel 2, some of the modelling effects cancel out when all assumptions are changed simultaneously (case 9, change all). For fuel 1 and 3, case 9 results in a lower RAD amplitude (but not as pronounced as when changing only the fuel pellet radius, probably because the boron content offset partly compensates for this). For one of the fuels (fuel 3), the more realistic assumptions in the modelling, results in the lowest RAD amplitude of all cases (although it is close to changing only the irradiation history).

In order to better understand why the RAD changes in the way it does, the changes of eight selected nuclide concentrations, identified to be of most importance when determining τ, were studied in detail. The isotopes, as identified in [16], are $^{239\text{-}241}$Pu, ^{241}Am, ^{235}U, ^{238}U, ^{155}Gd and ^{149}Sm. In addition, we decided to include ^{242}Cm and ^{244}Cm because they contribute to both spontaneous fission and a constant background in a real measurement situation. Figure 3 shows how the selected nuclides vary for the different cases (not including the case where guide tubes are included in MCNP 6, since the depletion calculations in Serpent2 are the same as for the default case), for fuel 1. However, for all three fuel assemblies studied here, the concentrations change in practically the same way. One can note that the concentrations for several of the nuclides in Figure 3 change in very similar ways as the RADs in Figure 2.

In absolute terms, the nuclide concentrations change the most for ^{238}U, followed by ^{239}Pu and ^{235}U for all three fuel assemblies. In relative terms, there are variations among the three fuel assemblies, but large relative increases are typically seen for the fission products ^{149}Sm and ^{155}Gd and the two Cm-isotopes, ^{242}Cm in particular (especially for fuel 3). Figure 3 shows that the concentrations of ^{239}Pu, ^{241}Pu and ^{235}U grow with increasing boron concentration, and that a lower water density also leads to a higher concentration (both changes make the neutron spectrum harder). Making the fuel pellet radius smaller or lowering the fuel temperature, gives lower plutonium concentrations than in the default case. Changing the UO_2 density does not impact the plutonium concentration much, neither does the actual irradiation history except in the cases of the ^{242}Cm and ^{241}Pu concentrations for fuel 3 (the same fuel assembly for which the RAD amplitude changes as a function of irradiation history). The lowest ^{239}Pu and ^{241}Pu

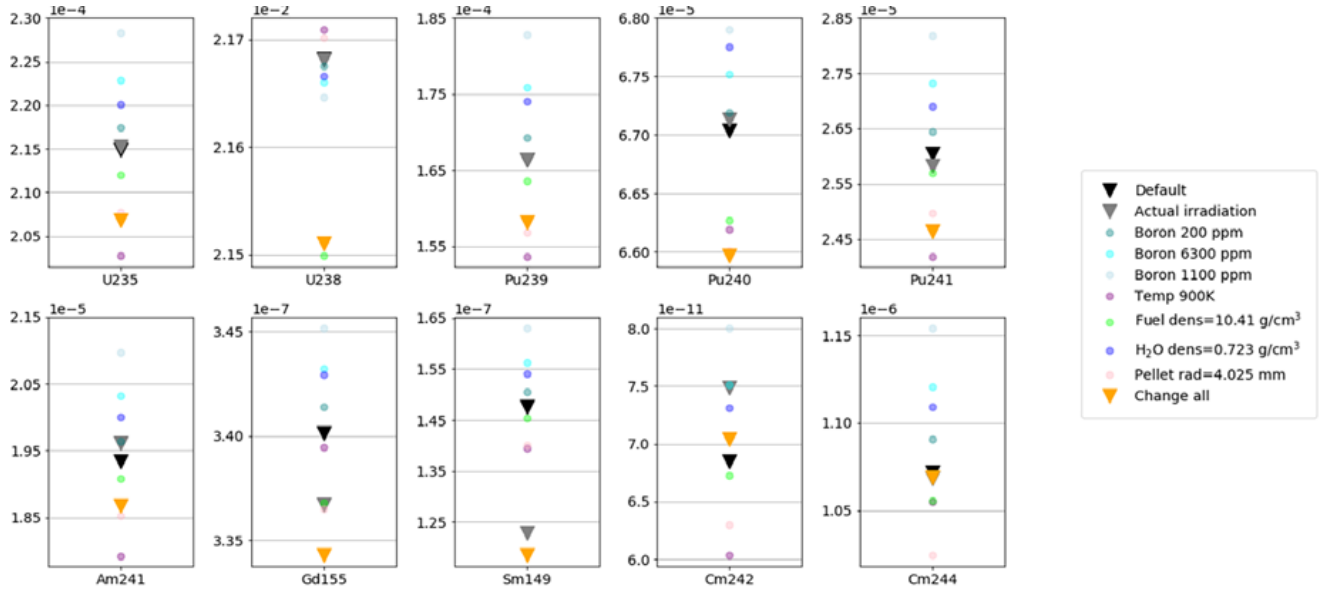

Figure 3: The subplots show how the selected nuclide concentrations (in units of 10^{24}/cm^3) vary for the different cases.

concentrations are found for a fuel temperature of 900 K and when all model assumptions are changed at the same time (case 9).

4.1.2 Results on τ

Values of τ for the simulated cases are shown in Table 2. They do not necessarily change in the same way as the RADs, since τ depends on the structure of the RAD. The values of τ for the fuel assembly with the highest initial enrichment (fuel 1) are consistently larger than for the two other fuel assemblies. It is not clear that increasing the boron content from 0 ppm (the default case), has an impact on τ. However, lowering the fuel temperature, the UO_2 density or making the fuel pellet radius smaller all seem to lower τ, although the magnitude of the effects are small in some cases. Lowering the water density has either a weak impact or no impact at all on τ. Making all changes at once, lowers τ in all three cases.

As seen in Table 2, modelling the actual irradiation history doesn't have a significant impact on τ, which remains the same when the uncertainties in the fits are taken into account, for all three fuel assemblies. The same holds true for changing the water density (even if this impacts the concentration of the three plutonium isotopes) or inserting guide tubes and an instrumentation tube. Increasing the boron content impacts τ, but differently for the different fuel assemblies. For fuel 1, a boron content of 200 ppm appears to considerably lower τ while increasing the boron content further restores τ to the same value as for no boron at all. For fuel 3, a boron content of 630 and 1100 ppm gives τ values, which are higher than for the default case. A lower fuel temperature gives a lower τ value for fuel 1, but not for the other two fuel assemblies. Lowering the fuel density lowers and decreasing the pellet radius lowers τ for fuel 1 and 3, but not for fuel 2.

4.2 Results for all fuel assemblies

For the remaining 17 fuel assemblies, three of the eleven assumptions were investigated: case 1, 2 and 9. For completeness, the results from the three fuels above can be found here as well.

4.2.1 Results on the RAD

The trend among the 17 spent nuclear fuel assemblies is that the irradiation history (case 2) has a low impact on the RAD amplitude. For the vast majority of the fuel assemblies, a visual inspection of the RAD data points reveal that these are the same within error bars, which show the uncertainty due to the number of simulated events in the Monte Carlo calculations, over the time interval 0-120 μs. In a few cases, the RADs do not completely overlap for times below 15 μs (fuels 19, 6 and 9), while the distributions sometimes overlap and sometimes not for another fuel (fuel 15). Only for one single fuel assembly (fuel 16), is the RAD associated with the actual irradiation history consistently lower than for the default irradiation. Inspecting the irradiation history for fuel 16 shows that it has undergone five irradiation cycles of rather varying length and cycle burnup, and resided outside the core for two years before being reinserted for a last irradiation cycle. For all fuel assemblies, the RAD amplitude for the most realistic case (case 9) is lower than, or approximately as large as, the RAD amplitude for the default case (case 1).

Cases investigated	Fuel 1		Fuel 2		Fuel 3	
	τ	Unc.	τ	Unc.	τ	Unc.
1. Default case	42.8	0.5	40.2	0.5	39.8	0.5
2. Actual irradiation	41.9	0.5	40.8	0.5	38.9	0.5
3.1. Boron concentration during irradiation = 200 ppm	41.3	0.4	40.8	0.5	39.7	0.5
3.2. Boron concentration during irradiation = 630 ppm	42.6	0.5	40.5	0.5	40.6	0.5
3.3. Boron concentration during irradiation = 1100 ppm	42.2	0.4	41.5	0.5	40.6	0.5
4. UO_2 fuel temperature = 900 K	40.8	0.5	39.7	0.5	38.6	0.5
5. H_2O density = 0.723 g/cm^3	42.3	0.5	40.6	0.5	39.8	0.5
6. Guide tubes and instrumentation tube present	41.9	0.5	41.0	0.5	38.9	0.5
7. UO_2 fuel density in Serpent and MCNP =10.41 g/cm^3	41.6	0.5	40.8	0.5	38.6	0.5
8. UO_2 fuel pellet radius in Serpent and MCNP=0.4025 cm	41.1	0.5	39.5	0.5	38.3	0.5
9. All of the above assumptions at once	40.9	0.4	39.6	0.5	37.6	0.4

Table 2. Determined τ values and the one sigma uncertainties in τ as determined by the fits, for the three selected fuel assemblies and the cases investigated in this work. All values are given in [μs].

4.2.2 Results on τ

With respect to the τ values, these are shown in Table 3 for all 20 fuel assemblies. One fuel assembly has a considerably higher τ than the other fuels; this fuel assembly has a relatively high initial enrichment and a medium discharge burnup after having been irradiated only two cycles. The fuel assembly with the lowest τ value is found to have a medium initial enrichment and a high burnup, having been irradiated for four cycles.

With respect to variations in τ with the modelling assumptions, the τ values for the default case (case 1) and the

Fuel	Default irradiation (case 1)		Actual irradiation (case 2)		Change all (case 9)	
	τ	Unc.	τ	Unc.	τ	Unc.
1	42.8	0.5	41.9	0.5	40.9	0.4
2	40.2	0.5	40.8	0.5	39.6	0.5
3	39.8	0.5	38.9	0.5	37.6	0.4
4	38.2	0.4	38.2	0.4	37.3	0.4
5	39.3	0.4	39.8	0.4	38.8	0.4
6	40.1	0.4	40.5	0.4	40.1	0.4
7	41.5	0.5	41.6	0.5	40.5	0.5
8	36.9	0.4	36.8	0.4	35.7	0.4
9	40.8	0.5	40.6	0.5	40.0	0.5
10	48.0	0.5	47.9	0.5	47.5	0.5
11	39.9	0.4	40.1	0.5	38.5	0.4
12	39.7	0.5	40.0	0.5	39.0	0.5
13	40.0	0.5	40.0	0.5	38.6	0.4
14	35.5	0.4	35.3	0.4	34.4	0.4
15	39.6	0.4	40.5	0.5	38.7	0.4
16	39.5	0.4	38.9	0.4	38.8	0.5
17	37.9	0.4	37.7	0.4	37.5	0.4
18	39.9	0.4	40.6	0.4	40.5	0.4
19	39.8	0.5	38.6	0.4	38.7	0.5
20	36.8	0.4	36.7	0.4	35.3	0.4

Table 3. The early die-away times τ and the one sigma uncertainties in τ as determined by the fit, for the 20 fuel assemblies and the three cases. All values are given in [μs].

actual irradiation (case 2) are the same when the uncertainties in the fits are taken into account, for all fuel assemblies except fuel 19. For fuel 19, the three RADs do not overlap below 15 μs, which results in a slightly different slope of the exponential fit and therefore also in τ. The τ values for case 9 appear, when compared to those in the default case (case 1), to be biased towards lower values for 18 of the 20 fuel assemblies. For ten fuel assemblies, the τ values for case 9 are in fact lower than for those of case 1, and in ten cases they are the same when the uncertainties in the fits are taken into account. This means that for 50% of the fuel assemblies, changing the fuel geometry and irradiation conditions results in a τ value which is lower when compared to the default case, with an average difference of 1.36 μs.

4.2.3 Relating effects in RAD and τ

Figure 4 plots τ versus the RAD amplitudes to visualize their interdependence. It shows τ versus the values of the RAD amplitudes at 5 μs, the data point closest in time to when the τ fit begins (at 4 μs), for all 20 fuel assemblies.

Comparing the RAD amplitudes for the two irradiation history cases (case 1 and case 2), shows that the largest impact on the RAD amplitude is found for one specific fuel assembly (fuel 16) and that minor discrepancies can be found for a small number of fuel assemblies. It can also be seen that for a large fraction of the fuel assemblies, mainly those with a relatively high RAD amplitude, the difference in RAD amplitude for the default case and the realistic case is noticeable. It can also be seen in Figure 4 that the RAD amplitudes in case 9 are considerably lower than for case 1 (the default case).

With respect to τ, Figure 4 shows that although the RAD amplitude does not change much with irradiation history, τ is seen to vary in all directions (remain the same, decrease and increase). Inspecting the irradiation histories of the fuel assemblies for which τ increases the most (fuels 2, 15, 5) or decreases the most (fuels 3, 19, 16, 1), provides no clear explanation for how τ changes. Both groups contain fuel assemblies with similar values of initial enrichment, burnup and cooling time. With respect to irradiation history and irradiation conditions, there is also no clear difference between the fuel assemblies in the two groups. Both of them contain fuel assemblies with unusually long and unusually short irradiation periods, low as well as high neutron fluxes, and fuel assemblies that have spent long periods of time outside the reactor before being reinserted. Only one of these seven fuel assemblies (fuel 19) has experienced an irradiation history similar to that in the default case. However, considering statistical uncertainties of Monte Carlo simulations, it is not surprising that the τ values fall outside the range of uncertainty from the fits in about a third of the cases. We have also made ten repeated simulations of the same case and seen that an average of the τ predictions are indeed normally distributed around the mean.

When comparing the RADs and the τ values for the default case (case 1) and the most realistic case (case 9), it is

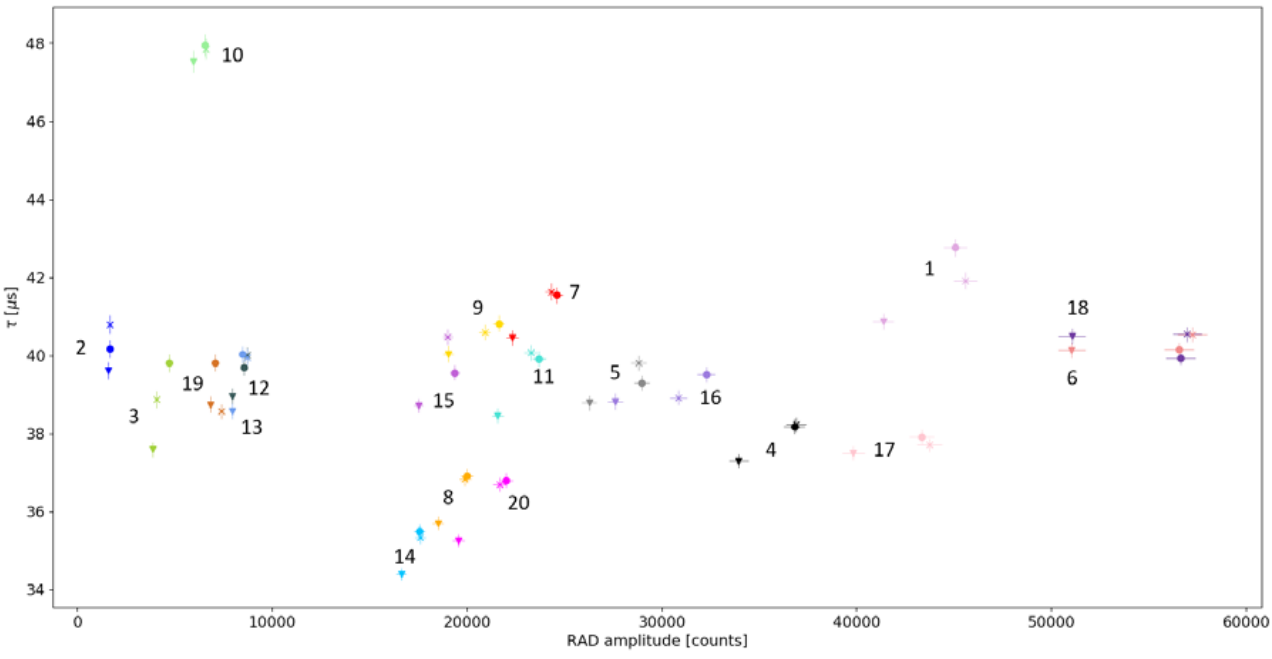

Figure 4: TValues of τ versus the RAD amplitude at 5 μs for all 20 fuel assemblies. The different markers denote the different cases: circles=case 1, x=case 2, and triangles=case 9. The different colours correspond to different fuel assemblies and the labels show the fuel ID.

seen that the RAD amplitude decreases for all fuel assemblies, and more so the higher the RAD amplitude is to start with. Among the nine fuel assemblies for which τ decreases the most (fuels 1, 3, 4, 7, 11, 13, 14, 15, 20), all but one fuel assemblies (fuel 1) have a fuel geometry consistent with that assumed in case 9. This indicates that using a more accurate fuel model leads to a lower τ value. The decrease in RAD amplitude seen for the 20 fuel assemblies in case 9 (as compared to case 1) is on average 2254 counts, and the decrease in τ is on average 0.92 μs.

For individual fuel assemblies, the largest change in τ between case 2 and case 1 (ie due to the irradiation history) is found for fuel 19, and it is 1.24 μs (or 3.12%). The largest change in τ between the case 9 and case 1 is found for fuel 3, and it is 2.22 μs (or 5.57%). The average change in τ between case 1 and 2 is 0.41 μs, and the average change in τ between case 1 and case 9 is 0.97 μs.

5. Summary and conclusion

The DDSI measurement technique offers a way to non-destructively assay the fissile material in spent nuclear fuel assemblies. It does so by quantifying the die-away time τ of the neutron population in a spent nuclear fuel assembly.

In this work, we have investigated how assumptions made in the modelling affect the resulting RADs and the τ values from the DDSI instrument. We have modelled a default irradiation history as well as the actual irradiation history, and we have made changes in the fuel geometry and the fuel irradiation conditions.

The results show that although each assumption in itself affects the RAD, most strikingly its amplitude, the τ values are less sensitive. The irradiation history, which can be both very difficult to obtain in practise and which for principal reasons should not be relied upon in safeguards evaluations, has very little or no impact on neither the RAD nor τ. However, lowering the fuel temperature, the fuel density or the pellet radius has an impact on both the RAD and τ. When making all changes simultaneously, the RAD amplitude is lowered for all fuel assemblies and τ is lowered for ten fuel assemblies (as compared to the default case). The largest change seen in τ between case 1 (the default case) and case 9 (change all) is 2.22 μs or 5.57%. The average change in τ is much lower, 0.97 μs. Based on these results, we consider the default model to be sufficiently good to estimate τ for different types of spent nuclear fuel assemblies with a 17x17 fuel geometry. However, considering that one of the objectives for developing the DDSI instrument was to estimate plutonium mass, we note that the modelling assumptions made in this work have a (varying) effect on the plutonium content of the spent nuclear fuel. The effect on the two fissile plutonium isotopes (^{239}Pu and ^{241}Pu) is larger than the resulting changes in τ. Although this may not be surprising, as τ captures the balance between fissile materials and neutron-absorbing materials and not the fissile material alone, it could be investigated in future work whether or not the simple model is suitable for estimating e.g. the plutonium mass or not.

Finally, we note that the depletion step in the model used for this work is based on a single-pin model, representative of all fuel rods in a fuel assembly. If there is information that indicates that this is not a valid assumption, such as the presence of Gd fuel rods in certain locations of the fuel assembly, a new model that does not assume that all fuel rods are identical needs to be developed to assess the impact of this on the RAD and τ.

6. Acknowledgement

The authors would like to thank the Swedish Radiation Safety Authority under contracts SSM2017-5979 and SSM2020-996, and express gratitude to our former colleague Klaes-Håkan Bejmer at Vattenfall for providing the fuel information.

7. References

[1] C. Kaplan, V. Henzl, H.O. Menlove, M.T. Swinhoe, A.P. Belian, M. Flaska, S.A.Pozzi, Utilizing simulated rossi-alpha distributions to develop new methods of characterizing spent nuclear fuel, in: PHYSOR Conference Proceedings, Kyoto, Japan, 2014

[2] S. Tobin, et al., “Experimental and Analytical Plans for the Nondestructive Assay System of the Swedish Encapsulation and Repository Facilities,” in IAEA Symposium, IAEA-CN-220-238, 2014.

[3] A. C. Trahan, Utilization of the Differential Die-Away Self-Interrogation Technique for Characterization and Verification of Spent Nuclear Fuel, Doctoral thesis, University of Michigan, 2016.

[4] A. C. Kaplan, V. Henzl, A. P. Belian, H. O. Menlove, M. T. Swinhoe, M. Flaska, S. A. Pozzi, “Determination of Spent Nuclear Fuel Assembly Multiplication with the Differential Die-Away Self-Interrogation Instrument,” Nuclear Instruments and Methods A, Vol. 757, No. 1, (2014).

[5] A. Trahan, G. E. McMath, P. Mendoza, H. Trellue, U. Backstrom, A. Sjoland, Preliminary Results from the Spent Nuclear Fuel Assembly Field Trials with the Differential Die-Away Self-Interrogation Instrument, 59th Annual Meeting of the Institute of Nuclear Materials Management (INMM 2018)

[6] A. Trahan et al., Results of the Swedish spent fuel measurement field trials with the Differential Die-Away Self-Interrogation Instrument, Nuclear Instruments and Methods in Physics Research Section A:

Accelerators, Spectrometers, Detectors and Associated Equipment, Volume 955, 1 March 2020, 163329, https://doi.org/10.1016/j.nima.2019.163329

[7] Nuclear Energy Agency, Spent Nuclear Fuel Assay Data for Isotopic Validation, State-of-the-art Report, NEA/NSC/WPNCS/DOC(2011), 5 June 2011

[8] G. E. Bosler, J. R. Phillips, W. B. Wilson, R. J. LaBauve and T. R. England, Production of Actinide Isotopes in Simulated PWR Fuel and Their Influence on Inherent Neutron Emission, LA--9343, DE82 021849, July 1982

[9] G. Radulescu I. C. Gauld G. Ilas, SCALE 5.1 Predictions of PWR Spent Nuclear Fuel Isotopic Compositions, ORNL/TM-2010/44, March 2010

[10] W. (B.J.) Marshall, B. J. Ade, S. Bowman, J. S. Martinez-Gonzalez , Axial Moderator Density Distributions, Control Blade Usage, and Axial Burnup Distributions for Extended BWR Burnup Credit, NUREG/CR-7224 ORNL/TM-2015/544

[11] Svensk Kärnbränslehantering AB, Spent nuclear fuel for disposal in the KBS-3 repository, Technical Report TR-10-13, https://skb.se/upload/publications/pdf/tr-10-13.pdf

[12] J. Leppänen et al., "The Serpent Monte Carlo code: Status, development and applications in 2013," Annals of Nuclear Energy, 82, pp. 142-150 (2015).

[13] MCNP6 user's manual version 1.0 edited by D. Pelowitz, LA-CP-13-00634 2013

[14] T. Goorley: Using MCNP5 for medical physics applications, LA-UR-05-2755

[15] Oak Ridge National Laboratory, Scale: A Comprehensive Modeling and Simulation Suite for Nuclear Safety Analysis and Design, ORNL/TM-2005/39 Version 6.1, June 2011

[16] L. Caldeira Balkeståhl, Zs. Elter, S. Grape, Parametrization of the differential die-away self-interrogation early die-away time for PWR spent fuel assemblies, ESARDA BULLETIN, No. 58, June 2019

Uncertainty quantification as presented in training courses for safeguards inspectors

Elisa Bonner[1], Thomas Burr[3], Thomas Krieger[4], Klaus Martin[1], Claude Norman[1], Peter Santi[2]

[1]IAEA/SGIM/Nuclear Fuel Cycle Information Analysis;
[2]IAEA/SGCP/Safeguards Training
[3]Los Alamos National Laboratory;
[4]Forschungszentrum Jülich GmbH

Summary

For safeguards evaluators to provide credible assurance that States are honoring their safeguards obligations, quantitative conclusions regarding non-diversion from States' nuclear material flows and inventories are needed. The statistical analysis used to reach these conclusions requires that each measurement method undergo uncertainty quantification (UQ). Training for safeguards inspectors includes measurement error models that must account for variation within and between groups, where a group is defined to be a calibration or inspection period. A typical model for multiplicative errors for the inspector (I) *is* $I_{jk} = \mu_{jk}(1 + S_{Ij} + R_{Ijk})$ *with* $S_{Ij} \sim N(0, \delta_{SI}^2)$ *and* $R_{Iij} \sim N(0, \delta_{RI}^2)$ *where* I_{jk} *is the inspector's measured value of item* k *in group* j, μ_{jk} *is the true value of item* k *from group* j, R_{Ijk} *is a random error of item* k *from group* j, S_{Ij} *is a short-term systematic error in group* j. *The notation* $S_{Ij} \sim N(0, \delta_{SI}^2)$ *means that values of* S_{Ij} *are assumed to have a normal distribution with mean* (0) *and variance* δ_{SI}^2. *This paper describes three main inspector UQ-related training topics. Topic one is analysis of variance to estimate the relative standard deviations (RSDs)* δ_{SI}^2 *and* δ_{RI} *(and the corresponding RSDs for the operator). Topic two is an example involving the uranium neutron coincidence collar (UNCL) to illustrate the need for inspector UQ training to include an understanding of the most important factors that impact the RSDs, which in turn also affect the rejection limits for comparing operator declarations to inspector measurements. For the UNCL method, it is important for inspectors to understand the fuel assembly design and IAEA neutron coincidence counting (INCC) software input requirements. Incorrect INCC declaration input is thought to be among the largest contributors to the observed UNCL uncertainty (as quantified by the RSDs). In response to needs arising from IAEA measurement evaluations, improved UQ methods have recently been developed, and the new methods described in topics one and two are beginning to be presented in training for safeguards inspectors, as will be described. Topic three is to use the estimated RSDs to evaluate material balances and to plan inspector sample sizes based on estimated material loss detection probabilities.*

Keywords: Nuclear Safeguards, Statistical Methodologies, Approximate Bayesian Computation (ABC), Data Analytics, Non-Destructive Assay (NDA)

1. Introduction

Inspector measurements are a cornerstone of IAEA safeguards, so it is important for inspectors to have a basic understanding of UQ. For example, suppose the operator's declared nuclear material (NM) mass for an item is 1.1 kg, and the inspector's measurement is 0.95 kg. Whether the 0.15 kg difference is a cause for concern depends on the uncertainty in the 1.1 kg and the 0.95 kg values. Effective UQ is critical in order to make quantitative safeguards conclusions based on inspector verification measurements.

This paper describes three UQ topics presented in training courses for safeguards inspectors. For background, the Guide to the Expression of Uncertainty in Measurement (GUM) provides guidance on the expression of measurement uncertainty [1]. UQ can be approached by comparing multiple measurements of the same item (top-down) or by assessing each step in the measurement procedure (bottom-up). The GUM briefly addresses top-down methods, but is most known for a bottom-up option using the measurement equation

$$Y = f(X_1, X_2, \ldots, X_p) \quad (1)$$

where Y is the estimate of the measurand, and $X_1, X_2, \ldots, X_p$ are inputs. The inputs can be measurement or adjustment factors, and can be regarded as having a joint probability distribution that can include covariances among the inputs. For example, some of the inputs can be estimated calibration parameters, others can be measured values, and others can be adjustment factors. The GUM applies uncertainty propagation to $X_1, X_2, \ldots, X_p$ and the function $f(\,)$ in Eq. (1) to estimate the uncertainty in the assay, defined as the standard deviation of Y. Informally, standard deviation quantifies measurement variability, defined as the square root of the variance, which is the average squared distance of the Y value from the mean of the

Y values. Safeguards metrology routinely partitions total variability into variability around the mean and variability around the true value into "random" and "systematic" components, respectively, and the GUM [1] combines random and systematic into a total variability as explained in inspector UQ training.

For verification purposes, paired (Operator (O), Inspector (I)) data are collected from inspections performed during site visits that occur once or a few times per year, and then for top-down UQ, several years of paired (O, I) data are analysed. An effective measurement error model must account for variation within and between groups, where a group is an inspection period. A typical top-down multiplicative error model used for the (I) (and similarly for O) is

$$I_{jk} = \mu_{jk}(1 + S_{Ij} + R_{Ijk}) \ , k = 1, \dots, n, j = 1, \dots, g, \quad (2)$$

where I_{jk} is the inspector's measured value of item k in group j, μ_{jk} is the true but unknown value of item k from group j, $R_{Ijk} \sim IIDN(0, \delta_{RI}^2)$ (IIDN is independently and identically distributed normal) is a random error of item k from group j, $S_{Ij} \sim IIDN(0, \delta_{SI}^2)$ is a short-term systematic error in group j [1-10]. Short-term systematic error remains constant for a short term when measurement conditions or settings, i.e., parameters of calibration curves, normalizations, and/or subtracted background etc. are not altered, but vary in a random way over the long term [2]. Long-term systematic error is sometimes also referred to as bias. In applications, the normality assumption is not usually critical in the error model depicted in Eq. (2); the important aspect of the modelling assumptions are that there are systematic and random components with RSDs δ_{SI} and δ_{RI}, respectively, that both bottom-up and top-down UQ aim to estimate [1-10]. Often, Top-down estimates $\hat{\delta}_{SI}$ and $\hat{\delta}_{RI}$ are larger than bottom-up estimates, and the gap is called "dark uncertainty" [2-8]. Note that in Eq. (2) the same number of measurements n per group is assumed for simplicity of presentation.

Figure 1 plots $n = 10$ simulated values of $(o - i)/o$ for each of $g = 5$ groups with parameters $\delta_{SO} = 0.001, \delta_{RO} = 0.001, \delta_{SI} = 0.027, \delta_{RI} = 0.027$ and $\delta_{\mu} = 0.003$. The within-group means are indicated by the horizontal within-group lines.

The need for quality control within UQ approaches provides motivation for excellent ongoing communication and collaboration among inspectors to reduce and better understand error variance components, which in turn provides partial validation that safeguards is properly implemented. Periodically, bottom-up and top-down estimates $\hat{\delta}_S$ and $\hat{\delta}_R$ should be compared (here the subscript I is dropped because the discussion also applies to operator measurements). It is not surprising that bottom-up UQ tends to lead to smaller estimates of $\hat{\delta}_S$ and $\hat{\delta}_R$ than does top-down, because small sources of variation are often neglected in bottom-up UQ. However, until the gap between top-down and bottom-up estimates is acceptably small, the fielded assay system is not fully understood. For example, Fig. 2 plots the estimated probability density of the bottom-up and top-down estimates $\hat{\delta}_T$ of the total RSD $\delta_T = \sqrt{\delta_S^2 + \delta_R^2}$ for the Uranium Neutron Coincidence Collar (UNCL) [5,11] measurement using approximate Bayesian Computation (ABC) [12-16]. The UNCL is the bottom-up UQ example in Section 3 that uses thermal neutrons to measure the ^{235}U content in fresh fuel assemblies. These measurements exhibit a gap between the bottom-up and top-down estimates of δ_T [5,11]. The vertical lines are the best point estimates, lying in the middle of the distribution, and the width of the distribution

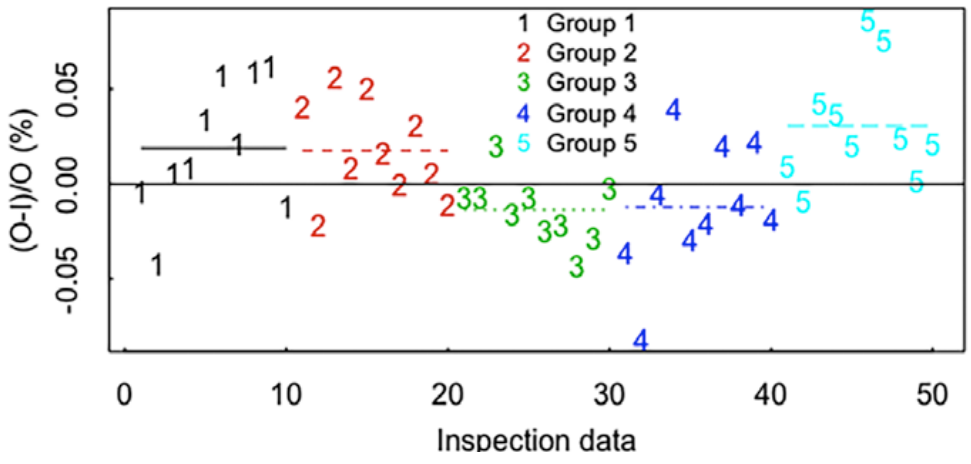

Figure 1: Ten simulated values of $(o - i)/o$ for each of g=5 groups.

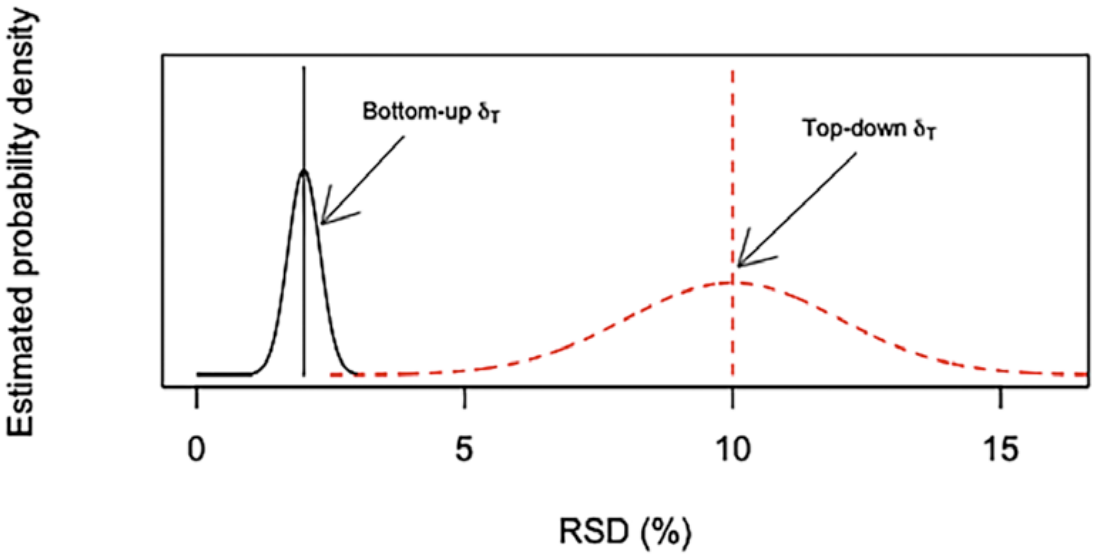

Figure 2: Uranium Neutron Collar example with a gap between top-down and bottom-up RSD estimates.

characterizes how well δ_T is estimated. Figure 2 indicates that the bottom-up estimate of δ_T is optimistically low compared to the top-down estimate because the two distributions have very little overlap (Section 3). Data sets having repeated measurements of the same item use top-down UQ to separately estimate variance arising from pure random effects from variance arising from item-specific effects (Section 2).

Inspectors need to understand both bottom-up and top-down UQ. Bottom-up UQ provides guidance regarding best measurement practice and protocol to understand and possibly reduce measurement uncertainty. This paper describes three main inspector UQ-related training topics. Topic one in Section 2 is analysis of variance to provide top-down estimate of the relative standard deviations (RSDs) δ_{SI} and δ_{RI} and (and the corresponding RSDs for the operator). Topic two in Section 3 is a bottom-up UQ example involving the UNCL to illustrate the need for inspector UQ training to include an understanding of the most important factors that impact the RSDs, which in turn also affect the rejection limits for comparing operator declarations to inspector measurements (Section 4.2). For the UNCL method, it is important for inspectors to understand the fuel assembly design and INCC (neutron coincidence counting software) input requirements. Incorrect INCC declaration input is thought to be among the largest contributors to the observed UNCL uncertainty (as quantified by the RSDs). Topic three in Section 4 is to use the estimated RSDs δ_S and δ_R for both the operator and inspector to evaluate material balances (MB) and to plan inspector sample sizes based on estimated material loss detection probabilities. Partitioning into random and systematic components has important implications for sample planning and MB evaluation.

2. Uncertainty Quantification (UQ) – an empirical (top-down) approach (ANOVA)

To be conservative (with regard to reducing false alarms), the IAEA's data evaluation group (nuclear fuel cycle information analysis) uses top-down-based UQ (rather than bottom-up UQ) to estimate the inspector's random and short-term systematic uncertainty components (RSDs) [2]. As explained in Section 4, the estimated RSDs are used in calculations to achieve target detection probabilities (DP) [17,18], and to perform error variance propagation in order to estimate the standard deviation of each material balance (MB) [1-12,19,20]. The published international target values (ITVs) for δ_R and δ_S are updated approximately every 10 years and the next updates are scheduled to be issued in early 2022 [2].

The basis of the top-down approach to UQ is an analysis of variance (ANOVA) with random effects based on operator-inspector relative differences. Such paired data arise when the operator and the inspector measure the same object once without measurement repetition. One goal is to estimate $\delta_R^2 = \delta_{RO}^2 + \delta_{RI}^2$ and $\delta_S^2 = \delta_{SO}^2 + \delta_{SI}^2$ for the relative differences. Another goal is to partition the total variance into four components, $\delta_{SO}^2, \delta_{RO}^2, \delta_{SI}^2$ and δ_{RI}^2.

Figure 1 illustrated an example in which paired operator (0) measurements (typically using Destructive Assay (DA)) and inspector (I) measurements (typically using Non-Destructive Assay (NDA)) from five previous inspection periods are used to estimate δ_R and δ_S for both the operator and inspector, and then to set alarm thresholds to detect possible data falsification in period six. The within-period variance is regarded as the random error variance, which includes the effects of item-specific bias. The between-period variance includes both random error variance (divided

by the number of measurements per period) [1-12] and short-term systematic effects such as instrument recalibration. Therefore, in Eq. (2), the errors R_{Ojk} and R_{Ijk} include "item-specific" bias because in verification data used for metrology, the measured items are not true replicates, that is, the relevant physical properties of the item being measured may vary randomly among items.

2.1 Estimating the variances of the relative differences $D = (o - i)/o$

For a balanced dataset with n paired differences in each of g groups $(N = ng)$ and under the assumption that no data are falsified by the operator, Eq. (2) yields for the relative differences $D_{jk}, j = 1, \dots, g, k = 1, \dots, n$,

$$D_{jk} = \frac{O_{jk} - I_{jk}}{O_{jk}} \approx \frac{O_{jk} - I_{jk}}{\mathbb{E}(O_{jk})} = S_j + R_j\,, \qquad (3)$$

where $S_j = S_{Oj} + S_{Ij}$ and $R_j = R_{Oj} + R_{Ij}$ and $\mathbb{E}(O_{jk})$ denotes the expected value of O_{jk}. Therefore, for the $n = 10$ sets of $g = 5$ groups values of $d = (o - i)/o$ as in Figure 1, standard ANOVA [21] can be applied to estimate δ_S^2 and δ_R^2. The validity of the approximation in Eq. (3) is shown in [10].

From standard ANOVA, it is well known that unbiased estimators of δ_R^2 and δ_S^2 are given by

$$\hat{\delta}_R^2 = \frac{1}{ng - g}\sum_{j=1}^{g}\sum_{k=1}^{n}(d_{jk} - \bar{\bar{d}})^2 \quad \text{and} \quad \hat{\delta}_S^2 = \frac{\sum_{j=1}^{g}(\bar{d}_j - \bar{\bar{d}})^2}{(g-1)} - \frac{\hat{\delta}_R^2}{n}, \qquad (4)$$

where $\bar{\bar{d}} = \sum_{j=1}^{g}\sum_{k=1}^{n} d_{jk}/(ng)$ is the overall unweighted average and $\bar{d}_j = \sum_{k=1}^{n} d_{jk}/n$ is the average measurement for item k. These formulas assume the same sample size (number of measurements is n) per group for simplicity of presentation here. Because the actual sample sizes n_i often vary across groups, weighted averages are actually used [21-24].

In standard one-way random effects ANOVA [10], if the relative error variances are not constant (which would mean that that the assumptions $R_{jk} \sim IIDN(0, \delta_R^2)$ and/or $S_j \sim IIDN(0, \delta_S^2)$ regarding the error variances in Eq. (2) are not correct), then it can be shown that $\sum_{j=1}^{g}\sum_{k=1}^{n}(d_{jk} - \bar{d}_j)^2/(n(g-1))$ is an unbiased estimate of the average relative variance $\sum_{j=1}^{g}\delta_{Rj}^2/g$ and $\hat{\delta}_S^2 = \sum_{j=1}^{g}(\bar{d}_j - \bar{\bar{d}})^2/(g-1) - \hat{\delta}_R^2/n$ is an unbiased estimate of the average relative variance $\sum_{j=1}^{g}\delta_{Sj}^2/g$ [21,22]. Note from Eq. (4) that it is possible that the estimate $\hat{\delta}_S^2 < 0$, in which case $\hat{\delta}_S^2$ is set to 0 (in a non-Bayesian framework, as presented here).

This same standard random-effects ANOVA just explained can also be applied to data sets for which there are repeated measurements on the same item in another common top-down approach to UQ [9]. In this case, the groups are not inspection periods, but are items, and the between-group variance is the variance of item-specific biases [9].

Typically, it is assumed that short-term systematic errors change across inspection periods from the groups used in the ANOVA. However, it may appear that the short-term systematic errors change at other times and thus the groups are unknown. The impact of unknown groups on the estimates of the variances of random and systematic errors in ANOVA is discussed in [24].

2.2 Grubbs estimator for paired (operator, inspector) data to estimate $\delta_{SO}, \delta_{RO}, \delta_{SI}$ and δ_{RI}

One-way ANOVA based on paired data allows us to estimate the measurement error variances of operators and inspectors. ANOVA requires the data to fall in groups, so that within-group and between-groups variances can be defined and estimated. In this example, the groups are the inspection periods. The basis of a Grubbs-based estimator [3-6,23,24] as applied to data assumed to be generated according to Eq. (2) in order to estimate $\delta_\mu^2, \delta_{SI}^2$ and δ_{RI}^2 ($\delta_{SO}^2, \delta_{RO}^2$ can be estimated accordingly) is that the covariance between operator and inspector measurements equals σ_μ^2, so can be estimated using (with $\bar{O}_j$ used to estimate the average true value μ)

$$\hat{\delta}_\mu^2 = \frac{1}{(n-1)g}\sum_{j=1}^{g}\frac{1}{\bar{O}_j{}^2}\sum_{k=1}^{n}(O_{jk} - \bar{O}_j)(I_{jk} - \bar{I}_j)\,. \qquad (5)$$

Note that the variance of the true values is estimated using the covariance between the operator and inspector measurements, and this provides a "teaching moment" in that the assumed error model in Eq. (2) implies zero covariance between operator and inspector measurements unless there is variability in the true values.

The measurement error model $I_{jk} = \mu_{jk}(1 + S_{Ij} + R_{Ijk})$ in Eq. (2) is the random variable μ_{jk} multiplied by the composite random variable $(1 + S_{Ij} + R_{Ijk})$. Therefore, a class exercise is to show that the variance of I_{jk} conditional on the value of S_{Ij} is given by the random variable $\mu^2(\delta_\mu^2\delta_{RI}^2 + \delta_\mu^2(1 + S_{Ij})^2 + \delta_{RI}^2)$, which has an expected value over inspection periods of

$\mu^2(\delta_\mu^2\delta_{RI}^2 + \delta_\mu^2(1+\delta_{SI}^2)+\delta_{RI}^2)$. Therefore, the expected between-group and within-group sums of squares involve both δ_{SI}^2 and δ_{RI}^2. Provided that δ_{SI}, δ_{RI}, and δ_μ are each less than approximately 0.15 (typically true for most safeguards measurements), the approximation $\mu^2(\delta_\mu^2\delta_{RI}^2 + \delta_\mu^2(1+\delta_{SI}^2)+\delta_{RI}^2) \approx \mu^2(\delta_\mu^2+\delta_{RI}^2)$ is adequate and will be used here. Then, the sample covariance between operator and inspector measurements can be subtracted from the sample variance of the inspector measurements to estimate δ_{RI}^2 (and similarly for estimating δ_{RO}^2. That is, within a single inspection period (group j), a reasonable estimate of δ_{RI}^2 is

$$\hat{\delta}_{RI,j}^2 = \frac{1}{\bar{O}_j^2(n-1)}\left(\sum_{k=1}^{n}(I_{jk}-\bar{I}_j)^2 - \sum_{k=1}^{n}(O_{jk}-\bar{O}_j)(I_{jk}-\bar{I}_j)\right).$$

The final estimate of the inspector's random error relative variance is then the average over groups,

$$\hat{\delta}_{RI}^2 = \frac{1}{g}\sum_{j=1}^{g}\hat{\delta}_{RI,j}^2. \quad (6)$$

The variance $\mathbb{V}(I_{jk})$ of I_{jk} is given by $\mathbb{V}(I_{jk}) = \mu^2(\delta_\mu^2(1+\delta_{SI}^2+\delta_{RI}^2)+\delta_{SI}^2+\delta_{RI}^2) \approx \mu^2(\delta_\mu^2+\delta_{RI}^2+\delta_{SI}^2)$, so the variance of the between group means (equal sample size with n observations per group) is $\sigma_{\text{Between},I}^2 \approx \mu^2(\delta_\mu^2/n + \delta_{RI}^2/n + \delta_{SI}^2)$, which yields by Eqs. (5) and (6)

$$\hat{\delta}_{SI}^2 = \frac{1}{\bar{O}^2}\frac{\sum_{j=1}^{g}(\bar{I}_j-\bar{I})^2}{g-1} - \frac{\hat{\delta}_\mu^2}{n} - \frac{\hat{\delta}_{RI}^2}{n}. \quad (7)$$

There is no guarantee that $\hat{\delta}_\mu^2, \hat{\delta}_{SI}^2$, or $\hat{\delta}_{RI}^2$ are non-negative, but the corresponding true quantities are non-negative $\delta_\mu^2 \geq 0, \delta_{SI}^2 \geq 0$ and $\delta_{RI}^2 \geq 0$, so constrained versions of the Grubbs' and ANOVA-based estimators are available; see [12-16] for Bayesian-type constraints and [23-24] for non-Bayesian constraints.

The original Grubbs' estimate [25] is for additive error models. The ABC framework [12-16] makes Grubbs' type estimation straightforward (constrained according to the prior distribution for each parameter) for either additive or multiplicative models. Using Eqs. (5), (6) and (7), the five summary statistics used in this application of ABC for n *(O,I)* pairs in each of g groups are $\hat{\delta}_\mu^2, \hat{\delta}_{RI}^2, \hat{\delta}_{RO}^2, \hat{\delta}_{SI}^2, \hat{\delta}_{SO}^2$.

As an example, Figure 3 plots the ABC-based posterior probability density function (pdf) for δ_{RI} using the ABC threshold $\varepsilon = 0.001, 0.02, 0.1$. The ABC-based [12-16] estimate of the pdf for δ_{RI} is computed as follows. First, ABC simulates synthetic data from Eq. (2) using many (105 in this example) candidate RSD values from a wide prior pdf, Second, ABC accepts all those candidate RSD values into the posterior pdf for which the corresponding five summary statistics above are close (within some small tolerance denoted ε) to those in the test data computed in this case as simulated data from Eq. (2). Regarding whether ABC is well calibrated, for $\varepsilon = 0.005, 0.01$ or 0.1, the predicted root mean squared error (RMSE) is 0.027 and the observed average standard deviation is 0.028, and the actual posterior probability coverages are 0.99, 0.96, and 0.91. The nominal interval coverages are 0.99, 0.95, and 0.90, so ABC is well calibrated. However, using $\varepsilon = 0.001$ leads in this example to a few unreasonably large accepted trial values of δ_{RI}, which shifts the mean upward from the true value of 0.027. Fortunately, the calibration check comparing nominal to actual coverages detects that $\varepsilon = 0.001$ leads to poor calibration, and so it is to be avoided. References [5,12,14-16] describe calibration checks for ABC in safeguards measurement applications, anticipating that the user will experiment to find an effective value of ε such that ABC is well calibrated. All analyses presented here are done in R [24].

Inspector training currently presents the original Grubbs' estimate [23] above in Eqs. (5)-(7) in a non-Bayesian framework. This paper emphasizes the need for all Safeguards professionals, including inspectors, to have a basic understanding of bottom-up and top-down UQ. The fact that dark uncertainty typically exists is most easily illustrated using a plot such as Fig. 2, where uncertainty in the bottom-up and top-down RSD estimates is also provided so that apparent gaps can be assessed for statistical significance. This section used simulated data from Eq. (2) to illustrate ABC as an effective option to provide a pdf for the top-down estimate of δ_{RI}. A Bayesian framework [3,4,54,7,8,12] naturally provides the uncertainty in the RSD estimates and is beginning to be presented as an option in training courses. Note that the non-negativity constraint on true RSDs forces truncation of negative estimates whether a Bayesian or non-Bayesian approach is used. Note also that while top-down UQ might lead to more realistic RSD estimates, there can be large uncertainty (wide posterior pdf) in top-down RSD estimates. Also, bottom-up RSD estimates are continually being improved, which leads to better understanding of the measurement process. It should be emphasized that the IAEA has unique opportunities to assess the quality of top-down and bottom-up UQ because inspector measurements are typically made using NDA while operator measurements are typically made using DA. As a consequence, dark uncertainty such as item-specific bias that is different for NDA than for DA of the same item is exposed when comparing operator declarations to inspector verification measurements of the same items. Therefore, topics one and two describe recent improvements to UQ methods, and the new methods are beginning to be presented in inspector training, which is

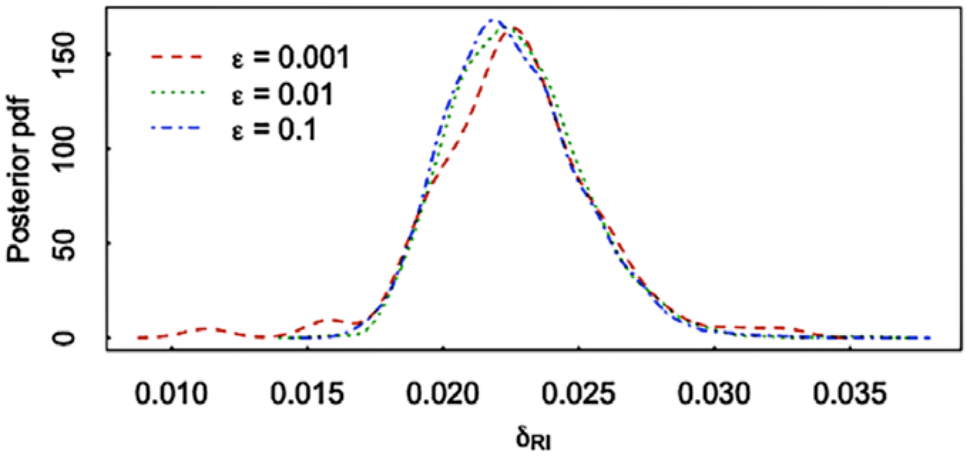

Figure 3: The posterior pdf for Grubbs'-type estimation of δ_{RI}. The posterior mean is 0.023 and the true value of δ_{RI} is 0.027 as was used to simulate the data in Fig. 1.

helping to overcome communication challenges involving the expression and quantification of uncertainty.

One of the main data sources used to estimate the IAEA's ITVs, is paired operator-inspector data such as that in Fig. 1 and analysed here without repeated measurements of items [2-5,21]. Recall that item-specific bias is often evident from applying Grubbs' estimation to paired data such as that used to generate the $d = (o - i)/o$ values in Fig. 1. The evidence for item-specific bias is that the estimated δ_{RI} is larger than predicted from bottom-up UQ (on the basis of non-overlapping pdfs such as in Fig. 2, but for δ_{RI}). As a result of such evidence, bottom-up UQ has only recently begun to consider sources of item-specific bias, such as departures from calibration items [2-5] or modelling assumptions [5,11,12]. Item-specific bias is random across items, so the effective random error RSD is

$$\delta_{R_{\text{effective}}} = \sqrt{\delta^2_{R_{repeat}} + \delta^2_{item-specific\ bias}} \quad .$$

The reported ITV values include item-specific bias effects if they are based on such paired data, and so δ_{RI} is actually $\delta_{R_{\text{effective}}}$.

3. A bottom-up UQ example: Uranium Neutron Coincidence Collar (UNCL)

The UNCL uses an active neutron source to induce fission in ^{235}U in fresh fuel assemblies [3,5,8]. Neutrons from fission are emitted in short bursts of time, and so exhibit non-Poisson bursts in detected count rates. Neutron coincidence counting is used to measure the "doubles" neutron coincidence rate Y, which can be used to estimate the linear density of ^{235}U in a fuel assembly (grams ^{235}U per cm) using calibration parameters a_1 and a_2. The rate Y is the observed rate of observing two neutrons in very short time gates, each of approximately 10-6 sec, and is attributable to fission events. The equation commonly used to convert the measured doubles rate Y to an estimate of X (grams ^{235}U per cm) is

$$X = \frac{kY}{a_1 - a_2 kY}, \tag{8}$$

where a_1 and a_2 are to be estimated, and $k = k_1k_2k_3k_4k_5$ is a product of correction factors that adjust Y to item-, detector-, and source-specific conditions in the calibration [5,11]. Therefore, Eq. (8) is a special case of GUM's Eq. (1), but with X and Y reversed here compared to that used by the GUM in Eq. (1) because conventionally in calibration, X is the measurand and Y is the measurement data, such as the neutron count rate. In Eq. (8), the net doubles rate Y, the two calibration parameters a_1 and a_2, and the correction factors in $k = k_1k_2k_3k_4k_5$ are among the X 's in Eq. (1).

Reference [8] showed that calibration is most effective (leading to smallest RMSE in the estimate of X, denoted $\hat{X}$) if there is no adjustment for errors in the predictor kY, and that errors $k_1k_2k_3k_4k_5$ should be included in synthetic calibration data. Note that by working with $1/X$ and $1/Y$, one can convert Eq. (8) to one that is linear in the transformed predictor $1/Y$.

Several recent UNCL measurements have exhibited a gap between the bottom-up and top-down total RSD estimate, $\delta_T = \sqrt{\delta_S^2 + \delta_R^2}$ [3,5,8]. Recall that Figure 2 is an example of the estimated pdf for δ_T using approximate Bayesian computation (ABC, see Section 2) for both the top-down

and bottom-up RSD estimates [3-5,7]. The bottom-up estimate shown in Fig. 2 was presented in [3,8] using ABC applied to simulated data from Eq. (8), where X is the ^{235}U content, and the item-specific adjustment factor $k = k_1k_2k_3k_4k_5$ is a product of correction factors that adjust the measured neutron doubles rate Y to item-, detector-, and source-specific conditions in the calibration. The correction factors are currently being examined more closely using modelling [3,5,8,11] and [5] indicates the need for better inspector training on measurement protocol, including the importance for inspectors to understand the fuel assembly design and the INCC software input because these requirements impact some of the factors in $k = k_1k_2k_3k_4k_5$. Incorrect INCC declaration input is thought to [5] be among the largest contributors to the observed UNCL uncertainty (as quantified by the RSDs), and consistent source positioning is also a non-negligible contributor to item-specific effects on $k = k_1k_2k_3k_4k_5$ [3,5,8,11].

Another potential contributor to the observed UNCL uncertainty (and more generally the uncertainty on any NDA measurement) is the purely random uncertainty associated with the measurement. A large factor that drives random error variance is measurement time. Given that the inspector determines UNCL measurement duration, an important aspect in training inspectors on UQ is to promote an understanding of how uncertainty quoted by INCC software (or any analysis software used for NDA techniques) relates to the total RSD δ_T that is calculated based on a top-down analysis using operator-inspector paired data. In the case of the UNCL, the uncertainties quoted by INCC are based on a bottom-up approach that takes into account estimated uncertainties in the calibration constants, uncertainties that are known for the various correction factors, as well as the random uncertainties associated with the doubles coincidence counting rate. To ensure that the quality of the current measurement is consistent with the historical δ_T that was determined for this particular set of UNCL measurements, the inspector is encouraged to compare the quoted uncertainty from the INCC code to the top-down historical δ_T for this measurement. If the bottom-up uncertainty estimation produced by the analysis software is similar in size to, or smaller than, the historical RSD, the quality of the current measurement is presumed to be consistent with the historical data used in modelling the top-down historical RSD for this measurement technique. On the other hand, if the bottom-up uncertainty estimation is significantly larger than the top-down historical RSD, it is presumed that the random uncertainty of the current measurement is unacceptably high which requires an increase in the measurement time to reduce the bottom-up uncertainty estimation. Training inspectors how to perform a quality control check on each measurement using such a simple guideline helps reduce the chances that the historical δ_T will become large over time due to the inclusion of poor-quality data.

4. Two main applications for RSD estimates of $\delta_{SI}, \delta_{RI}, \delta_{SO}$ and δ_{RO}

Within safeguards, there are two main applications for the estimated values of $\delta_{SI}, \delta_{RI}, \delta_{SO}$ and δ_{RO}. The first application is material balance evaluation where $\delta_{SI}, \delta_{RI}, \delta_{SO}$ and δ_{RO} are used in variance propagation to estimate the standard deviation of the material balance. The second application is designing inspection plans to have a desired detection probability.

4.1 Material balance evaluation

The MB sequence is fundamental to material accounting [19,20]. For example, in a sequence of 12 monthly MBs over a one-year analysis period, a key task is to classify the period as having no loss or having non-zero loss. Nuclear material accountancy (NMA) at a facility that processes nuclear material requires measuring facility input transfers T_{in}, output transfers T_{out}, and inventory I to compute a material balance defined for balance period j as $MB_j = (I_{j-1} + T_{in,j} - T_{out,j}) - I_j$, which equals "book inventory" minus "physical inventory," where $(I_{j-1} + T_{in,j} - T_{out,j})$ is the book inventory.

Typically, many measurements are combined to estimate the terms T_{in}, T_{out}, I_{begin} and I_{end} in the MB; therefore, the central limit effect and years of experience suggests that MBs will be approximately normally distributed with mean equal to the true NM loss μ and standard deviation σ_{MB}, which is expressed as $MB \sim N(\mu, \sigma_{\text{MB}})$, where X denotes the MB [19,20]. Therefore, a sequence of n MBs are assumed to have approximately a multivariate normal distribution, $MB_1, MB_2, \ldots, MB_n \sim \text{MVN}(\mu, \Sigma)$, where the $n \times n$ covariance matrix is

$$\Sigma = \begin{pmatrix} \sigma_{11}^2 & \sigma_{12}^2 & \cdots & \sigma_{1n}^2 \\ \sigma_{21}^2 & \sigma_{22}^2 & \cdots & \sigma_{2n}^2 \\ \vdots & \vdots & \ddots & \vdots \\ \sigma_{n1}^2 & \sigma_{n2}^2 & \cdots & \sigma_{nn}^2 \end{pmatrix},$$

with variances on the diagonal and covariances on the off-diagonals.

One common goal is for the loss DP to be at least 0.95 if $\mu \geq 1$ SQ (significant quantity, which is 8 kg Pu or Uranium-233 or 25 kg of uranium-235 in HEU), which is accomplished if $\sigma_{MB} \leq SQ/3.61$ (Figure 4). The factor 3.61=1.96+1.65 where the alarm rule $|MB| < 1.96\,\sigma_{MB}$ is used in two-sided testing (testing for either loss or gain of NM) for approximately a 0.05 false alarm probability. Therefore, if a loss of $1.96\,\sigma_{MB}$ occurs, then the DP is only 0.50. But if a loss of (1.96+1.65) σ_{MB}, then the DP is 0.95

(Figure 4). If $\sigma_{MB} > SQ/3.61$, this can be mitigated either by reducing the typical magnitude of measurement errors to achieve $\sigma_{MB} > SQ/3.61$ (if feasible), and/or by closing the balances more frequently so there is less nuclear material transferred per balance period, which reduces σ_{MB} .

In order to address large throughput facilities Near Real Time Accountancy (NRTA) was introduced in the mid 1990's. NRTA is frequent material balance closure, such as one per 10 to 30 days instead of only annually in conjunction with the annual physical inventory taking at the time of plant shutdown. As explained in inspector UQ training, large throughput facilities cannot typically achieve DP ≥ 0.95 for a loss of $\mu \geq 1$ SQ over a long time period such as one year. And, NRTA is not a panacea, because, as shown in [20], if a facility slowly diverts NM over, for example, one year, then a single yearly statistical test based on the annual cumulative material balance (known as CUMUF), $\sum_{i=1}^{n} X_i$ has larger DP than frequent statistical testing during the year. Of course, if the facility diverts NM abruptly, such as over one day, then NRTA will have much larger DP than a single annual statistical test. It is therefore generally accepted that NRTA is a valuable safeguards measure, despite leading to slightly smaller DP than in using annual MBs for protracted loss detection. Most safeguards studies consider a yearly analysis period, corresponding to the time of the annual scheduled physical inventory. But, if the facility diverts material, for example, $SQ/2$ in year one and $SQ/2$ in year two, then the DP is lowered compared to diverting one SQ in the analysis year. See Figure 5; however, the required diversion time would be longer than one calendar year, in this figure, lasting from period 7 to 18.

Grubbs' estimation [23] (or ABC based on Grubbs') produces the parameter estimates $\hat{\delta}_{SO}^2$, $\hat{\delta}_{RO}^2$, $\hat{\delta}_{SI}^2$ and $\hat{\delta}_{RI}^2$, which, as just explained, are needed for MB evaluation. Note that verifications rely on relative difference $(o-i)/o$ and δ_R^2 and δ_S^2 as given by Eq. (4) are the only parameters required for verification checks as described in Section 4.2. However, because MB evaluation is conducted separately for the operator, the estimates $\hat{\delta}_{SO}^2$ and $\hat{\delta}_{RO}^2$ are required.

The law of error propagation is described in the GUM [1] in the context of bottom-up UQ. The original law of error propagation by Gauss was designed for random errors only. Gauss realized after his publication that this was not always adequate. Therefore, the law of error propagation was modified to allow for measurement values to be correlated. The mode of error propagation for correlated values is a minor extension from purely independent (random) values. Specifically, formula (E.3) of JCGM 100:2008 [1] illustrates error propagation applied to the measurand equation $Y = f(X_1, X_2, \ldots, X_N)$ using the approximate result (based on a linear Taylor series approximation)

$$\sigma_Y^2 \approx \sum_{i=1}^{N} \left(\frac{\partial f}{\partial x_i}\right)^2 \sigma_i^2 + 2 \sum_{i=1}^{N-1} \sum_{j=i+1}^{N} \frac{\partial f}{\partial x_i} \frac{\partial f}{\partial x_j} \sigma_i \sigma_j \rho_{i,j} \,, \quad (9)$$

where σ_i^2 is the variance of X_i, $\rho_{ij} = v(X_i, X_j)/(\sigma_i \sigma_j)$ is the correlation coefficient of X_i and X_j, and $v(X_i, X_j)$ is the covariance of X_i and X_j. The first term on the right side of

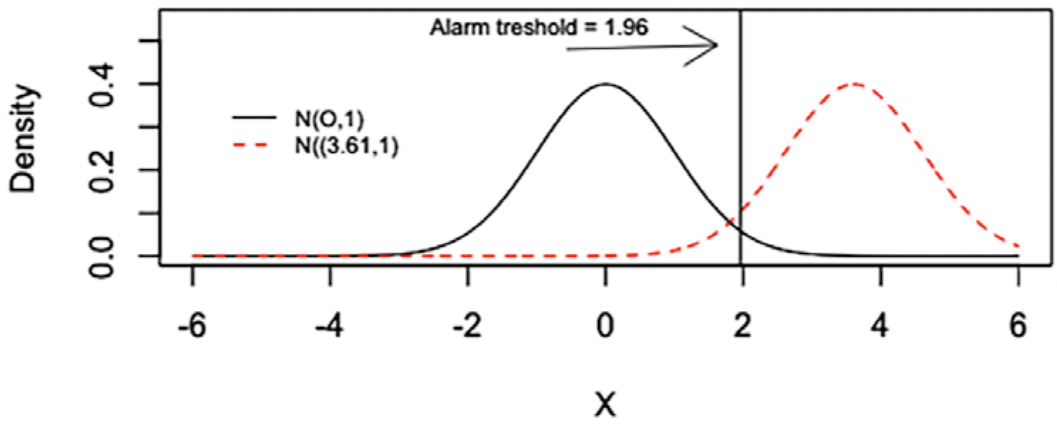

Figure 4: A $N(0,1)$ and a $N(3.61,1)$ distribution with threshold 1.96 for 2-sided testing.

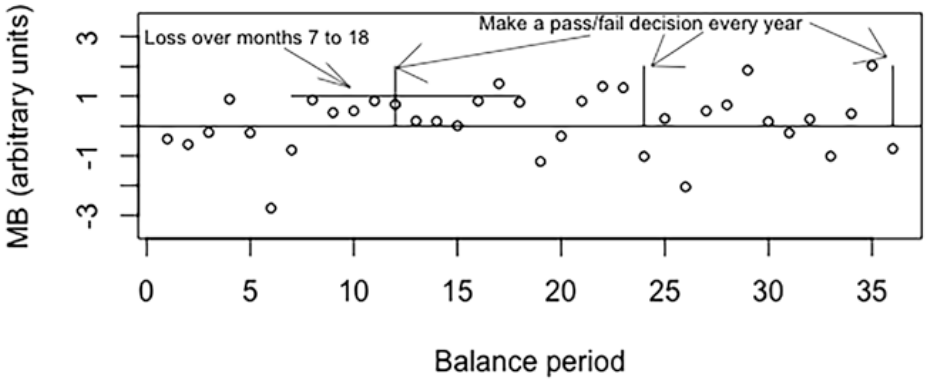

Figure 5: TMB sequences over 36 months using fixed-period (annual) decision periods.

Eq. (9) is the original law of Gauss for independent errors. The second term allows for correlated errors.

It is instructive in UQ training to illustrate how the MBE assumptions implement propagation of variance. Suppose that the total material mass declared by the operator is simply $Y = X_1 + X_2 + \cdots + X_N$ where X_i is the mass of item i. Assuming this model, then the variance of Y denoted by σ_Y^2 is given by applying Eq. (9) and accounting for the fact that the random and systematic error estimates propagate differently. Note that $\frac{\partial f}{\partial x_i} = 1$ for $f(X_1, X_2, \ldots, X_N) = X_1 + X_2 + \cdots + X_N$, and also note that the variance of an individual item is assumed to be the same for all items, that is $\sigma_i^2 = \sigma_X^2$ for all i, and the correlations $\rho_{i,j}$ are also assumed constant for each i, j. It then follows that Eq. (9) is an exact expression, and

$$\begin{aligned} \sigma_Y^2 &= \sum_{i=1}^{N} \left(\frac{\partial f}{\partial x_i}\right)^2 \sigma_i^2 + 2 \sum_{i=1}^{N-1} \sum_{j=i+1}^{N} \frac{\partial f}{\partial x_i} \frac{\partial f}{\partial x_j} \sigma_i \sigma_j \rho_{i,j} \\ &= N(\sigma_S^2 + \sigma_R^2) + N(N-1)\sigma_S^2 = N^2 \left(\sigma_S^2 + \frac{\sigma_R^2}{N}\right), \end{aligned} \tag{10}$$

because in nuclear safeguards the total error variance for measurement of one item is assumed as in Eq. (10) to be $\sigma_X^2 = \sigma_R^2 + \sigma_S^2$ and $\sigma_S^2 = \mathrm{cov}(X_i, X_j) = \rho \sigma_X^2$ is the variance of the short-term systematic measurement errors. Note that Eq. (10) is assuming negligible variation in the true values, so assuming $\mu_1 = \mu_2 = \cdots = \mu_N = \mu$, the same result is obtained by using Eq. (2),

$$Y = \sum_{i=1}^{N} \mu_i (1 + S + R_i) = \sum_{i=1}^{N} \mu_i + N\mu S + \mu \sum_{i=1}^{N} R_i,$$

which has variance $N^2(\sigma_S^2 + \sigma_R^2/N)$. Similarly, the absolute variance of $I_{11} + I_{12}$ is easily shown in a course exercise reviewing variance propagation to be $\sigma_{I_{11}+I_{12}}^2 = (\mu_{11}^2 + \mu_{11}^2)\delta_{RI}^2 + (\mu_{11} + \mu_{11})^2 \delta_{SI}^2$, which equals $2^2(\sigma_{SI}^2 + \sigma_R^2/2)$ for the case $N = 2$.

4.2 Sample size calculations for verification tests

Data such as the paired (O, I) data in Figure 1 are collected for verifying operator declarations. Recall the example from Section 1: suppose the operator's declared NM mass for an item is 1.1 kg, and the inspector's verification measurement is 0.95 kg. Whether the 0.15 kg difference is a cause for concern depends on the uncertainty (as quantified using RSDs as explained in Section 2) in the 1.1 kg and the 0.95 kg values.

Section 2.2 described how Grubbs' estimation can be applied to such (O, I) data to estimate the four RSDs $\delta_{SI}, \delta_{RI}, \delta_{SO}, \delta_{RO}$. Section 2.1 applied standard ANOVA to estimate the total RSD $\delta_T = \sqrt{\delta_{SO}^2 + \delta_{RO}^2 + \delta_{SI}^2 + \delta_{RI}^2}$ of $d = (o - i)/o$. The IAEA has historically used zero-defect sampling, which means that the only acceptable (passing) sample is one for which no defects are found according to the pass/fail test $|d| < 3\delta_T$ [17,18]. Because here we consider the case that the operator overstates the amount of NM present in a defective item by a certain amount (see below), the pass/fail test is one-sided: An alarm is raised if and only if $d > 3\delta_T$.

The non-detection probability β is the probability that no defects are found in a sample of size n when r (r is one or more) true defective items are in the population of size N. For one-item-at-a-time testing and under the assumption that only one measurement method is applied (extensions to more than one method see [18]), the non-detection probability β is given by

$$\beta = \text{Prob(discover 0 defects in a sample of size } n\text{)} = \sum_{i=Max(0,n-(N-r))}^{Min(n,r)} (A_i \times B_i) \quad (11)$$

where the selection probability term A_i is the probability $\mathbb{P}(N,r,n,i)$ that the selected sample contains i truly defective items, which is given by the hypergeometric distribution, i.e.,

$$\mathbb{P}(N,r,n,i) = \frac{\binom{r}{i}\binom{N-r}{n-i}}{\binom{N}{n}}.$$

The non-identification probability, B_i, is the probability that none of the i truly defective items is inferred to be defective based on the individual tests whether $d < 3\delta_T$. The value of B_i depends on the metrology, the defect size (defined as the amount by which the declared item nuclear material mass differs from its best accountancy value), and the alarm threshold (which is typically $3\delta_T$). Assuming a purely random error model, i.e., a multiplicative error model as in Eq. (2) for the inspector measurement (and similarly for the operator) with no systematic errors, and the case that the operator overstates the material present by the amount $M/(\bar{x}r)$ in each defective item, the non-identification probability [17,18] is

$$B_i = \left(\Phi\left(\frac{3\delta_T - \frac{M}{\bar{x}r}}{(1-\frac{M}{\bar{x}r})\,\delta_T} \right) \right)^i,$$

where δ_T is the total RSD (random plus systematic) for the one measurement method, M is the diverted amount of NM (usually M is the significant quantity), $\bar{x}$ is the average amount of NM per item, and $\Phi()$ is the cumulative normal distribution function.

Using Eq. (11), the non-detection probability β is given by

$$\beta(N,n,r,\delta,M,\bar{x}) = \sum_{=Max(0,n-(N-r))}^{Min(r,n)} \frac{\binom{r}{i}\binom{N-r}{n-i}}{\binom{N}{n}} \left(\Phi\left(\frac{3\delta_T - \frac{M}{\bar{x}r}}{(1-\frac{M}{\bar{x}r})\,\delta_T} \right) \right)^i. \quad (12)$$

For simplicity, sample size calculations currently regard all errors as random, but the total RSD $\delta_T = \sqrt{\delta_S^2 + \delta_R^2}$ includes the effects of both systematic and random errors [17,18]. From Section 2, it is evident that δ_T must be estimated using $\hat{\delta}_T$, which has estimation error; therefore because the DP is estimated by substituting $\hat{\delta}_T$ in Eq. (12) for δ_T, the calculated DP also has estimation error and confidence bands can be constructed around plots of DP versus sample size or plots of DP versus the number of defective items for a chosen sample size n. Also, reference [10] uses concepts from tolerance interval construction to show how to control the false alarm rate in future measurements when δ_R and δ_S are estimated from a few previous inspection periods as in Figure 1.

It is to be emphasized that Eq. (11) is quite general; it allows for the non-identification probability B_i to be a user-defined probability density function, such as the familiar normal density, or any other specified density that is suggested by measurement evaluations. Most commonly, B_i as given above is assumed. Also, the requested sample size n is then based on the minimum detection probability (maximum non-detection probability) over a range of possible r values (r is the true number of defective items in the population of size N), assuming each defective item has the same defect size.

5. Summary

IAEA safeguards training courses serve many types of students, including inspectors, who need to understand bottom-up and top-down UQ. Bottom-up UQ is primarily presented in NDA training. Top-down UQ is presented by the statistical analysis team and includes Grubbs' estimation as described in Section 3. Grubbs' estimation training includes related topics such as screening for outliers, choosing the appropriate groups if by inspection period is not the appropriate grouping [24], alternatives to Grubbs' estimation to reduce variability in RSD estimates, and subsampling to make more homogeneous strata if item masses have large variability (which increases the variability in the Grubbs' estimates). Section 4 briefly described two main applications for the estimates of the four main RSDs, $\delta_{SI}, \delta_{RI}, \delta_{SO}$, and δ_{RO}.

As UQ utilizes a holistic means to assess and estimate total uncertainty, performing a proper UQ can be challenging and tedious. Effective bottom-up and top-down UQ help to further reveal the so called "dark uncertainty" which exists in-between. Without this complete assessment, all sources of uncertainty cannot be properly identified and accounted for. The aim for effective UQ is part of ongoing quality control for measurements, and collaborations regarding any gaps between bottom-up and top-down RSD estimates (with attention to uncertainty in the RSD estimates – see Fig. 2) which can lead to fruitful communication among nuclear safeguards professionals.

6. References

[1] Evaluation of measurement data — Guide to the expression of uncertainty in measurement, JCGM 100:2008

GUM 1995 with minor, https://www.bipm.org/utils/common/documents/jcgm/JCGM_100_2008_E.pdf, 2008.

[2] Zhao, K., et al., International Target Values 2010 for Measurement Uncertainties for Safeguarding Nuclear Safeguards, STR 368, IAEA, 2010.

[3] Burr, T., Croft, S., Jarman, K., Nicholson, A., Norman, C., Walsh, S., Improved Uncertainty Quantification in NonDestructive Assay for Nonproliferation, Chemometrics, 159, 164-173, 2016.

[4] Bonner, E., Burr, T., Krieger, T., Martin, K., Norman, C., Comprehensive Uncertainty Quantification in Nuclear Safeguards, Science and Technology of Nuclear Installations, 1-16, 10.1155/2017/2679243, 2017.

[5] Bonner, E., Burr, T., Guzzardo, T., Krieger, T., Norman, C., Zhao, K., Beddingfield, D., Geist, W., Laughter, M., Lee, T., Ensuring the Effectiveness of Safeguards through Comprehensive Uncertainty Quantification, Journal of Nuclear Materials Management 44(2), 53-61, 2016.

[6] Walsh, S., Burr, T., Martin, K., Discussion of the IAEA Error Approach to Producing Variance Estimates for use in Material Balance Evaluation and the International Target Values, and Comparison to Metrological Definitions of Precision, Journal of Nuclear Materials Management, 45(2), 4-14, 2017.

[7] Burr, T., Croft, S., Favalli, A, Krieger, T., Weaver, B., Bottom-up and Top-Down Uncertainty Quantification for Measurements, Chemometrics and Intelligent Laboratory Systems 209, 104224, 2021.

[8] Burr, T., Croft, S., Krieger, T., Martin, K., Norman, C. Walsh, S., Uncertainty Quantification for Radiation Measurements: Bottom-Up Error Variance Estimation Using Calibration Information, Applied Radiation and Isotopes, 108,49-57, 2015.

[9] Burr, T., Sampson, T., Vo, D., Statistical Evaluation of FRAM Gamma-ray Isotopic Analysis Data, Applied Radiation and Isotopes 62, 931-940, 2005.

[10] Burr, T., Bonner, E., Krzysztoszek, K., Norman, C., Setting Alarm Thresholds in Measurements with Systematic and Random Errors, Stats 2(2), 259-271, doi.org/10.3390/stats2020020, 2019.

[11] Croft, S., Burr, T., Favalli, A., Nicholson, A., Analysis of Calibration Data for the Uranium Active Neutron Coincidence Counting Collar with Attention to Errors in the Measured Neutron Coincidence Rate, Nuclear Instruments and Methods in Physics Research A 811. 70-75, 2016.

[12] Burr, T., Krieger, T., Norman, C., Approximate Bayesian Computation applied to Metrology for Nuclear Safeguards ESARDA Bulletin No. 57, 52-59, 2018.

[13] Carlin, B., John, B., Stern, H., Rubin, D., Bayesian Data Analysis (1st ed), Chapman and Hall, 1995.

[14] Burr, T., Skurikhin, A, Selecting Summary Statistics in Approximate Bayesian Computation for Calibrating Stochastic Models, BioMed Research International, Vol20 2013, Article ID 210646, 10 pages, 2013. doi:10.1155/2013/210646, 2013.

[15] Blum, M., Nunes, M., Prangle, D., Sisson, S., A Comparative Review of Dimension Reduction Methods in Approximate Bayesian Computation, Statistical Science 28(2), 189–208, 2013.

[16] Nunes, M. Prangle, D., abctools: an R package for Tuning Approximate Bayesian Computation Analyses, The R Journal 7(2), 189–205, 2016.

[17] Krieger, T., Burr, T., Avenhaus, R., Statistical tests for verification sampling plans, Proceedings 61st Annual INMM meeting, 2019.

[18] Burr, T., Krieger, T., Norman, C., Zhao, K, The Impact of Metrology Study Sample Size on Verification Sample Size Calculations in IAEA Safeguards, European Journal Nuclear Science and Technology, 2, 36, 2016.

[19] Picard, R., Sequential Analysis of Material Balances, Journal of Nuclear Materials Management 15(2), 38-42, 1987.

[20] Avenhaus, R., Jaech, J., On Subdividing Material Balances in Time and/or Space, Journal of Nuclear Materials Management, 10, 24-34, 1981.

[21] Miller, R., Beyond ANOVA: Basics of Applied Statistics, Chapman & Hall, 1998.

[22] Vardeman, S., Wendelberger, J., The Expected Sample Variance of Uncorrelated Random Variables with a Common Mean and Some Applications in Unbalanced Random Effects Models, Journal of Statistics Education 13, 1, 2005, available online at lib.dr.iastate.edu/cgi/viewcontent.cgi?article=1064&context=stat_las_pubs.

[23] Martin, K., Böckenhoff, A., Analysis of variance of paired data without repetition of measurement, Allgemeines Statistisches Archiv, volume 90, pages 365–384, 2006.

[24] Burr, T., Martin, K., Norman, C., Zhao, K., Analysis of Variance for Item Differences in Verification Data with Unknown Groups, Hindawi, Science and Technology of Nuclear Installations, Volume 2019, Article ID 1769149, 10 pages, https://doi.org/10.1155/2019/1769149, 2019.

[25] Grubbs, F., On Estimating Precision of Measuring Instruments and Product Variablity, Journal of the American Statistical Association, 43, 243-264, 1948.

[26] R Core Team. R: A language and environment for statistical computing. R Foundation for Statistical Computing, Vienna, Austria. ISBN 3-900051-07-0, www.R-project.org, 2017.

Fast neutron dose rate monitoring using off the shelf Helium-4 scintillation detectors

Paolo Tancioni, Rico Chandra, Marco Panniello, Ulisse Gendotti
Arktis Radiation Detectors Ltd
Räffelstrasse 11, 8045 Zürich, Switzerland

Abstract

The capability to measure neutron dose rate with an accuracy of +/- 20% is demonstrated for the helium-4 fast neutron scintillation detector model s670 by Arktis Radiation Detectors. Measurements were performed utilizing quasi-monoenergetic neutron fluxes in an energy range between 0.144 and 14.8 MeV as well as using calibrated Cf-252 and Americium-Beryllium (Am-Be) sources.

The elastic scattering reaction between neutrons and (_^4)He enables detection of neutrons whilst preserving the information about their energy. This measurement technique does not require neutron moderators, resulting in a remarkably lighter configuration. The readings from the detector were plotted against neutron energy to obtain energy calibration curves. Neutron fluence rates measured by certified laboratory detectors were used to calculate intrinsic efficiency values for various irradiation energies.

Fluence per unit dose equivalent factors were used to derive the ambient dose equivalent rate values from the measured neutron energy spectra. The results are used to implement a dose rate calculation in the system software, capable of providing neutron ambient dose equivalent rate values. The accuracy of the computed values is validated with calibrated Cf-252 and Am-Be sources. This work highlights the versatility of such a system, which extends to applications where not only simple neutron counting is required but neutron energy information is also of interest to assess the radiological risk caused by a neutron flux. This system can be used in a variety of applications ranging from dose monitoring in nuclear power plants to risk-assessment of nuclear waste drums coming from the decommissioning of nuclear facilities.

Keywords: neutron; safety; helium-4; dose

1. Introduction

Fast neutrons fluxes are generally coming from sealed radionuclide sources, nuclear power plants, fuel enrichment facilities and particles accelerators. Neutron sources are also used for various industrial purposes.

The major difficulties in detecting fast neutron and measuring their energy arise from the wide energy range a neutron flux can present, the important dependence of the medium cross section with neutron energy and the possible presence of different types of radiation in the same environment, especially gamma rays. The system described in this work, a high-pressure ^{4}He gas scintillation detector model s670 by Arktis Radiation Detectors Ltd, was irradiated with quasi-monoenergetic neutron fluxes ranging from 0.144 to 14.8 MeV. In this region, the most probable interaction of neutrons with light nuclei such as helium is elastic scattering.

He-4-based neutron detection technologies, characterized by higher availability and lower cost of the scintillation gas medium compared to ^{3}He, have been gaining increasing interest as a reliable and affordable neutron detection technology. Moreover, unlike ^{3}He detectors which rely on the absorption of a thermal neutron, ^{4}He detectors exploit excellent fast neutron elastic scattering properties of the gas. This enables the manufacturing of detection systems without utilizing moderators, thus preserving neutron energy information. Using helium-4 as a detection medium, a fast neutron can lose up to around 64% of its initial kinetic energy in a single elastic scattering interaction. This information was used to characterize the detector response at different irradiation energies, allowing to obtain accurate energy calibration curves.

Moreover, helium's low atomic number (Z = 2) results in a low electron density, which reduces the probability of gamma interaction. Additionally, gamma interactions in the active volume generate recoil electrons, which are characterised by low rate of energy deposition. These electrons will be more likely to hit the detector wall before depositing all of its energy. Gamma rays are also characterised by lower light yield in helium scintillation if compared to neutron interactions, which makes this detection technique more advantageous than liquid scintillation detection systems when operating in intense gamma field. In gaseous

helium, these combined effects result in the slow component of the scintillation pulse of a gamma event being up to 8 times smaller than that of a neutron event [1], allowing pulse shape discrimination (PSD).

For neutron spectrometry applications, ^{4}He scintillation techniques have the additional advantage of having an elastic scattering cross section of the scintillation medium which is characterized by a peak for the scattering angle resulting in the maximum energy deposit. This behaviour is not visible for other neutron detection techniques which relies on proton-recoil interactions, being characterized by an elastic scattering cross-section that is almost constant for increasing scattering angles [3].

In this work, pressurized ^{4}He fast neutron scintillation detector model s670 by Arktis Radiation Detectors Ltd is used to implement an ambient dose equivalent rate calculation for dose monitoring purposes, highlighting the possibility to exploit this technology in every environment that is characterized by a high fast neutron radiation component, improving radiological safety of workers.

2. The detection system

Arktis Radiation Detectors model s670 fast neutron detector, shown in figure 1, consists of a stainless-steel tube filled with pressurized ^{4}He, divided into three optically decoupled and identical segments, each containing 8 Silicon Photomultipliers (SiPM) for light collection. The electronic board for signal processing is mounted on one end of the tube, where the TTL output is visible as well.

2.1 Working principle and operational parameters

When fast neutrons interact with helium nuclei through elastic scattering, kinetic energy is transferred from the neutron to the target helium nucleus. The nucleus slows down in the pressurized gas, producing excited and ionized species that de-excite emitting scintillation light.

The 24 SiPMs operating in the s670 fast neutron detector convert the light pulse into an electric signal, which is subsequently processed by the electronic board.

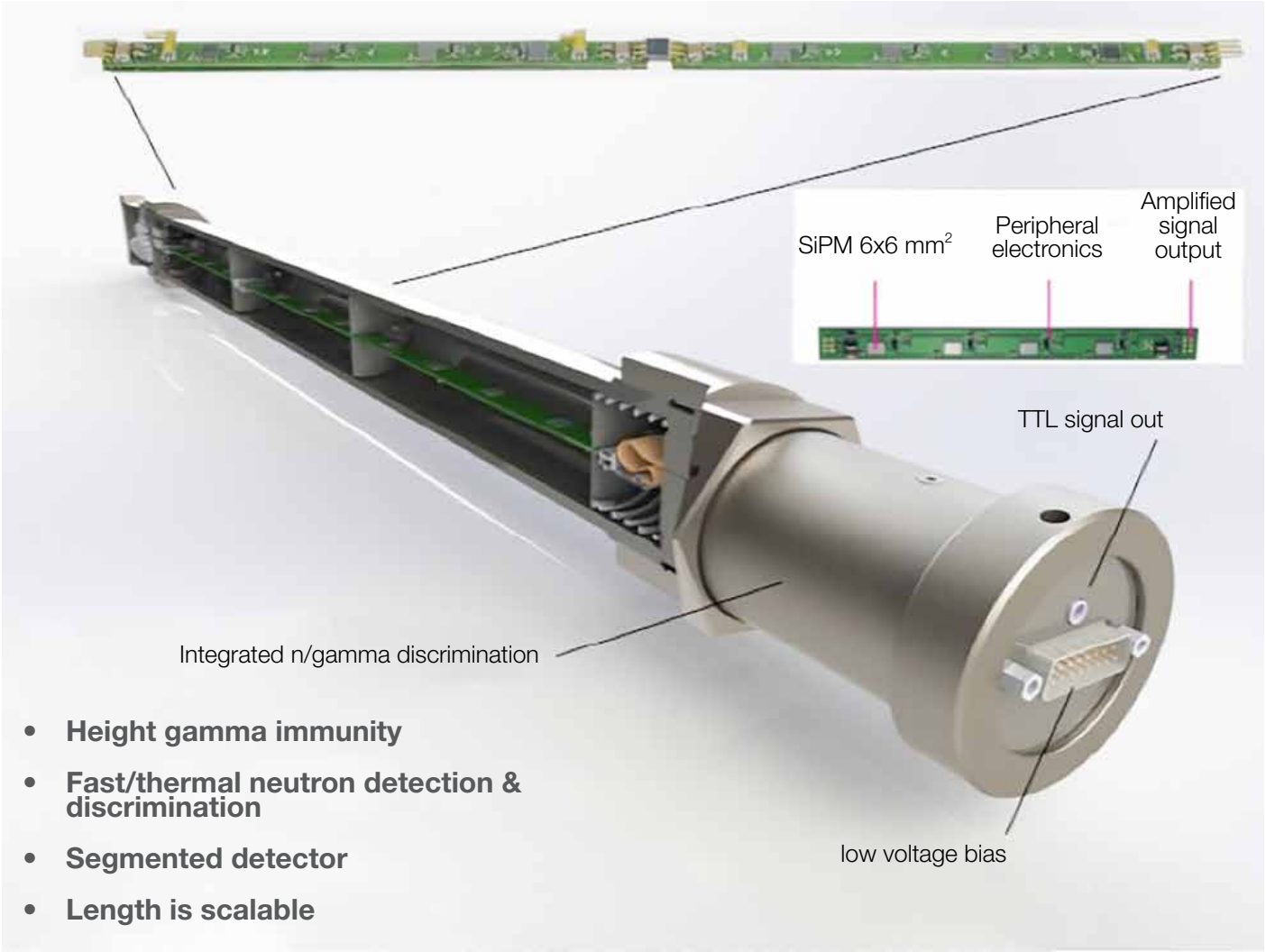

Figure 1: High-pressure He-4 scintillation detector model s670 by Arktis Radiation Detectors Ltd.

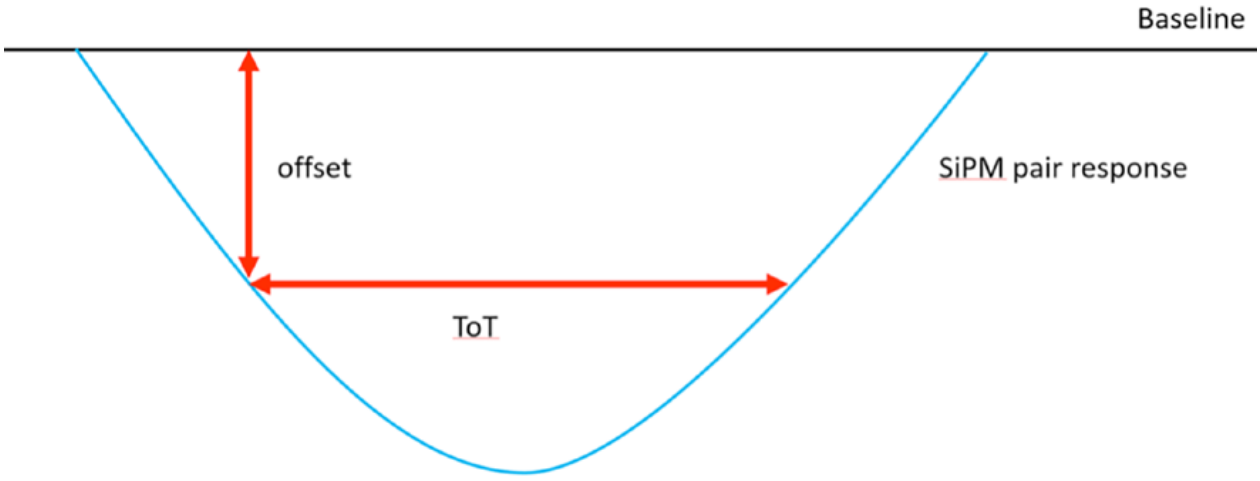

Figure 2: Definition of the parameters “Time-over-Threshold” and “offset”.

The output information of the detector is a Time-over-Threshold (ToT), i.e. the time duration during which the response amplitude of the signal coming from the SiPMs is above a tunable threshold. This electronic threshold is called offset, and it can be adjusted separately for each segment to tailor the sensitivity to the specific application. The offset value is set such that only signals of a certain height are accepted as valid and hence are stored for post analysis. Depending on the value of the ToT signal generated by one event inside the tube, a different TTL signal is produced.

A schematic description of these parameters is shown in Figure 2.

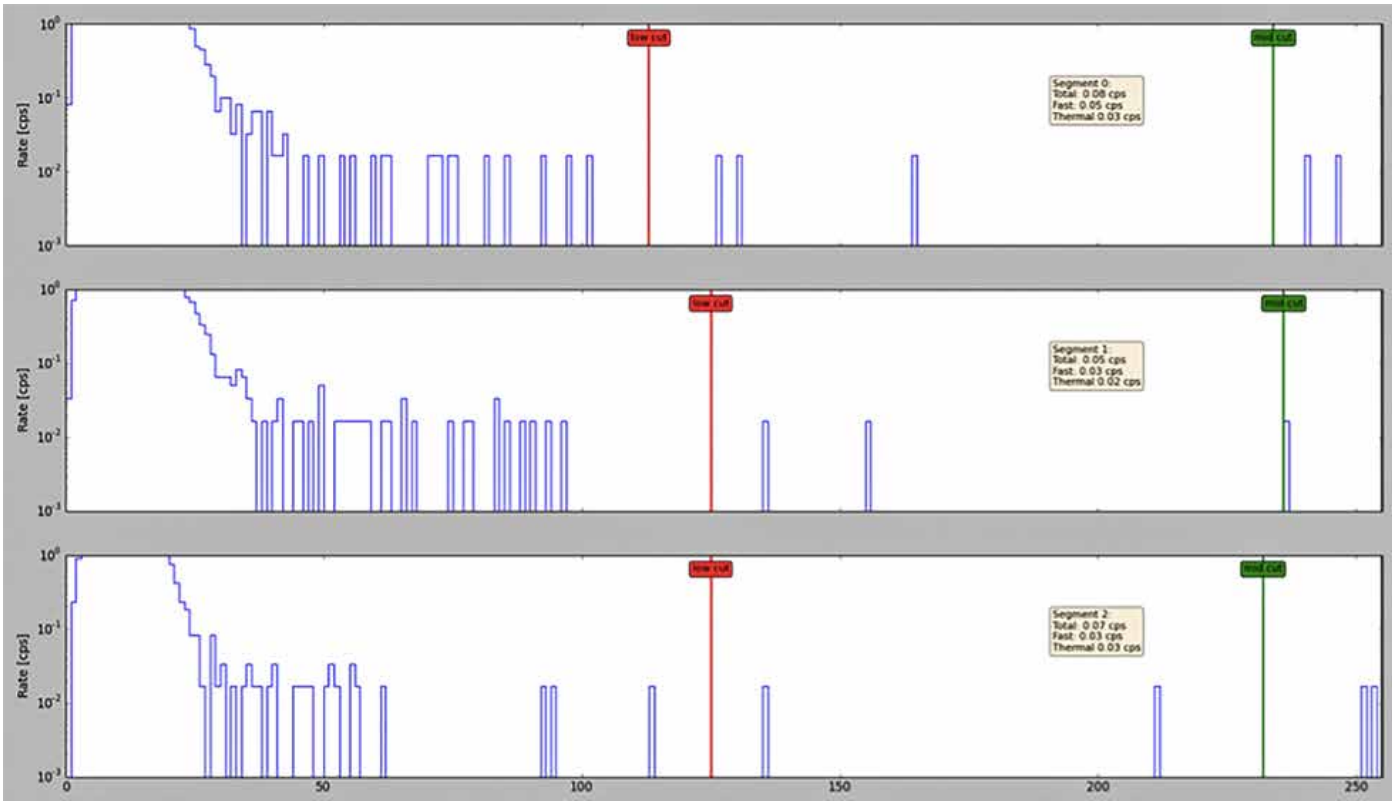

Figure 3: Output histogram showing background count rate versus ToT channel for the three segments of the s670 neutron detector. Different ToT regions are identified by the low-cut (red), mid-cut (green) and high-cut (coinciding with the right end of the x-axis).

Another parameter of importance acting on the ToT histograms is the cut. Applying a “low-cut”, “mid-cut”, and “high-cut” on the ToT signal width, it is possible to define an optimal gamma-rejection ToT region for the detector and to focus on well-defined regions of interest based on the width of the signals that generate counts in those regions.

A typical output of a background measurement reporting count rate versus ToT channel is shown in Figure 3 for each of the three optically decoupled segments. The desired gamma-rejection is set by the low-cut (red), while mid-cut (green) and high-cut (here coinciding with the right end of the x-axis) can be set to focus on a particular ToT region of interest.

3. Measurement campaign

3.1 Irradiation tests with monoenergetic neutron fields

To assess the detector performance for various neutron energies, an extensive experimental campaign was conducted at the neutron irradiation facility (PIAF) at Physikalisch-Technische Bundesanstalt (PTB) in Berlin, Germany [5].

Quasi-monoenergetic neutron fields were utilized to irradiate an array of s670 neutron detectors and acquire data for neutron energies of 0.144, 0.565, 1.2, 2.5, 5, 14.8 MeV.

The measurements took place in a low-scattering measurement hall, where two s670 detectors were positioned at

reaction	target	θ_n	E_n [MeV]	ΔE_n [keV]	ϕsc/ϕdir
^{7}Li(p,n)^{7}Be	LiF 75 µg/cm^2	0°	0.144	12	0.020(5)
^{7}Li(p,n)^{7}Be	LiF 75 µg/cm^2	0°	0.565	8	0.016(4)
^{3}H(p,n)^{3}He	Ti(T) 0.955 mg/cm^2	0°	1.2	74	0.034(8)
^{3}H(p,n)^{3}He	Ti(T) 0.955 mg/cm^3	0°	2.5	52	0.015(4)
^{3}H(d,n)^{4}He	Ti(T) 1.076 mg/cm^4	0°	14.8	434	0.015(4)

Table 1. Informational data on the monoenergetic neutron fields at PTB.

Figure 4: Picture of the experimental set-up in the low-scattering measurement hall at PTB. Target-to-detector distance is indicated by the red line.

Detectors numbers	MS number	t (s)	ϕ_{dir} (10^5 cm^{-2}
#100413 / #100497	4	299.6	0.80(4)
#100413 / #100497	5	308.6	0.84(4)
#100413 / #100497	6	316.7	0.86(4)
#100413 / #100497	7	298.3	0.80(3)
#100508 / #100520	8	896.7	2.41(10)
#100508 / #100520	9	630.7	1.70(7)
#100508 / #100520	10	51.8	0.140(6)
#100508 / #100520	11	601.0	1.62(7)
#100508 / #100520	12	410.9	1.11(5)
#100508 / #100520	13	522.1	1.41(6)

Table 2. Measurement time duration and direct neutron fluence rate for irradiation tests with a monoenergetic 2.5 MeV neutron field.

a distance of 300 cm from the neutron generator. The detectors were supported and enclosed by foamed material, and the distance from the detectors to the neutron production target was measured along the direction of the ion beam between the plane containing the axis of the detector housings and the neutron production target. The direction of the ion beam hits this plane in the middle between the centers of the sensitive volumes. The experimental set-up is shown in Figure 4.

Table 1 shows informational data on the monoenergetic neutron fields, such as the type of nuclear reaction exploited to generate the neutron field, nominal values of neutron energies and FWHMs of the irradiation fields.

In Table 1, the neutron emission angle θ_n, the neutron field energy E_n, and the width ΔE_n (FWHM) of the direct neutron distribution are nominal values. Standard measurement uncertainties (k = 1) are given for the ratio ($\varnothing_{sc}/\varnothing_{dir}$) of the fluence values of scattered and direct neutrons. As for the measured neutron fluence values that were used as a reference for each irradiation field, the related uncertainties are expanded measurement uncertainties obtained by multiplying the standard measurement uncertainties by a coverage factor (k = 2). They have been

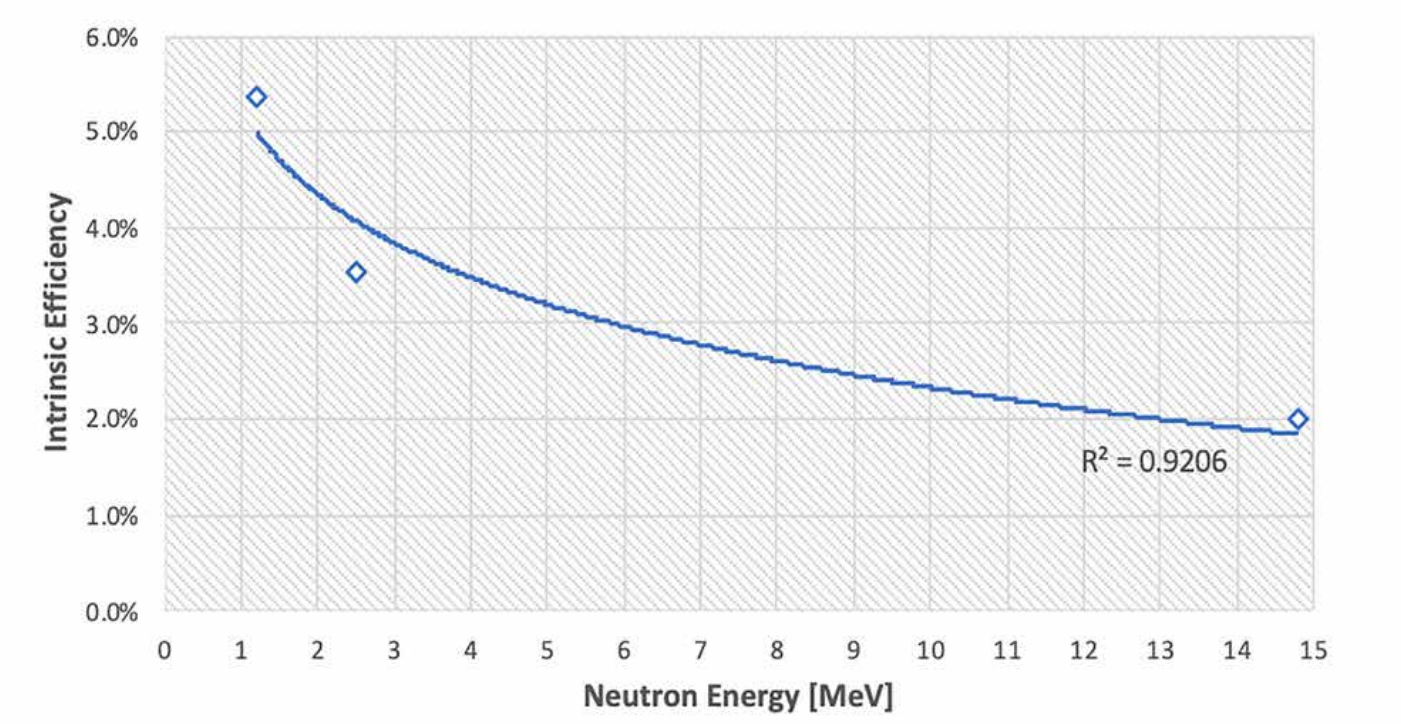

Figure 5: Intrinsic efficiency values calculated for 1.2, 2.5, 14.8 MeV neutron energies, together with the analytical fit.

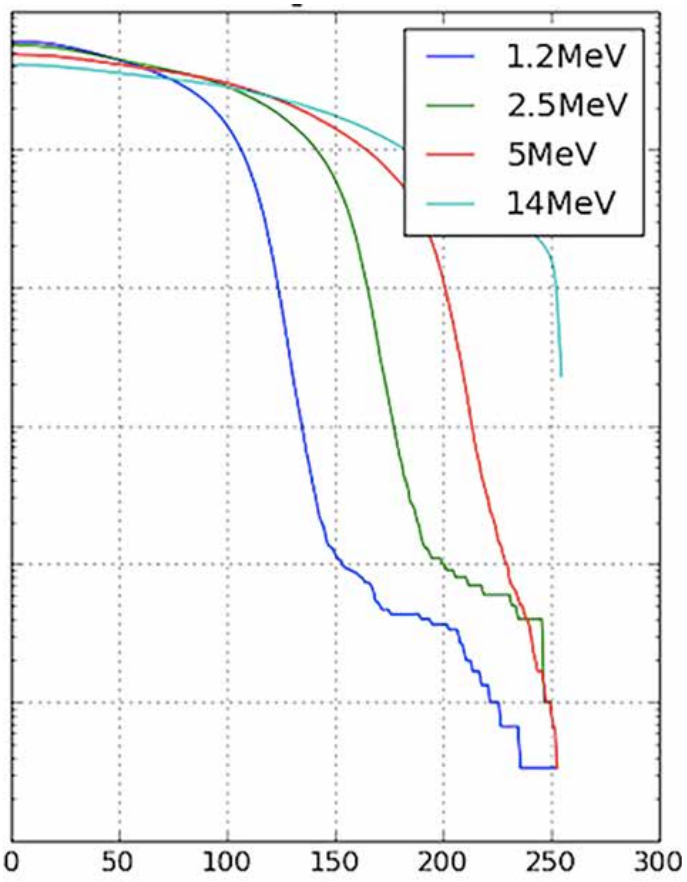

Figure 6: Detector response to various monoenergetic neutron fields in terms of cumulative count rate versus ToT channel.

determined in accordance with the Guide to the Expression of Uncertainty in Measurement (GUM) [7]. The value of the measurand then normally lies, with a probability of 95%, within the attributed coverage interval.

These neutron fluence measured values, together with the time duration of the test and the generator-to-detector distance, were used to calculate the neutron fluence rate at the detector surface in units of $cm^{-2}s^{-1}$.

For each measurement performed with the s670 neutron detector, the detector output is a histogram in which for every event generating a signal that is above the offset, a count is stored in a histogram and distributed over 255 ToT channels depending on the amplitude of the light pulse generated by that event. By summing over all the counts above the low-cut (set to achieve the desired gamma-immunity) and dividing by the measurement time duration, the measurement count rate is calculated for each irradiation energy. By subtraction of the background count rate, the net neutron count rate has been calculated for all the irradiation tests.

Moreover, by multiplying the neutron fluence rate at the detector surface by the sensitive cross-sectional area of the tube, the number of neutrons hitting the detector per unit time was calculated.

From the ratio between the net neutron count rate and the number of neutrons hitting the detector per unit time, the intrinsic efficiency of the detector was calculated for all the irradiation energies.

In Table 2 the reference neutron fluence values and irradiation time for the 2.5 MeV irradiation tests are shown as an example.

3.2 Intrinsic efficiency assessment and energy calibration

The intrinsic efficiency values calculated for energies of 1.2, 2.5 and 14.8 MeV are plotted in figure 5, where the analytical fit is shown as well.

This analytical fit was then used when implementing the dose rate calibration in the system software, in order to calculate the neutron fluence rate from the detector count rate for neutron energies in this range.

In Figure 6, the response of the s670 detector to irradiation energies of 1.2, 2.5, 5.0 and 14.8 MeV are shown in terms of the cumulative count rate versus ToT channel.

The response curves are clearly characterised by an increasing cut-off ToT channel number with increasing irradiation energy. The positions of these cut-off points were then used to calibrate in energy the ToT histograms in order to have direct information about the neutron field energy out of a measurement histogram.

From the physics of the elastic scattering interaction between a neutron and a helium nucleus, it is easily calculated that a neutron can deposit up to 64% of its initial kinetic energy to the target nucleus [3].

Thus, it is straightforward to associate the maximum deposited energy (and then the initial neutron energy) to the ToT channel where the irradiation of the detector with a field of that energy would show a cut-off. The energy calibration points, and the related analytical fit implemented into the system software are shown in the graph in figure 7.

Neutrons effective dose per fluence factors (in units of pSv cm^{-2}) from ICRP Publication 116 (Table A.5, mono-energetic particles incident in various geometries) were used to implement the dose rate calculation in the system software [4]. For each energy region resulting from the ToT histograms calibration, a set of neutron effective dose per fluence factors was used to estimate the dose rate delivered by neutrons belonging to that region.

After the implementation of this dose-rate calculation in the detector software, the final tests were performed at Paul Scherrer Institut (PSI) Calibration Laboratory [6]. A

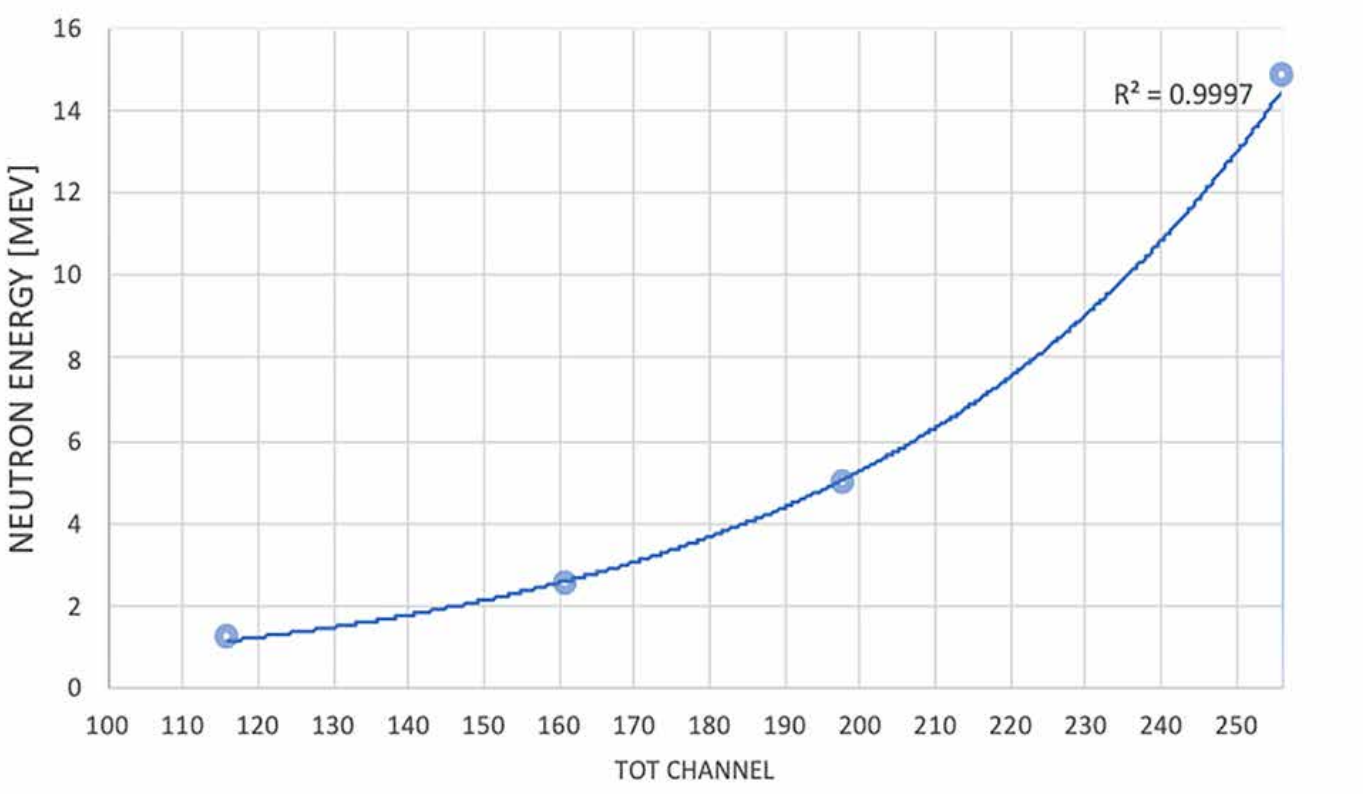

Figure 7: Energy Calibration points and analytical fit in the energy range 1.2 – 14.8 MeV..

spontaneous fission ^{252}Cf and an alpha-neutron ^{241}Am—Be source were used.

Characteristics of these neutron sources are shown in Table 3.

The PSI Calibration Lab uses a Berthold LB6411 neutron detector with an UMO LB 123 neutron dosimeter as a secondary standard. The expanded combined uncertainty (k = 2) of the dose rate values used as reference was estimated by PSI to be 6% for ^{252}Cf and 7-8% for ^{241}Am-Be for distances larger than 50 cm. Higher uncertainty for ^{241}Am-Be is due to the uncertainty of a field-specific correction factor to the calibration of the secondary standard LB6411, which was calibrated in a direct neutron field from a ^{252}Cf source.

Nuclide	^{241}Am-Be	^{252}Cf
Nominal Activity [GBq]	185	19.68
Neutron source strength [n/s]	9.15E+06	2.29E+09
Reference Date	10.10.59	05.12.01

Table 3. Characteristics of the neutron sources used at PSI Calibration Laboratory [5].

4. Results

Defining the Response Factor (RF) as the ratio between the measured ambient dose rate value at distance d from the source and the reference ambient dose rate value at the same distance certified by PSI for each source, the detector performance was evaluated for both sources at various source-to-detector distances and for various measurement duration. Two s670 detectors were irradiated (serial numbers 100488 and 100509, as shown in Table 4).

The acceptance range for the Response Factor is set as to have a maximum error of +/- 20% with respect to the dose rate value declared by PSI. Results of the ambient dose equivalent rate measurements for these two sources are shown in Table 3 for source-to-detector distances of 1 m and 3 m and measurement duration of 60 s and 10 s. The measurement at 3 m with duration of 10 s is shown to represent the worst-case scenario for this fixed source activities and measurement setup.

5. Conclusions

The results presented in Table 4 show that the accuracy of the dose rate calculation is inside the defined acceptance range for both sources and for different source-to-detector distances and durations of the measurements, giving an overall average accuracy of 92.5% calculated over all the

distance = 1m; duration 60s	Reference H*(10) [uSv/h]	100488 [uSv/h]	100488 RF [0.8-1.2]	100509 [uSv/h]	100509 RF [0.8-1.2]	100488 Calib.	100509 Calib.
AmBe	115.2	106.5	0.92	127.2	1.10	passed	passed
Cf-252	222.3	217.9	0.98	247.4	1.11	passed	passed

distance = 3m; duration 60s	Reference H*(10) [uSv/h]	100488 [uSv/h]	100488 RF [0.8-1.2]	100509 [uSv/h]	100509 RF [0.8-1.2]	100488 Calib.	100509 Calib.
AmBe	20.2	17.2	0.85	19.4	0.96	passed	passed
Cf-252	38.2	35.6	0.93	40.0	1.05	passed	passed

distance = 1m; duration 10s	Reference H*(10) [uSv/h]	100488 [uSv/h]	100488 RF [0.8-1.2]	100509 [uSv/h]	100509 RF [0.8-1.2]	100488 Calib.	100509 Calib.
AmBe	115.2	105.1	0.91	125.6	1.09	passed	passed
Cf-252	222.3	223.0	1.00	238.9	1.07	passed	passed

distance = 3m; duration 10s	Reference H*(10) [uSv/h]	100488 [uSv/h]	100488 RF [0.8-1.2]	100509 [uSv/h]	100509 RF [0.8-1.2]	100488 Calib.	100509 Calib.
AmBe	20.2	17.8	0.88	21.7	1.07	passed	passed
Cf-252	38.2	36.1	0.94	40.1	1.05	passed	passed

Table 4: Results of the dose rate measurements with radionuclide neutron sources at PSI for the s670 neutron detectors #100488 and #100509

measurements shown in Table 4. This clearly shows how this fast neutron detection system can serve as a neutron dose meter for radiological safety purposes in environments where neutron dose rate of neutron fluxes in the fission energy range must be constantly monitored, such as nuclear power plants, fuel reprocessing facilities and nuclear waste analysis laboratories. The National Institute of Metrology of China (NIM) certified the first s670 fast neutron detector as a neutron dose meter in China in 2020. Avoiding the use of helium-3 and the employment of large volumes of moderating material, the s670 fast neutron detector can represent a robust, compact and versatile alternative to these detectors, with the additional feature of providing an accurate dose rate calculation for fast neutrons in the fission energy range.

References

[1] R. Chandra et al. Fast neutron detection with pressurized 4He scintillation detectors. JINST 7 C03035. 2012.

[2] Murer D.E. He-4 Fast Neutron Detectors in Nuclear Security Applications. ETH Zürich. 2014.

[3] Knoll G. F. Radiation Detection and Measurements, 4th Ed.

[4] Conversion Coefficients for Radiological Protection Quantities for External Radiation Exposures. Table A.5. ICRP Publication 116, Ann. ICRP 40(2–5). 2010.

[5] URL: https://www.ptb.de/cms/en/ptb/fachabteilungen/abt6/measurement-and-calibration-capabilities/neutron-radiation.html

[6] URL: https://www.psi.ch/de/asi/facilities

[7] International Organization for Standardization (ISO). Evaluation of measurement data. Guide to the expression of uncertainty in measurement. JCGM 100:2008.

Supporting the Additional Protocol declarations on nuclear research and technology by the JRC TIM DU platform

Filippo Sevini[1], Enzo Caponetti[2], Christos Charatsis[1], Xavier Arnes-Novau[1]

[1]European Commission, Joint Research Centre (JRC), Ispra, Italy
Directorate Nuclear Safety and Safeguards
E-mail: filippo.sevini@ec.europa.eu
[2]Liege University, European Studies Unit

Abstract

Research subject to dual-use trade controls may play an important role in proliferation programmes because the exchanges among research entities are traditionally open and prone to be exploited by third countries' illicit developments.

For these reasons, apart from information "in the public domain" or "basic scientific research", transfers of nuclear technology are subject to export authorisation requirements and government-to-government assurances like the export of tangible goods, as specified by the Nuclear Suppliers Group's guidelines and national export control laws.

Also the requirements of the Model Additional Protocol to the Agreement(s) between States and the International Atomic Energy Agency for the Application of Safeguards include declarations about national research and development activities related to the nuclear fuel cycle, but do not require declarations of technology transfers to third countries.

The European Commission JRC, in collaboration with Liege University, has developed the Tools for Innovation Monitoring Dual-use (TIM DU) platform that can facilitate the identification of entities publishing research with a dual-use potential in the various countries. Together with many dual-use goods and emerging technologies, TIM DU maps nuclear-fuel cycle activities' results included in scientific abstracts, patents, and EU-funded projects, allowing analysts to gather lists of documents, geographical distributions, collaborations, and authors related to these activities.

These results can help the national authorities submitting declarations to IAEA in accordance with Additional Protocol's Article 2.a, both to identify also previously unknown national research actors and their collaboration networks, as well as to raise the awareness of national research entities about potential sensitivities with external collaborators. The IAEA could also use TIM DU to support the verification of the completeness and correctness of the declarations concerning nuclear fuel cycle research.

Keywords: export control; nuclear safeguards; non-proliferation; dual-use; research; strategic trade; intangible technology transfers.

1. Research and technology

Research is essential to support technological development as well as education. It is usually divided into fundamental - more typical of the academic sphere - and applied, in support to industry. This distinction is however not so clear-cut, especially considering the increasing collaborations between academia and industry, which will be discussed when analysing the TIM DU results in the second part of this article [1, 4].

Various actors are involved in research, ranging from universities to research and development organisations, as well as governmental agencies, industries, consulting companies, and even hospitals.

Research can share technological developments in multiple ways, primarily involving intangible technology transfers (ITT) through international projects and collaborations, exchanges of researchers, training, technical assistance, and scientific publications [5].

Transfers of sensitive dual-use technology are subject to export controls, both from the civil and the military side, respectively represented in the EU by the so-called "EU Dual-use Regulation" (i.e. EC Regulation 428/2009, about to be Recast in 2021 [6,7]) and the EU Common Military List.

Export control of ITT is particularly challenging because they are difficult to monitor and stop, as there is no crossing of borders of physical goods.

The EU Dual-use Regulation contains in its Annex I the dual-use items, definitions, and various decontrol notes deriving from the Nuclear Suppliers Group - as well as the Wassenaar Arrangement, Missile Technology Control Regime, Australia Group, and the Chemical Weapons Convention [8-12], integrated into the annually amended Commission Delegated Regulation [13].

The definitions used are therefore essentially the same both in the Dual-use Regulation and the Nuclear Suppliers Group, which will be considered as references in this paper, in particular referred to nuclear technology.

2. Important definitions related to dual-use research controls

According to the EU Dual-use Regulation, 'dual-use items' shall mean items, including software and technology, which can be used for both civil and military purposes, and shall include all goods which can be used for both non-explosive uses and assisting in any way in the manufacture of nuclear weapons or other nuclear explosive devices.

Dual-use technology is the specific knowledge or information needed for the development, production or use of dual-use goods. Together with software, it is hence subject to export controls just like tangible goods, such as systems, equipment, components; test, inspection and production equipment; or materials.

Technology can take the form of technical assistance or technical data.

2.1 Technical data

Technical data include blueprints, models, formulae, tables, engineering designs and specifications, manuals and instructions written or recorded on media or devices.

The approval of any dual-use item for export also authorises the export to the same end-user of the minimum "technology" required for the installation, operation, maintenance, and repair of the item.

Important to notice is that according to the Nuclear Suppliers Guidelines and the EU Regulation, controls on "technology" transfer do not apply to information "in the public domain"[1] or to "basic scientific research"[2].

These are key decontrol notes that, save verification of their actual relevance, may apply to most research activities, making them not subject to export authorisations and traceability requirements.

Compliance by organisations engaged in research subject to dual-use controls is a topic of increasing concern. To assist researchers, the EU is about to issue a Commission Recommendation tailored to the needs of academic and research communities, providing guidance for implementing internal compliance controls in different research settings. The draft of the Recommendation was supported by a public consultation of all concerned stakeholders (e.g. academia and research institutions) that was closed on 30 November 2020 [14]. This follows a previous Commission Recommendation dedicated to dual-use suppliers in general [15].

2.2 Technical assistance

"Technical assistance" includes instructions, skills, training, working knowledge, consulting services and may involve the transfer of technical data.

Also the provision of technical assistance and associated technology transfer to third countries is subject to national authorisation.

The Dual-use Regulation's recast expected in 2021 will directly include technical assistance, not only provided abroad but also to third country's nationals "temporarily present in the customs territory of the Union" [7].

Technical assistance is also an activity performed by the IAEA itself through its Technical Cooperation programme with third countries [16].

3. Strategic export control and nuclear safeguards

After this preamble about dual-use research, it is important to briefly recall that, as already described in [17], strategic export control is a barrier against proliferation called for by United Nations Security Council Resolution 1540 [18], aiming at preventing unauthorised access to strategic technology and goods.

Export control and nuclear safeguards developed in parallel, as two intimately linked elements of the non-proliferation framework. This link is evident in both the Non Proliferation Treaty [19] and the Nuclear Suppliers Group (NSG) Trigger List guidelines [20]:

- The Non Proliferation Treaty's Art. III.2., conditions the export of equipment or material especially designed or prepared for the processing, use or production of special fissionable material to any non-nuclear-weapon State to international nuclear safeguards;[3]
- The Nuclear Suppliers Group's Trigger List guidelines state that safeguards are a condition of supply for nuclear goods [20, Art. 4].

1 "Technology" or "software" that has been made available without restrictions upon its further dissemination.

2 Experimental or theoretical work undertaken principally to acquire new knowledge of the fundamental principles of phenomena and observable facts, not primarily directed towards a specific practical aim or objective.

3 Similar obligations are provided for in regional non-proliferation treaties (e.g. the Tlatelolco Treaty, the Rarotonga Treaty, the Bangkok Treaty and the Pelindaba Treaty), EURATOM.

The "NSG Guidelines for transfers of nuclear-related dual-use equipment, materials, software and related technology", containing in annex the Dual-Use List (DUL) [21] were developed after the discovery of undeclared proliferation activities in Iraq in 1991. This determined also another turning point in the international safeguards framework, leading to the introduction in 1997 of the "Model Protocol Additional to the Agreement(s) between State(s) and the International Atomic Energy Agency for the Application of Safeguards" (AP - INFCIRC/540) [22].

This event highlights the complementarity between the IAEA safeguards system and strategic export controls. Thanks to more comprehensive States' reports and inspections, the IAEA can obtain a better insight into a State's nuclear fuel cycle-related activities and capabilities [23-25]. Yet, this does not include the control of nuclear exports, which is of course left to the states, organised - or not – according to principles and control lists set by multilateral arrangements such as the NSG [26].

The controls set by the NSG and other export control regimes on technology needed for the development, production or use of WMD are as important, or even more important, than strategic commodities themselves because technology is critical to the use of the controlled goods and the development of indigenous WMD-related production capabilities, as the A.Q. Khan proliferation case demonstrated [17 5, 6, 2].

4. Nuclear Suppliers Group and technology controls

Most of the provisions of the NSG guidelines are incorporated into the EU Regulation, it is however interesting to comment on those related to technology.

The NSG Part 1 guidelines speak extensively of technology, as e.g. "facility, or equipment or technology therefor".

The same applies to NSG Part 2 guidelines, mentioning "equipment, materials, software, and related technology".

According to both Nuclear Suppliers Group guidelines, "Technology" directly associated with any controlled item will be subject to as great a degree of scrutiny and control as will the item itself, to the extent permitted by national legislation.

In addition to controls on "technology" transfer for nuclear non-proliferation reasons, suppliers should promote protection of technology for the design, construction, and operation of trigger list facilities in consideration of the risk of terrorist attacks, and should stress to recipients the necessity of doing so.

5. Model Additional Protocol's requirements

The Additional Protocol (AP) [22] expanded the set of information that States are required to transmit to the Agency under their report¬ing obligations and expanded the verification toolkit at the IAEA disposal to exclude the presence of possible unde¬clared nuclear material and activities in a State.

5.1 Additional Protocol and nuclear research

While INFCIRC 153 does not make any reference to technology and research, the AP does not explicitly refer to nuclear technology, but implicitly includes technology in connection to the provision of information about research activities, or – indirectly - description about facilities, sites and locations, as important indicators of the overall country's potential and declared list of activities.

The Additional Protocol's Article 2.a. requires that States:

> ..... *shall provide the Agency with a declaration containing:*
>
> (i) A general description of and information specifying the location of nuclear fuel cycle-related research and development activities not involving nuclear material…
>
> 2.a.(i) allows the IAEA to get information about research activities which could also involve technology subject to export control provisions.

Important to note are also AP art. 2.a.(x)'s requirements to provide:

> (x) General plans for the succeeding ten-year period relevant to the development of the nuclear fuel cycle (including planned nuclear fuel cycle-related research and development activities) when approved by the appropriate authorities

And art. 2.b.(i) concerning the provision to the Agency of:

> (i) A general description of and information specifying the location of nuclear fuel cycle-related research and development activities not involving nuclear material which are specifically related to enrichment, reprocessing of nuclear fuel or the processing of intermediate or high-level waste containing plutonium, high enriched uranium or uranium-233… that are carried out anywhere in ..... but which are not funded, specifically authorized or controlled by, or carried out on behalf of, ...

Article 18 illustrates the research areas of interest mentioned throughout the Additional Protocol:

a. Nuclear fuel cycle-related research and development activities means those activities which are specifically related to any process or system development aspect of any of the following:

- conversion of nuclear material,
- enrichment of nuclear material,
- nuclear fuel fabrication,
- reactors,
- critical facilities,
- reprocessing of nuclear fuel,
- processing (not including repackaging or conditioning not involving the separation of elements, for storage or disposal) of intermediate or high-level waste containing plutonium, high enriched uranium or uranium-233

Echoing the NSG guidelines, also the AP specifies that these activities do not include activities related to theoretical or basic scientific research, or to research and development on industrial radioisotope applications, medical, hydrological and agricultural applications, health and environmental effects and improved maintenance.

5.2 Additional Protocol Annex I

A key requirement in article 2.a is the provision of:

> *(iv) A description of the scale of operations for each location engaged in the activities specified in Annex I to this Protocol.*

Where Annex I lists fifteen key manufacturing steps in the nuclear fuel cycle:

i. The manufacture of centrifuge rotor tubes or the assembly of gas centrifuges.

ii. The manufacture of diffusion barriers.

iii. The manufacture or assembly of laser-based systems.

iv. The manufacture or assembly of electromagnetic isotope separators.

v. The manufacture or assembly of columns or extraction equipment.

vi. The manufacture of aerodynamic separation nozzles or vortex tubes.

vii. The manufacture or assembly of uranium plasma generation systems.

viii. The manufacture of zirconium tubes.

ix. The manufacture or upgrading of heavy water or deuterium.

x. The manufacture of nuclear grade graphite.

xi. The manufacture of flasks for irradiated fuel.

xii. The manufacture of reactor control rods.

xiii. The manufacture of criticality safe tanks and vessels.

xiv. The manufacture of irradiated fuel element chopping machines.

xv. The construction of hot cells.

Besides being captured by the requirement of art. 2.a.(i), R&D and university sites - or other actors outside the specific facilities - might also be relevant to the declarations under art. 2.a.(iv) because of their involvement in research supporting the actual manufacturing activities, i.e. “technology” for the “development, production or use” of controlled items. To acquire a more comprehensive overview of information suitable for the AP declarations, it is therefore useful to analyse also research publications related to these activities. This may also bring to the attention of the authorities unknown relevant national research actors, which could be contacted to raise their awareness about the risk of sensitive technology transfers involved in international research collaborations.

5.3 Additional Protocol Annex II

The AP also requires export declarations of items listed in its Annex II.

Art. 2.a.(ix) of the AP requires that States:

> *…shall provide the Agency with a declaration containing the following information regarding specified equipment and non-nuclear material listed in Annex II:*
>
> *For each export: the identity, quantity, location of intended use in the receiving State and date … of export;*
>
> *Upon specific request, confirmation as importing State of information provided by another State concerning the export of such equipment and material.*

Annex II lists the items contained in the NSG Trigger List (INFCIRC 254/Part 1) available in 1995 (Rev. 2). Unfortunately, AP Annex II list has not been amended thereafter, unlike the NSG Trigger List, amended already several times (the current version being Rev. 14 of 2019). This omission creates discrepancies to exporters and

authorities which is addressed in various practical ways as outlined in [23,26].

More relevant to the scope of this paper, is also the fact that Annex II refers only to EQUIPMENT AND NON-NUCLEAR MATERIAL and not to "technology" (except for one occurrence). It is therefore strictly limited to tangible items, unlike the NSG "Guidelines for the Export of Nuclear Material, Equipment and Technology" which already in 1995 extensively referred also to "technology".

5.4 Comments to this section

According to the Model Additional Protocol, the information about technology required to be reported to the IAEA is hence limited to the information provided under art. 2.a. and possibly also associated to Annex I's activities, as well as art. 2.b.(i).

Although the availability of technology (and software to model, assist the processes) may be described in association to AP Annex I's list of indigenous activities, their transfer to third country's entities is not due to be declared to IAEA. There is therefore an inconsistency and distortion with respect to the national export control systems and the NSG guidelines. Moreover, the extent of research activities within the specific country, which must be described to IAEA, may also involve international collaborations and hence technology transfers which could be captured by scientific documents, and which might not be reported in States' declarations.

The verification of the completeness and correctness of the declarations to the IAEA is an important element of the analyses and inspection activities leading to the conclusion about the absence of undeclared activities.

From the IAEA's verification perspective, it would therefore be useful also to analyse the research publications related to the AP Annex I's list of activities, as well as Annex II's items. This may bring additional information about relevant research actors, as well as their possible international research collaborations.

6. TIM Dual-use

TIM Dual-Use is a web-based platform focused on dual-use research developed by the European Commission Joint Research Centre in collaboration with the European Studies Unit of the University of Liège [27].

It is part of the broader Tools for Innovation Monitoring (TIM) developed by the Joint Research Centre to support policy-making in the European Institutions in the field of innovation and technological development.

The TIM DU's database contains three types of documents:

- All the scientific publications contained in SCOPUS, which is the largest abstract and citation database of peer-reviewed literature, covering over 45 million publications in all languages provided that at least the title and the abstract are written in English;
- World-patents from the European Patent Office PATSTAT, covering more than 22 million patents issued by more than 90 patent authorities, including all the major countries, published in English;
- all EU - funded research projects throughout various research Framework Programmes, retrieved from the CORDIS web-site.

The documents date back to 1996, and the database is regularly updated twice a year.

TIM DU has been designed to map scientific abstracts, patents and EU-funded projects against the EU dual-use control list, including of course the nuclear-fuel cycle activities under Category 0.

The data are retrieved on the basis of queries combining keywords related to the controlled items, which are searched in some specific fields, such as the title, the text of the article abstracts, the authors or the organisations' name. Boolean operators (AND, OR, NOT) connect these terms to maximise the number of meaningful results and minimise the irrelevant ones.

TIM DU presents the results and the associated information in various formats, such as connectivity network charts, heatmaps, tables, bar graphs, lists of relevant documents (linked to the original sources, e.g. journals, in which case the access to the full paper depends on the user subscriptions), organisations with their geographical distributions and even authors' names.

A module based on disambiguation algorithms, called Entity Matcher, is applied in order to associate the organisations' names to a location (e.g. in case of an umbrella organisation or daughter companies is the headquarter or the most frequent location in the data that characterises the geographical affiliation), to harmonize the information of the various databases (Scopus, Patstat, and Cordis), as well as to adjust duplicates and mistakes which are sometimes present in the original data of these databases. In addition to that, any residual error can be reported to the TIM administrators and manually fixed.

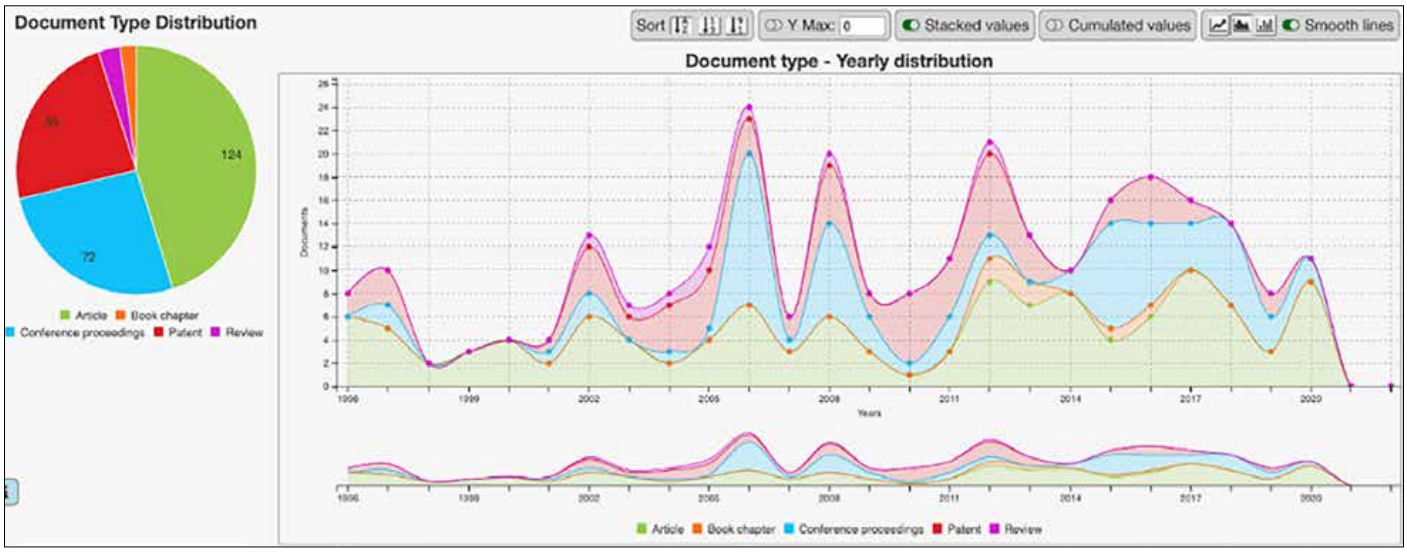

Figure 1: Type of activities related to (i) Gas centrifuges and their evolution over time.

7. TIM DU analyses of AP Annex I activities

The analysis that follows is based on the mapping of some of the fifteen key nuclear fuel cycle-related activities listed in Annex I to the Model Additional Protocol. The results presented are only a fraction of the data collected by TIM DU, considering the limits and the purpose of this paper.

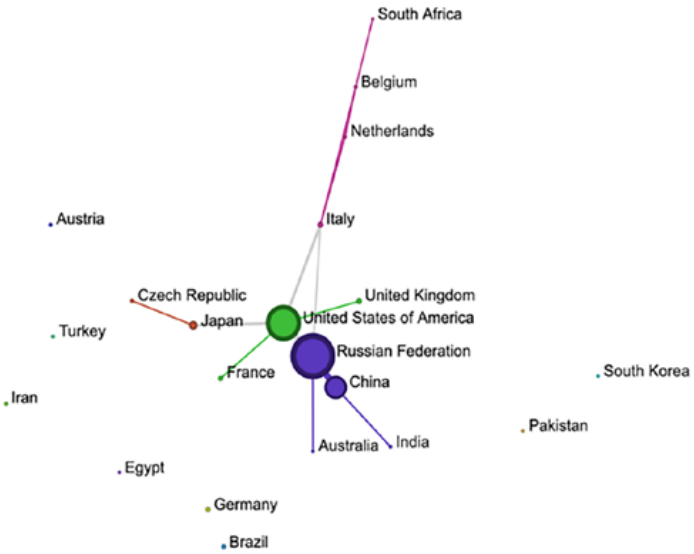

Figure 2: Countries involved in activities related to (i) Gas centrifuges

(i) The manufacture of centrifuge rotor tubes or the assembly of gas centrifuges

This paragraph will focus on the research activities and associated technology relative to the manufacture of centrifuge rotor tubes or the assembly of gas centrifuges.

Type of activities

On the basis of the constructed query, TIM Dual-Use retrieved 485 documents. The graph below shows the type of activities carried and their evolution over time between 1996 and 2020.

Around 38% of the activities are scientific publications, 34% patents, and 28% conference proceedings. No EU-funded projects were retrieved by TIM Dual-Use on the basis of our query.

Involved countries

These documents were produced by entities based in the following 21 countries: Australia, Austria, Belgium, Brazil, China, Czech Republic, Egypt, France, Germany, India, Iran, Italy, Japan, Netherlands, Pakistan, Russian Federation, South Africa, Republic of Korea, Turkey, United Kingdom, and United States of America.

Russia is the leading country with 84 documents associated (35 articles, 30 conference proceedings and 19 patents), whereas the United States, the country with the 2nd largest number of documents, presents mainly scientific publications, with only 2 patents dating back to the '90. China, with 40 associated documents, is the third most active country with 23 articles, 13 conference proceedings, and 4 recent patents.

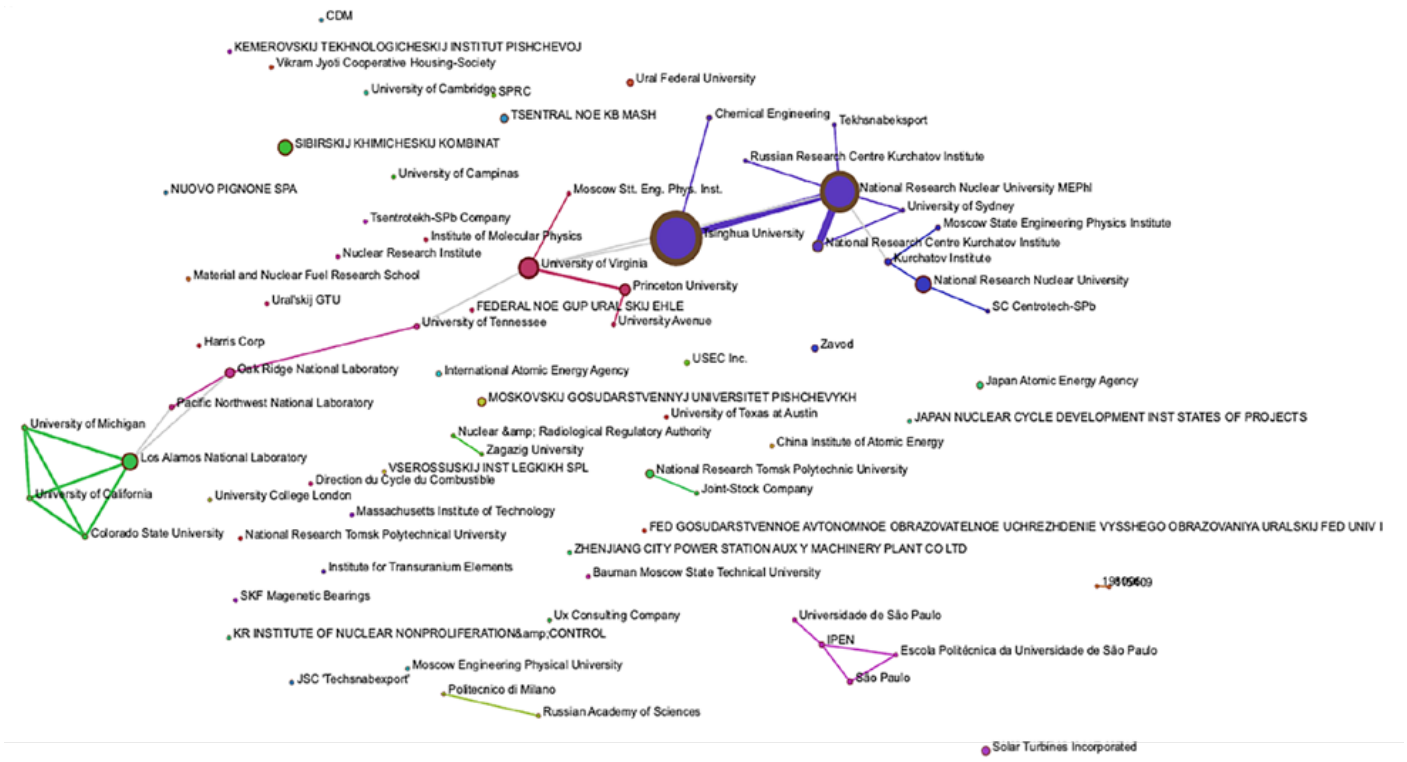

Figure 3: Organisations involved in activities related to (i) Gas centrifuges.

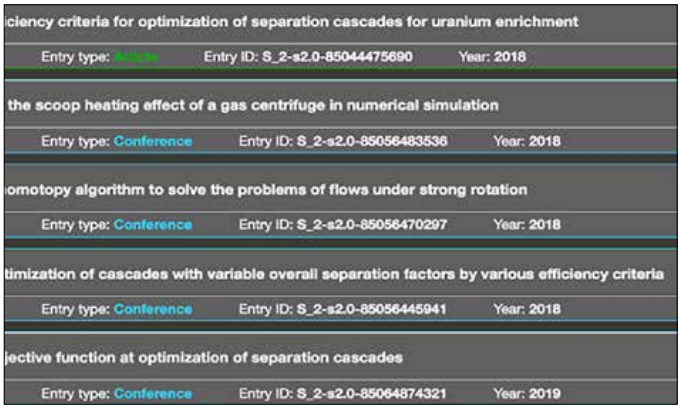

Figure 4: Collaborations between MEPhI and Tsinghua University

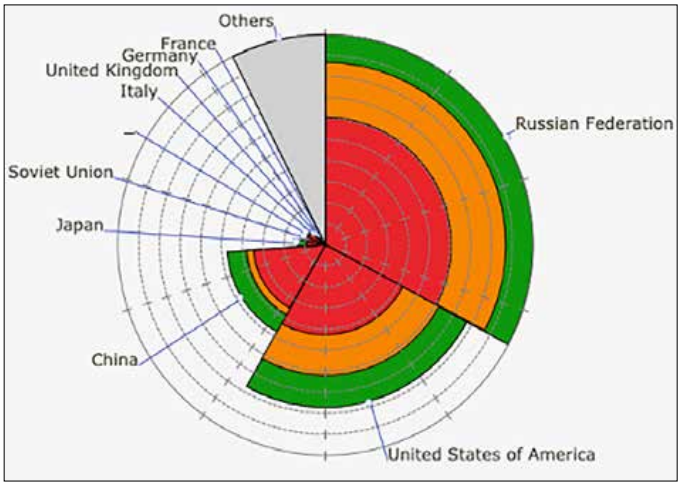

Figure 5: Countries' collaborations

Top 10 involved organisations and their international scientific collaborations

TIM DU identified more than 300 organisations undertaking research & development activities related to gas centrifuges. Among them the top 10 are:

1. National Research Nuclear University MEPhI (Russia);
2. Tsinghua University (China);
3. University of Virginia (USA);
4. Los Alamos National Laboratory (USA);
5. Siberian Chemical Combine - Sibirskij Khimicheskij Kombinat (Russia);
6. Princeton University (USA);
7. National Research Centre Kurchatov Institute (Russia);
8. Oak Ridge National Laboratory (USA);
9. National Research Tomsk Polytechnic University (Russia);
10. Tsentralnoe Konstruktorskoye Byuro Mashinostroyeniya - Design Bureau for Special Machine-Building (Russia).

It is interesting to note that China, and to a lesser extent also Russia, displays a high level of concentration of the activities, carried out by a few organisations, with Tsinghua University at the top.

TIM DU identifies Russia as the most active country and China as its main partner. The National Research Nuclear University MEPhI, the most active organisation, shares five collaborations with the Tsinghua University (China), the second most active organisation.

The collaborations are quite recent, dating from 2018 to 2019, and they concern the optimization of separation cascades for uranium enrichment and the scoop heating effect of a gas centrifuge in numerical simulation. It's also interesting to note that the authors of the publications are almost always the same ones.

MEPhI also collaborated twice with the University of Virginia (USA) even though it dates back to 1999 and 2008. Once again, the authors are the same in both publications, noticing as well that the two Russian authors are also the same ones collaborating with China, even though this time the research focused on the separation of multi-isotope mixtures. The last international collaboration of MEPhI is with the University of Sidney (Australia), an article published in 2020 exploring a new type of plasma centrifuge for isotope separation.

In addition to the collaborations with the MEPhI, the Tsinghua University co-published a study with the University of Virginia (USA) in 2015 on the simulation of the feed, withdrawals, and scoops in the flow field of a gas centrifuge by using Onsager's pancake.

Besides the publications with the MEPhI and Tsinghua University, the University of Virginia has also led a joint study with the Saclay Nuclear Research Centre (France) on the optimization of separative performance using the hypothetical gas centrifuge parameters of the so-called "Iguacu machine". Also here, the American author is still the same one.

Zeng S.	27
Borisevich V.D.	23
Wood H.G.	15
Sulaberidze G.A.	15
Bogovalov S.V.	14
Tronin I.V.	13
Smirnov A.Y.	10
Ying C.	9
Jiang D.	9
VODOLAZSKIKH VIK...	8

Figure 6: Top 10 authors' names

The rest of the scientific collaborations of the other organisations, all took place at the national level.

Top 10 authors' names

TIM DU not only can tell which author worked on a topic and with whom, it can also gather all the documents data and elaborate a list of the authors or inventors in order of their level of activity, showing on how many documents they participated. Figure 7 is an extract of the top 10 authors/inventors' names.

(iii) The manufacture or assembly of laser-based systems

Types of activities

For the research activities related to (iii) Laser-based isotopes separation, TIM DU retrieved 68 documents, which might be indicative of a lesser interest in the topic. This

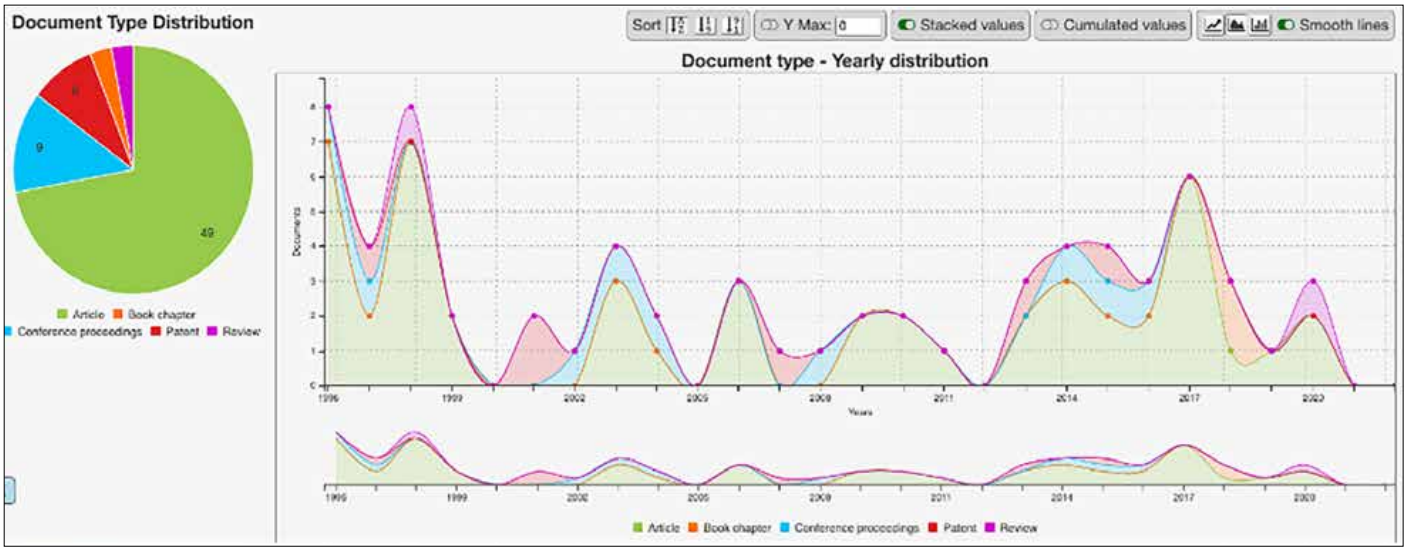

Figure 7: Types of activities related to (iii) Laser-based isotopes separation

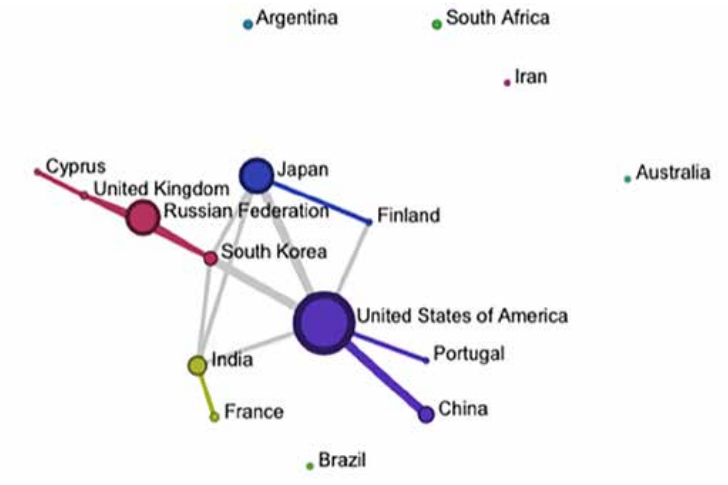

Figure 8: Countries involved in activities related to (iii) Laser-based isotopes separation

consideration might be even more applicable for other activities listed in Annex I to AP, such as the ones related to electromagnetic isotope separators, aerodynamic separation nozzles or vortex tubes, or uranium plasma generation systems. For these topics, TIM DU suggests an even lower level of activity.

Among these 68 documents, the outright majority are scientific articles, while no EU-funded project was found.

Involved countries

TIM DU identified 18 countries as being involved in research and development activities related to (iii)

Laser-based isotope separation: Argentina, Australia, Brazil, Canada, China, Cyprus, Finland, France, India, Iran, Israel, Japan, Portugal, Russian Federation, South Africa, South Korea, United Kingdom, United States of America.

Among these countries, only Japan and the United States own patents.

Top 10 involved organisations

TIM Dual-Use identified more than 70 organisations. Among them the top 10 are:

1. Russian Academy of Sciences (Russia);
2. University of Missouri (USA);
3. University of California (USA);
4. Lawrence Berkeley National Laboratory (USA);
5. University of Michigan (USA);
6. Inst. of Phys. and Chemical Research (Japan);
7. Power Reactor and Nuclear Fuel Development Corporation (Japan);
8. Pacific Northwest National Laboratory (USA);
9. Bhabha Atomic Research Centre (India);
10. Pennsylvania State University (USA).

The Russian Academy of Sciences is at the first place with nine scientific publications, followed by the University of Missouri with three. However, the Russian Academy of Sciences seems to have only national collaborations, namely with the Troitsk Institute for Innovation and Fusion Research and the company 'Lad' Research and Production Association.

Whereas, the University of Missouri co-published a study in 2010 with the Korea Atomic Energy Research Institute on the separation of gaseous molecules in supersonic free jets by laser-assisted selective condensation repression.

The University of California realized two joint studies in 2013, one with the South China University of Technology and one with the Bhabha Atomic Research Centre, both focusing on laser ablation molecular isotopic spectrometry.

While the Lawrence Berkeley National Laboratory co-published with the Spanish Instituto Tecnológico e Nuclear in 2009 a study on the laser synthesis of uranium oxide anions in the gas phase, and in 2015 collaborated with the Ocean University of China on a zirconium isotope analysis using laser ablation molecular isotopic spectrometry. In 2017 the American Laboratory published a joint study with the Korea Institute of Nuclear Safety focusing on uranium optical isotopic analysis in laser induced plasma spectrometry.

The rest of the scientific collaborations were all with national partners.

(x) The manufacture of nuclear grade graphite

Type of activities

Among the 273 documents almost 80% consist in articles and conference proceedings retrieved from SCOPUS, while the rest are patents, with the exception of a single EU project. In fact, as the connectivity graph of the organisations will show, a significant part of the entities are companies.

Involved countries

TIM DU lists 32 countries as involved in activities related to (x) Nuclear grade graphite: Argentina, Australia, Austria, Brazil, Bulgaria, China, Denmark, France, Germany, Greece, Hong Kong, India, Indonesia, Iran, Italy, Japan, Lithuania, Luxembourg, Pakistan, Poland, Romania, Russian Federation, Saudi Arabia, Singapore, South Africa, South Korea, Spain, Taiwan, Turkey, Ukraine, United Kingdom, United States of America.

The United States ranks at the first place with 86 documents, consisting of scientific publications and participation in the EU-funded project.

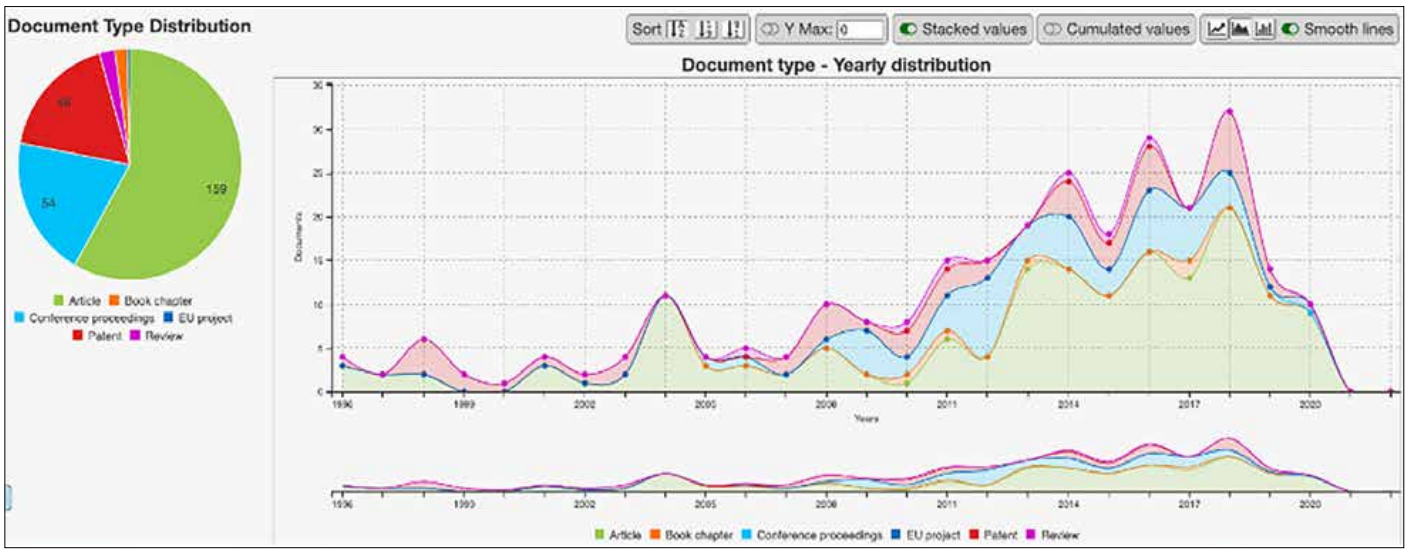

Figure 10: Type of activities related to (x) Nuclear grade graphite

The connectivity graph particularly highlights some strong connections between the country and the United Kingdom, Japan and the Republic of Korea.

Top 10 involved organisations

The organisations identified by TIM DU as being the most active in activities related to (x) nuclear grade graphite are:

1. Tsinghua University (China);
2. Idaho National Laboratory (USA);
3. University of Manchester (UK);
4. Oak Ridge National Laboratory (USA);
5. Korea Atomic Energy Research Institute (Rep. of Korea);
6. University of Missouri (USA);
7. Chinese Academy Of Sciences (China);
8. University of Oxford (UK);
9. University of New Mexico (USA);
10. University of Bristol (UK).

The Tsinghua University had an international scientific collaboration with the University of Hong Kong and University of Minnesota. In 2013 they co-published a study on the fracture properties of two types of nuclear-grade graphite, the Japanese IG11 graphite and Chinese NG-CT-01 graphite. While more recently in 2019, it realized a joint study with the Tokyo Institute of Technology on the kinetic recovery process of low dose neutron-irradiated graphite.

The second most active organisation is the American Idaho National Laboratory. In 2015 it co-published an experimental investigation of the cross flow of the Prismatic Modular Reactor (PMR) with the Seoul National University and Hanyang University.

In 2017 the Laboratory realized a study with the Helmholtz Research Centre (Germany) and University of Leeds (UK) on the neutron irradiation-induced structural changes in nuclear grade graphite types PCEA and PCIB.

While in 2020, it published an article in collaboration with the European Commission JRC based in Karlsruhe (Germany), the Royal School of Mines (UK) and the company EDF Energy Nuclear Generation Ltd (UK) investigating the thermal properties of unirradiated nuclear grade graphite between 750 and 2500 kelvin.

At the third place stands the University of Manchester, which realized in 2011 a joint study with the University of Cape Town (South Africa) and University of Oxford analysing the damage, crack growth and fracture characteristics of nuclear grade graphite using the double torsion technique.

In 2013, it published a study realized with the Celâl Bayar University (Turkey) and still the University of Oxford on the flexural strength and defect behaviour of polygranular graphite under different states of stress.

In 2020 the British University also participated in an EU funded project along with other European organisations from Spain, France, Italy and Lithuania aiming at studying innovative tools for the dismantling of graphite moderated nuclear reactors.

The Oak Ridge National Laboratory collaborated several times with the Japanese Tokai Carbon Co. Ltd.. In 2011 they published along with the Japan Atomic Energy Agency a conference proceeding on the development of new nuclear grade graphite (Fine-grained isotropic graphite) for

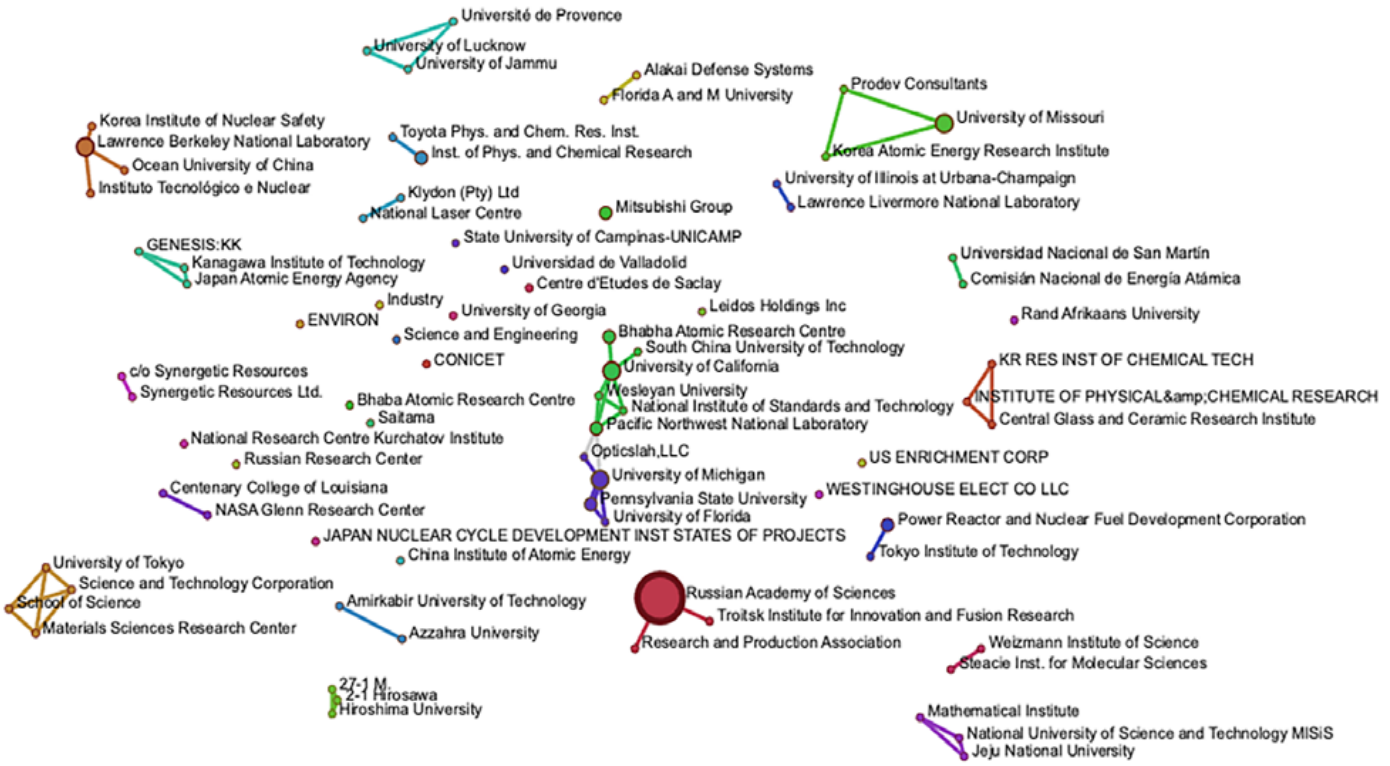

Figure 11: Countries involved in activities related to (x) Nuclear grade graphite

application to Very High Temperature Reactor (VHTR). In 2013 they published another conference proceeding, a microstructural analysis of nuclear grade graphite materials. While in 2016 they co-published an article analysing the property changes of g347a graphite due to neutron irradiation.

In 2011, the Oak Ridge National Laboratory also collaborated with the Korea Atomic Energy Research Institute, they co-published a study on the characterization of tensile strength and fracture toughness of nuclear graphite nbg-18 using subsize specimens.

In addition to the collaboration with the Oak Ridge National Laboratory in 2011, the Korea Atomic Energy Research Institute also collaborated with the Japan Atomic Energy Agency in 2013, publishing a study on the oxidation behaviour and property degradation of nuclear-grade c/c composites oxidized in air.

Besides the publications with the University of Cape Town and Celâl Bayar University realized along with the University of Manchester, the University of Oxford, co-published in 2017 a study on damage tolerance of nuclear graphite at elevated temperatures with the University of Bristol (UK), the American Lawrence Berkeley National Laboratory, University of California, and the Australian School of Mechanical and Manufacturing Engineering.

(xii) The manufacture of reactor control rods

Type of activities

The constructed query resulted in 1980 documents, with the peculiarity of having more than half of them constituted by patents, distributed almost homogeneously over the years.

Both the amount of results and their distribution over time suggest an active interest on the technology associated to the topic.

Involved countries

TIM DU detected the involvement of 51 countries in the research and development activities related to (xii) Reactor control rods: Argentina, Australia, Austria, Bangladesh, Belgium, Brazil, Bulgaria, Canada, China, Croatia, Czech Republic, Egypt, Finland, France, Georgia, Germany, Ghana, Greece, Hong Kong, Hungary, India, Indonesia, Iran, Italy, Japan, Jordan, Lithuania, Malaysia, Mexico, Netherlands, Nigeria, Norway, Pakistan, Poland, Romania, Russian Federation, Saudi Arabia, Singapore, Slovakia, Slovenia, South Africa, South Korea, Spain, Sweden, Switzerland, Syria, Taiwan, Turkey, Ukraine, United Kingdom, United States of America.

However, taking into consideration only the patenting activities, the map limits the number of countries to fifteen (see figure 16 here below).

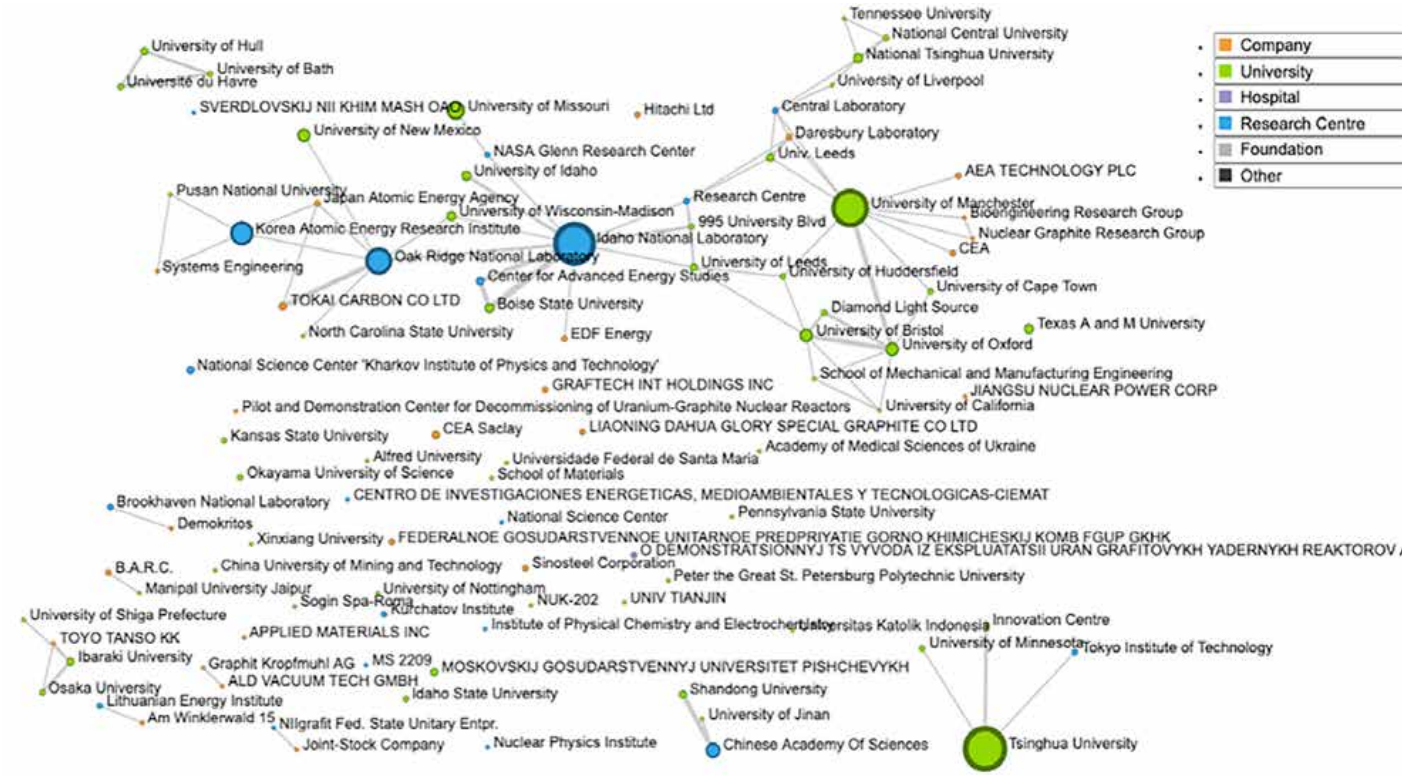

Figure 12: Organisations, shown per type, involved in activities related to (x) Nuclear grade graphite

At the first place is China with 628 documents, half of which are made up of patents. The same proportion applies to the United States, even though Chinese activities are three times more than the ones associated to US organisations. While for Japan, patents account for more than 85% of its 586 activities.

Top 10 involved organisations

Among the top 10 organisations listed by TIM DU, seven of them are companies:

1. Toshiba Corp (Japan);
2. Hitachi Ltd (Japan);
3. Nuclear Power Institute of China (China);
4. Tsinghua University (China);
5. Mitsubishi Group (Japan);
6. CHINA GENERAL NUCLEAR POWER(China);
7. CGN POWER CO., LTD. (China);
8. WESTINGHOUSE ELECT CO LLC (USA);
9. CHINA NUCLEAR POWER ENG CO LTD (China);
10. Korea Atomic Energy Research Institute (Rep. of Korea).

Both Tohiba Corp and Hitachi Ltd realized almost exclusively patents and without any international collaboration. Also the Nuclear Power Institute of China had only domestic collaborations. While the Tsinghua University realized only one international scientific collaboration with the German Karlsruhe Institute of Technology and the American Washington University in Saint Louis. It took place in 2020 and concerned a review of sensors to measure control rod position for nuclear reactor.

The WESTINGHOUSE ELECT CO LLC published a conference proceeding with the Taiwanese National Tsing Hua University on the analysis of PWR reactor vessel upper plenum sections (flow simulation in control rod guide tubes), and a collective conference proceeding with the participation of institutes from Mexico, Japan, Brazil, Italy and Croatia concerning the integral design description of the International Reactor Innovative and Secure (IRIS), including its control rod drive mechanisms.

The Korea Atomic Energy Research Institute contributed to a conference proceeding with several Japanese institutes, including the Japan Atomic Energy Agency, dating back to 2011. The study analysed the fracture behaviour of 2d-c/c composite for application to control rod of very high temperature reactor.

While in 2018, the Korea Atomic Energy Research Institute co-published a study with the Saudi research and governmental entity “King Abdullah City for Atomic and Renewable Energy”. The paper studied the applicability of reed switch type rod position indicator for a nuclear reactor.

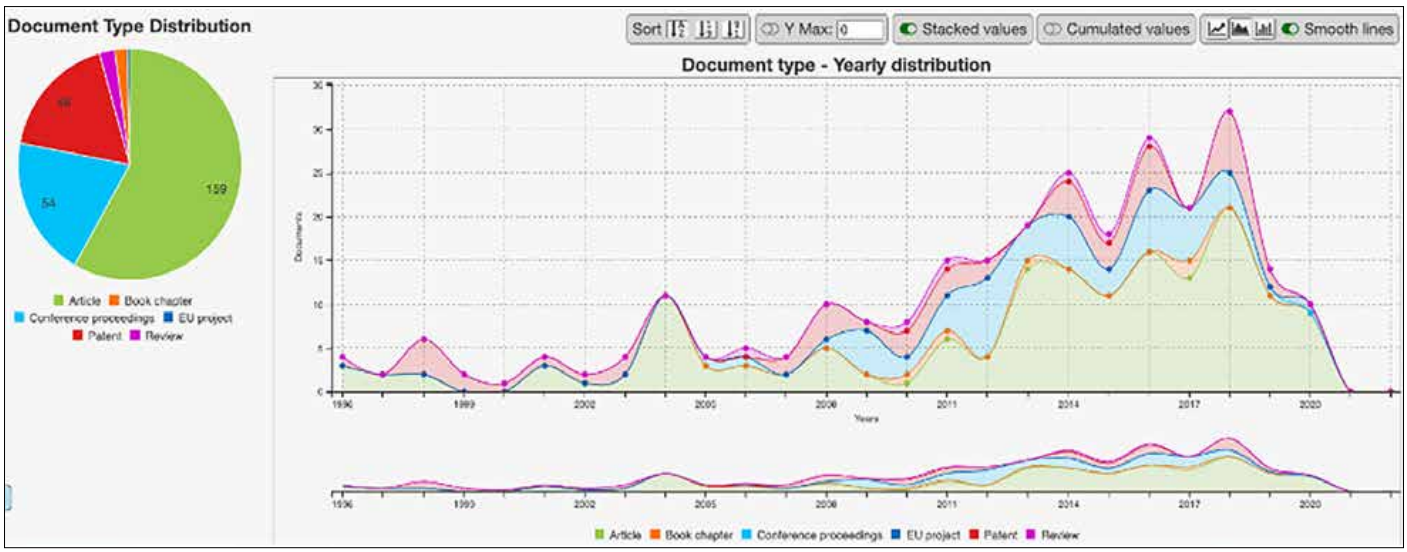

Figure 13: Types of activities related to (xii) Reactor control rods

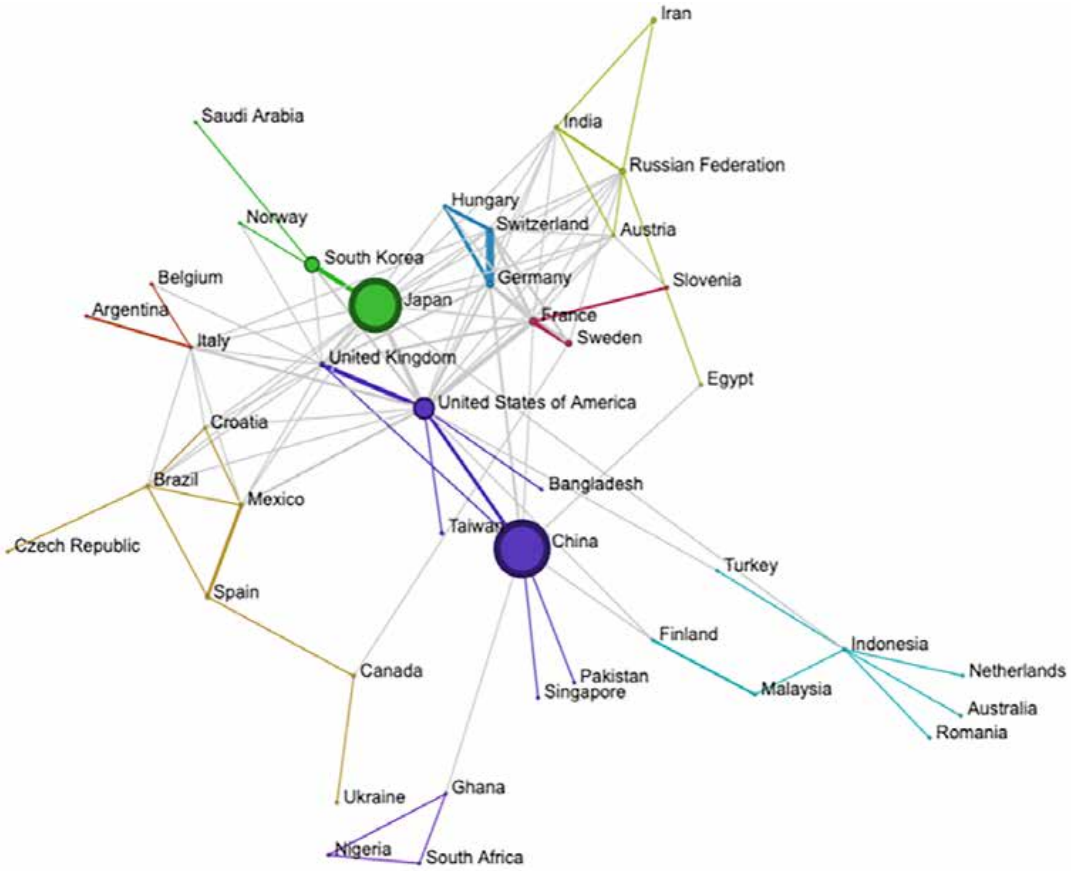

Figure 14: Countries involved in activities related to (xii) Reactor control rods

8. Comments on the TIM DU analyses

The analyses show how TIM DU can provide useful insights both to the national authorities, in charge to provide to the IAEA the information required by the Model Additional Protocol, and to the IAEA to verify the completeness and correctness of the information.

National authorities could get a more complete information about the research carried out in the country about Trigger List related items, including also international research collaborations previously not known and worthwhile to be considered as potential sources of technology transfers.

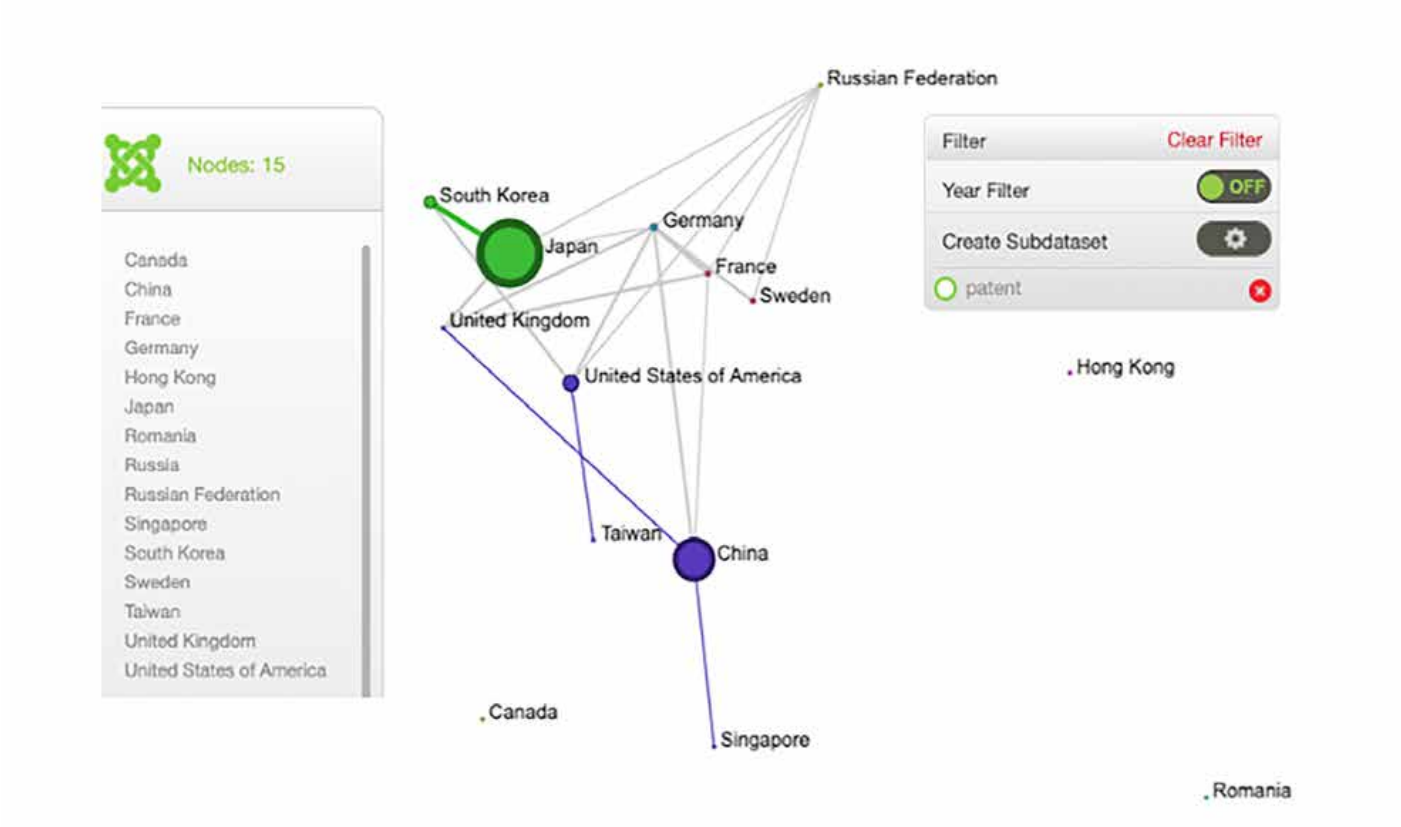

Figure 15: Countries involved in activities related to (xii) Reactor control rods

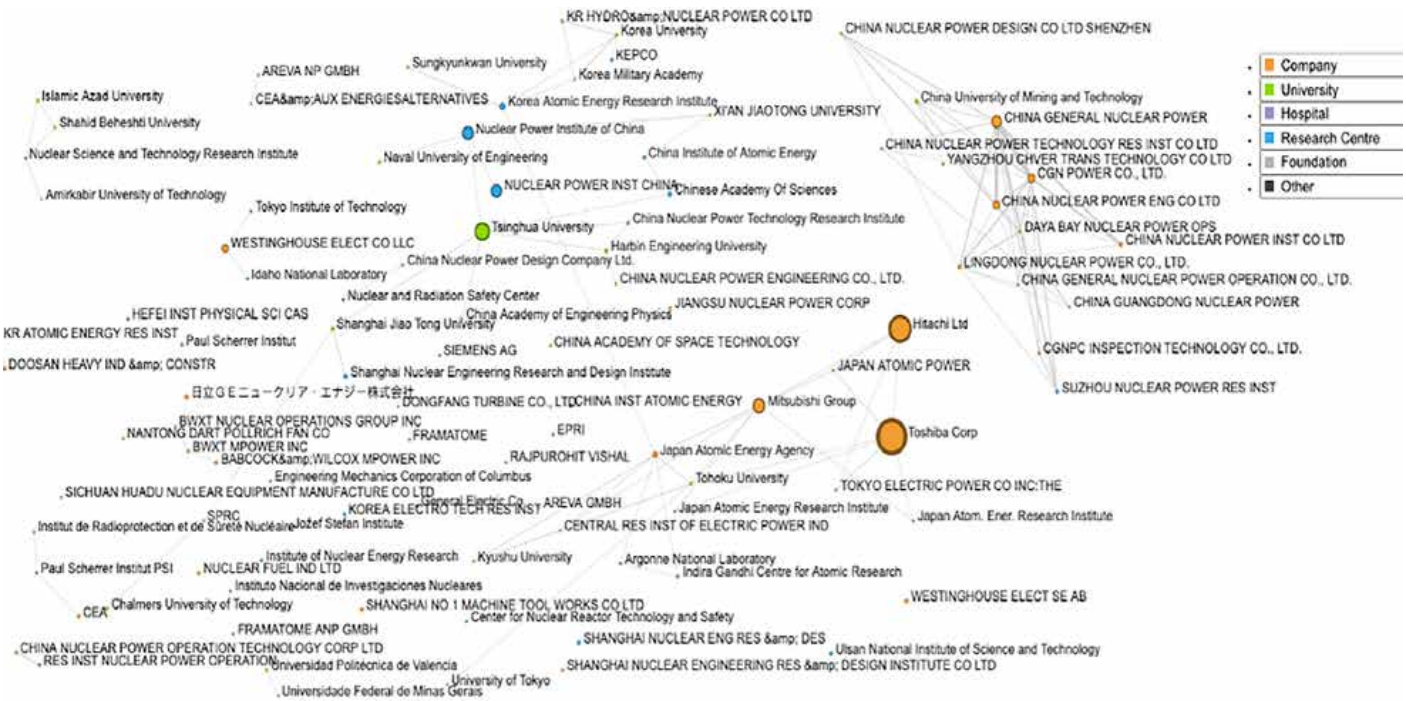

Figure 15: Countries involved in activities related to (xii) Reactor control rods

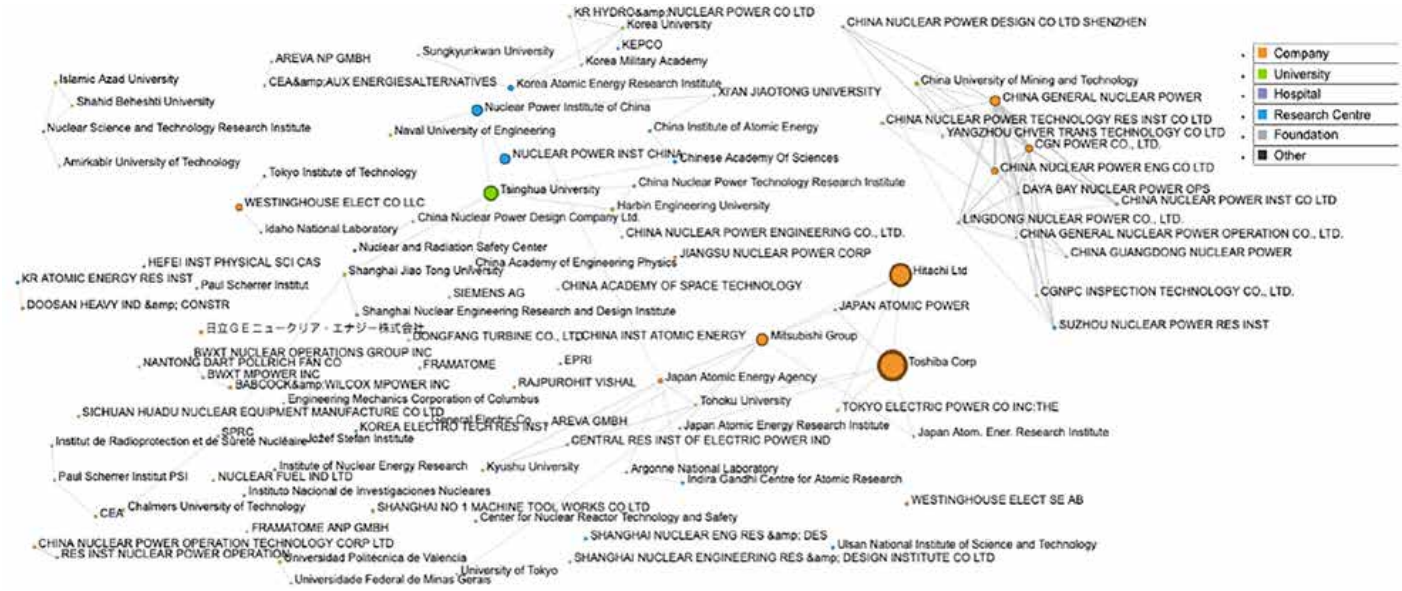

Figure 16: Organisations, shown per type, involved in activities related to (xii) Reactor control rods

For the IAEA, the analyses could be interesting to look at the big picture of indigenous research in connection to international scientific collaborations, possibly involving also technology transfers and technical assistance.

As a starting point, we considered to assess publications and patents related to Annex I's fifteen key nuclear fuel cycle-related activities, because although related to "manufacturing", they have of course also to encompass research activities and the associated technology, i.e. technical data and possibly also technical assistance (art. 2.a.iv).

To be more complete, one could also look at the entire breadth of nuclear research and associated technology by checking with TIM DU the results related to the entire NSG TL, for which queries are also available (Category 0).

By extension, also the verification of the declarations containing export-related information regarding specified equipment and non-nuclear material listed in Annex II (art. 2.a.ix) could be complemented by assessing possible nuclear technology transfers by TIM DU datasets covering both the NSG lists, noting also that the minimum technology for installation and maintenance is automatically included in the export authorisation of tangible goods.

Along this line, we would add as a final observation that, although not called for by the AP, we consider essential to verification also checking the items listed in the Nuclear Suppliers Group Dual-Use List, including goods, software and technology. As shown by the most notorious proliferation cases, dual-use items are indeed integral, and sometimes alternative, key elements for undeclared illicit manufacturing activities, that could involve also research and intangible technology transfers.

TIM DU is also a valuable export compliance support to researchers, called to comply with export regulations. By detecting past scientific production potentially involving dual-use items, TIM DU could be a valuable help for better targeting specific research entities to raise their awareness and encourage them to tailor their internal compliance programmes .

An in depth assessment of the material obtained (full paper of the abstracts, public patents) is anyway needed, also before concluding that the documents might have required export authorisations. TIM DU's datasets include the list of abstracts retrieved by the query, with hyperlinks to the original journal, where the full article may be available or purchased. For patents, the hyperlink leads to the information contained in PATSTAT; the same happens for an EU-funded project stored in the CORDIS database.

A disclaiming note is also necessary: TIM DU's queries allow retrieving documents possibly related to dual-use controlled items, but a certain degree of uncertainty is inherently present. The collections of datasets retrieved may not be complete, nor always fully relevant to the object of the query. As previously outlined, at times, there might be errors deriving from incorrect downloading of the database records. Depending on the original information provided to the journals and then sent to SCOPUS, organisations' names might differ for the use of full titles, acronyms etc. Part of the analysis is dedicated to cleaning the data accordingly.

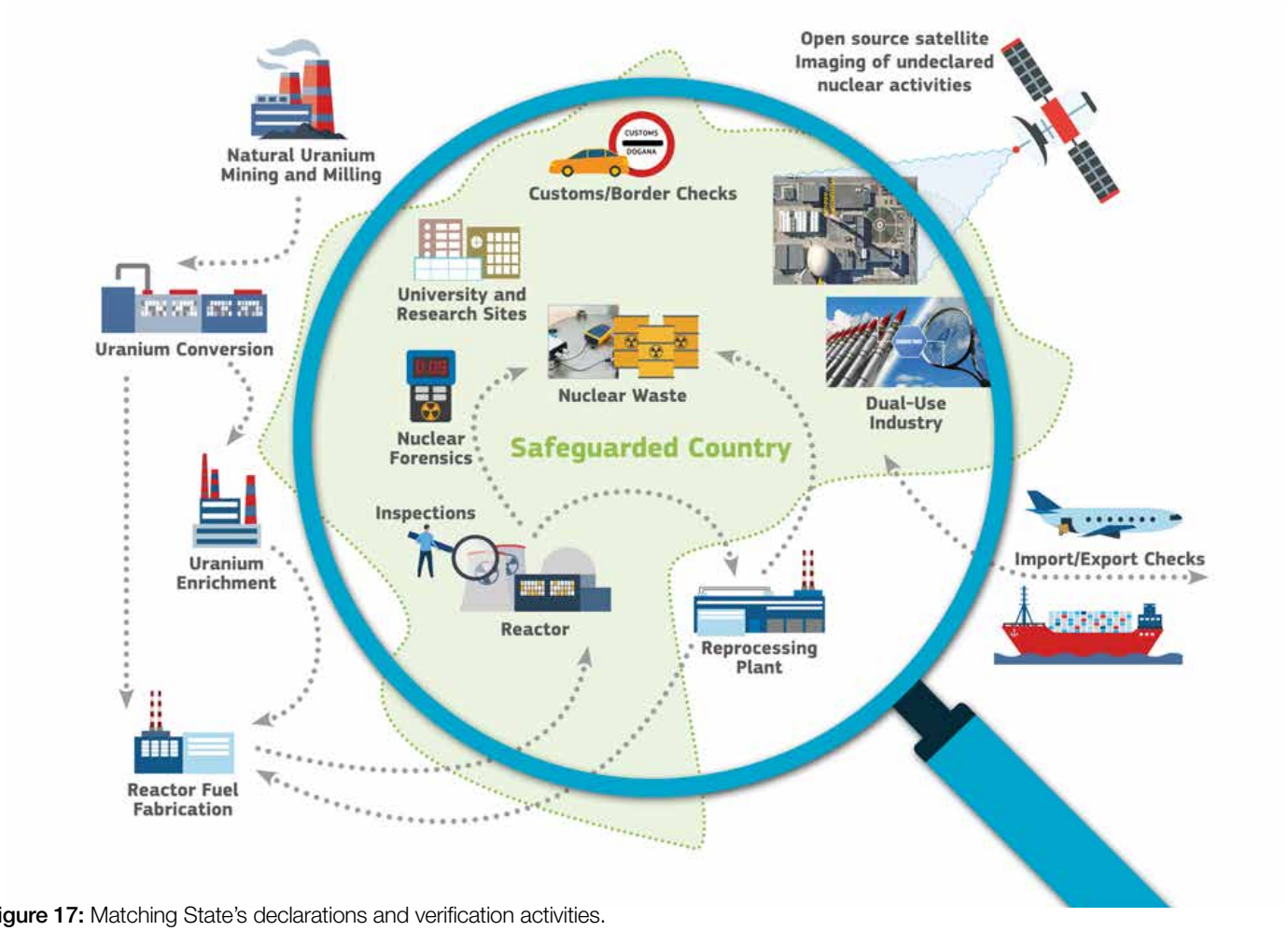

Figure 17: Matching State's declarations and verification activities.

9. Conclusions

Strategic export controls are a barrier against proliferation and the unauthorised access to strategic technology and goods, which developed in parallel to nuclear safeguards for decades.

The verification of the completeness and correctness of the declarations to the IAEA is an important element of the analyses and inspection activities leading to the conclusion about the absence of undeclared activities, as summarised in Figure 17.

Besides manufacturing activities and exports of tangible items, also research activities and transfers of nuclear technology may play an important role in proliferation programmes.

Various types of information are required by the Model Additional Protocol, including nuclear research in areas pertaining to the nuclear fuel cycle, also not involving nuclear materials.

Together with many dual-use goods and emerging technologies, TIM DU maps nuclear-fuel cycle activities' scientific abstracts, patents, and EU-funded projects, allowing to gather lists of documents, geographical distributions, collaborations, and authors, providing a quantitative and qualitative overview of the potential issues and to identify areas of possible risk.

These results can be helpful to the national authorities submitting declarations to IAEA in accordance to Additional Protocol's Article 2.a, both to identify previously unknown national research actors and to raise the awareness of national research entities about potential sensitivities with external collaborators.

The IAEA could also use TIM DU to support the verification of the completeness and correctness of declaration concerning research about the nuclear fuel cycle.

Research organisations and other involved entities could also consult TIM DU to identify their past scientific production, which could include dual-use aspects and tailor their compliance programmes accordingly.

TIM DU has been launched in January 2021 and is under continuous testing and validation. Any useful feed-back will be precious and enabling our future improvements. While the nuclear controls are extensively mapped, more queries may be necessary to complete the other dual-use categories.

10. Acknowledgements

The authors would like to thank the European Commission Joint Research Centre's Text and Data Mining unit for the valuable support in the development of the TIM DU platform.

11. References

1. Paile, S., Michel, Q., Caponetti, L., Charatsis, C., & Marrone, E. (2018). Do academic activities contribute to WMD proliferation?. Chaudfontaine Group, European Studies Unit (University of Liege)
2. Stewart, I. (2016). Examining Intangible Controls. Project Alpha, King's College London
3. Brockmann, K. and Kelley, R. (2018). The challenge of emerging technologies to non-proliferation efforts: Controlling Additive Manufacturing and Intangible Transfers of Technology. SIPRI.
4. Charatsis, C. (2017). Dual-use Research and Trade Controls: Opportunities and Controversies. Strategic Trade Review, Vol. 3(4) (Spring 2017), pp.47-68
5. Bromley, M. and Maletta, G. (2018). The challenge of software and technology transfers to non-proliferation efforts: Implementing and complying with export controls. SIPRI
6. Council Regulation No 428/2009 of 5 May 2009 setting up a Community regime for the control of exports, transfer, brokering and transit of dual-use items (Recast), (2009).
7. European Parliament legislative resolution of 25 March 2021 on the proposal for a regulation of the European Parliament and of the Council setting up a Union regime for the control of exports, transfer, brokering, technical assistance and transit of dual-use items (recast) (COM(2016)0616 – C8-0393/2016 – 2016/0295(COD))
8. Nuclear Suppliers Group, NSG, www.nuclearsuppliersgroup.org
9. Missile Technology Control Regime, www.mtcr.info
10. Australia Group, www.australiagroup.net
11. Wassenaar Arrangement www.wassenaar.org
12. Organisation for the Prohibition of Chemical Weapons, OPCW, http://www.opcw.org/
13. COMMISSION DELEGATED REGULATION (EU) 2020/1749
14. European Commission, Targeted consultation on draft EU compliance guidance for research involving dual-use items (https://trade.ec.europa.eu/consultations/index.cfm?consul_id=292).
15. Commission Recommendation 2019/1318 on internal compliance programmes for dual-use trade controls under Regulation 428/2009.
16. IAEA INFCIRC/267 (March 1979), THE REVISED GUIDING PRINCIPLES AND GENERAL OPERATING RULES TO GOVERN THE PROVISION OF TECHNICAL ASSISTANCE BY THE AGENCY
17. F. Sevini, G. Renda, S. Cagno, X. Arnes Novau, C. Charatsis, W. Janssens, Export control and nuclear safeguards, ESARDA BULLETIN, No. 60, June 2020
18. United Nations Security Council. Resolution 1540 Adopted by the Security Council at its 4956th Meeting, on 28 April 2004, S/RES/1540, 2004
19. IAEA INFCIRC/140 - TREATY ON THE NON-PROLIFERATION OF NUCLEAR WEAPONS (1970)
20. IAEA INFCIRC/254/Rev.14/Part 1, GUIDELINES FOR NUCLEAR material, equipment and technology, available at www.nuclearsuppliersgroup.org
21. IAEA INFCIRC/254/Rev.11/Part 2 GUIDELINES FOR TRANSFERS OF NUCLEAR-RELATED DUAL-USE EQUIPMENT, MATERIALS, SOFTWARE, AND RELATED TECHNOLOGY, available at www.nuclearsuppliersgroup.org
22. IAEA INFCIRC/540 (Corrected). Model Protocol Additional to the Agreement(S) Between State(S) and the International Atomic Energy Agency for the Application of Safeguards, (1997).
23. Filippo Sevini, Renaud Chatelus, Malin Ardhammar, Jacqueline Idinger, Peter Heine, States' reporting of Annex II exports (AP) and the significance for safeguards evaluation, IAEA SG Symposium 2014
24. F. Sevini et al., Some ESARDA Parties' experience with Additional Protocol export control declarations, paper presented at the 33rd ESARDA Symposium, Budapest 2011, available at https://esarda.jrc.ec.europa.eu/
25. M. Ardhammar, "Trade and procurement analysis in the context of IAEA safeguards", Presentation at ESARDA Joint meeting on "IAEA State Level Concept", Nov 12, 2013, Ispra ,12 November 2013; M. Ardhammar, "Responding to Verification Challenges Caused by Increasing Nuclear-Related Trade", Presentation at Symposium on International Safeguards, 5-9 November 2018.
26. Persbo, A., & Woodward, A. (2014). Detection, deterrence and confidence-building: improving multilateral technology controls. In Meier, O. (2014). Technology transfers and non-proliferation: between control and cooperation. Routledge, pp. 76-95.
27. TIM Dual-Use: https://knowledge4policy.ec.europa.eu/text-mining/tim-dual-use_en

Three properties of Distributed Ledger Technology systems applied in the nuclear sector adding value to safeguards – immutability, timestamping and auditability

Marco Sachy, Roberto Spigolon and Stefan Nonneman

European Commission, Joint Research Centre (JRC), Ispra, Italy
Directorate G - Nuclear Safety and Security
Nuclear Security Unit
E-mail: marco.sachy@ec.europa.eu, roberto.spigolon@ec.europa.eu, stefan.nonneman@ec.europa.eu

Abstract

We present our preliminary findings from the exploratory research project Shared Ledger Technologies for Nuclear Safeguards (SLT4SFG) conducted at the Joint Research Centre of the European Commission. As long as nuclear fuel (fresh or spent) is stored in facilities of a state, that state should always comply with the international non-proliferation treaty. Safeguards' verification processes will be affected also by the digital transformation. The exploratory research project SLT4SFG, has the objective to provide an evidence-based analysis on the benefits and challenges of Distributed Ledger Technology (DLT) systems for the nuclear sector, with special emphasis on safeguards. After presenting background knowledge on DLT systems, we discuss three key properties adding value to nuclear safeguards processes: (1) practical immutability can improve security of sensors identity management; (2) data anchoring through decentralised timestamping can provide proofs of existence and non-alteration of relevant data; and (3) auditability can increase efficiency in data sharing and become a source of forensic evidence to help determine legal liability. We inferred these three properties of DLT systems by endorsing a deductive methodology for the definition of nuclear sector use cases on containment and surveillance and radiation protection. Our aim is to frame a Proof-of-Concept strategy of software implementations intended to be ultimately exploited in nuclear safeguards. We conclude pointing to future research on performance tests simulated on the JRC Experimental Infrastructure for Internet Contingencies. We will aim at offering metrics to quantitatively measure the performance and derive added value of DLT systems properties applied to nuclear safeguards

Keywords: Distributed Ledger Technology; blockchain; safeguards; immutability; timestamping; auditability.

1. Introduction

In the nuclear industry, the regulatory requirement to avoid the diversion of nuclear material from its intended uses shall be met for many years to come [1]. Indeed, nuclear safeguards will be required in both the near and distant future to ensure that nuclear material will be used only within regulatory constraints. In order to lower operational costs and increase efficiency in the management of nuclear safeguards business processes such as – but not limited to – containment and surveillance and nuclear material accountancy, the digital transformation in the nuclear industry will arguably have a significant impact also on safeguards.

Among many technologies such as robotics, the Internet of Things or still Artificial Intelligence, the European Commission considers also Distributed Ledger Technology (henceforth, DLT) systems, such as blockchains, as innovations with a high transformative potential. In this context, the European Union is promoting initiatives such as the European Blockchain Partnership [2], the EU Blockchain Observatory and Forum [3] together with open consultations for the European Blockchain Services Infrastructure [4] and the European Blockchain Pre-Commercial Procurement [5].

As a contribution to a strategy on "continuity of knowledge and data for very long periods", the European Commission's Joint Research Centre is providing insights and foresight on DLT systems in various domains. While we leave political and legal considerations to future research, the scope and purpose of this paper is exclusively to present our preliminary evidence-based technical research outputs from the exploratory research project Shared Ledger Technologies for Nuclear Safeguards (SLT4SFG) [6]. The objective of the SLT4SFG explorative research project is to provide evidence-based answers on whether and to what extent DLT systems and their properties can improve and add value to nuclear safeguards business processes.

Roughly put, DLT systems implement peer-to-peer networks deployed to validate digital assets' transaction history on an append-only and tamper-evident log, replicated to all participating nodes. DLT systems leverage applied cryptography and distributed computing to achieve consensus on global system state among either completely or partially distrusting parties.

While they periodically experience 'hype' phases, DLT systems form a new family of technologies that has not been yet thoroughly explored and validated. Our preliminary evidence-based findings suggest that individual properties of DLT systems can already add value to nuclear safeguards business processes by becoming a features' layer firstly added to, and in the future possibly replacing, legacy systems. In other words, as we will argue more in detail in the sections below, DLTs systems' properties can add a synergistic layer of functionality to legacy systems, viz. a series of complementary modules that can be initially identified by the three properties discussed in this paper. In the future, especially in the case where DLT systems will be validated and standardised, various properties that today we propose to deploy autonomously in concert with legacy systems could entirely replace them.

Accordingly, below we discuss three key DLT systems' properties, i.e. practical immutability, decentralised timestamping and structural auditability. In our view, they offer benefits and add value to nuclear safeguards data management techniques. These properties emerged as the most relevant ones for testing use cases in different nuclear sector's domains: nuclear safeguards - with a focus on containment and surveillance - and radiation protection. For the use cases on radiation protection, we indicate how the same principles could be relevant for nuclear safeguards.

Firstly, we introduce practical immutability as a property related to public distributed ledgers through a use case in the context of containment and surveillance that does not involve any sensitive data. We propose to leverage practical immutability of data stored on a public blockchain for Public Key Infrastructure management to prevent that a malicious insider forge a valid digital identity for a sensor used in safeguards containment and surveillance without leaving any trace. Alongside increased cybersecurity, adding a blockchain-based module to Public Key Infrastructure management can contribute to deploy new systems for remote monitoring (e.g. with the use of digital seals). This could desirably impact inspections planning activities with potential cost savings related to the deployment of human resources.

Secondly, we introduce decentralised timestamping as another property inherent to public distributed ledgers that can be used as a data anchoring service for datasets, proving both the existence of data at a certain moment in time and the absence of alterations. We identified the benefits of this property in the radiation protection context, as an integrity layer to prove in the future that historical data on absorbed doses of personnel will not have been modified. The same property can be leveraged by nuclear installations operators in the context of nuclear material regular mailbox declarations, especially in the case where such declarations are not sent to the inspectorate but remain inside the facility. Moreover, decentralised timestamping offers a supplementary layer of integrity for databases and datasets backups.

Thirdly, we introduce structural auditability as a property of distributed ledgers in general. We studied the benefits of this property on the digitalisation of the radiation passbook used by workers (and inspectors as well) when travelling between different nuclear sites. By virtue of its internal structure as a chain of transactions, a digital radiation passbook implemented with a permissioned DLT system structurally provides an auditable trail of the history of records related to workers exposed to ionizing radiation. Considering also the non-repudiation property (i.e. who committed a transaction cannot repudiate it), DLT systems can thus become a source of forensic evidence that can be used to help determine legal liability in case of disputes.

Moreover, the deployment of smart contracts (i.e. computer programs encoding a business logic whose output is stored on each node of a distributed ledger) automates and enforces the execution of workflows and lowers the rate of clerical errors. Because information exchange would take place on a commonly shared system, rather than through different centralised databases still processed with a significant degree of human intervention as for current practices, it follows that a DLT-based system would be even more easily auditable from a backend perspective. The same kind of approach could be applied also in the domain of Nuclear Material Accountancy and Control as a way to integrate and coordinate the execution of the workflows related to nuclear material accountancy, ease both data sharing procedures and the auditability of the whole process.

Although not all of them are strictly related to nuclear safeguards, the use cases presented below have been selected by endorsing a broad deductive methodology. From the DLT systems' properties, we inferred use cases through a top-down scientific experimental approach to test them in the nuclear sector. For each use case, we then endorsed the best fit-for-purpose software development methodology to implement a Proof-of-Concept strategy. In this way, we could better assess whether and to what extent our deductions were corroborated by evidence to prove the correctness, or lack thereof, about our ideas on the applicability of DLT systems properties to the nuclear sector with special focus on added value for nuclear safeguards.

The remainder of this paper is structured as follows. Section 2 briefly presents related work and elicits background knowledge on DLT systems by providing an analysis of their general benefits and challenges. Section 3 concisely elicits our methodological choices. Section 4 analyses three key DLT systems' properties, their benefits and added value to nuclear safeguards. We conclude the paper in Section 5 pointing to a potential way forward for future research on performance testing with the emulation of use

case implementations on the JRC Experimental Platform for Internet Contingencies (EPIC). This will enable us to reproduce the performance of DLT systems behaviour in real world network conditions, under a fully controllable experimentation environment. In this way, we will aim to establish more granular quantitative metrics to measure both benefits and added value of DLT systems' properties applied to nuclear safeguards.

2. Related work and background knowledge on DLT systems

2.1 A brief introduction to DLT systems

The European Commission is not the only organization currently exploring the applicability of DLT systems in the nuclear safeguards domain. To our knowledge, there are other active actors in the field, especially in research institutes in the United States of America, also with international collaborations, for instance experimenting on nuclear safeguards data management [7], transit matching [8] and on aspects of DLT systems deployment for UF6 cylinder tracking and process monitoring [9].

First, to our knowledge the Stimson Centre is currently the main actor in the United States landscape that is exploring DLTs added value applications in this domain [10] through its "Blockchain in practice" program. Together with the University of New South Wales (UNSW) and the Finnish Radiation and Nuclear Safety Authority (STUK), they launched the SLAFKA prototype: a permissioned blockchain system that enables nuclear facilities to record nuclear material assets on a distributed ledger. It is implemented using Hyperledger Fabric [11], an open source permissioned DLT project maintained by the Linux Foundation. SLAFKA has been implemented to test DLT and how such technology performed in handling safeguards transactions: instead of having a primary role of the regulators to settle the transactions, nuclear facilities would be able to transact assets whilst being supervised by regulators. SLAFKA's prototype outcomes are:

1. The introduction of a distributed networking approach to safeguards reporting.
2. A way to reduce reconciliation time among State and operators.
3. A single source of truth for the management of safeguards information.

Secondly, the Pacific Northwest National Laboratory (PNNL) simulated a transit matching system based on DLT, experimenting with both Hyperledger Fabric and Ethereum [8]. Their main goal was to understand whether a DLT system could bring benefits in comparison to the current IAEA approach. The outcomes on this prototype are:

1. a DLT system could improve the efficiency of the process through real-time match attempts of all transactions posted to the ledger.
2. Using "graded scores" applied to match attempts could represent a useful source of information for increasing the effectiveness of safeguards inspections.
3. Since the DLT system is a tamper-evident record of transactions, transit matching operations performed on such a system could lead to an increased confidence on IAEA safeguards conclusions through transparent reconciliation of transit matching reports.

Because they are converting a legacy system into a DLTs-based one, they also highlight that among these three findings, only the last one is really dependent on the technology used (i.e.: a distributed ledger), while the first two could be achieved also with "traditional" technologies.

Finally, Sandia National Laboratories built their DLT-based prototypes on the field. According to information shared during the 2020 Institute of Nuclear Material Management (INMM) Annual Meeting [9], they built a prototype based on a private version of Ethereum where they stored together Inventory Change Reports data and sensors data such as gamma-ray events and video cameras recordings. The idea was to enable workflows, e.g. retrieving of sensors data to validate an inventory change.

In terms of background knowledge on DLT systems, the past decade witnessed significant advancements in integrated and applied cryptography for the innovation of distributed computing with the introduction of public blockchains such as Bitcoin [12] and more in general DLT systems [13] as blockchains are a subset of this larger class. Fully aware that the cryptologic history of these systems dates back decades, here we limit ourselves to an overview on this family of technologies by referring to the conceptual genealogy of the notion of 'blockchain', both in applied cryptography and in the nuclear industry.

Because a genealogy of a concept researches its original meaning to then provide current definitions, we will begin by presenting an etymology of this term. In applied cryptography, the term 'block-chain' can be traced back to block cyphers modes of operation algorithms [14]. In particular, the algorithm for Cipher Block Chaining (CBC) mode is defined such that "the plaintext is XORed with the previous ciphertext block before it is encrypted" [15]. Similarly, in the nuclear sector, the idea of using cryptographic techniques to ensure that data acquired to verify treaty compliance be trustworthy is also not new [16]. In effect, during the 20th century, cryptographers operating in the nuclear sector developed techniques to solve problems of mutual distrust, whereby "data as well as the redundant identifying information would be block-chain encrypted" [16].

What has been novel in the more recent past, perhaps relies in the fact that cipher block-chaining evolved and coalesced with other advancements in cryptology for digital cash applications such as e-cash [17] [18] and hashcash as a Proof-of-Work system [19] [20] into increasingly popular public blockchain protocols. After an initial focus on the seminal application, i.e. cryptocurrency, it became increasingly clear that the underlying blockchain technology had farther reaching implications and the potential to bring innovation to entire industries.

From a genealogical point of view, the reference implementation for DLT systems, i.e. the Bitcoin blockchain is a data structure representing the ledger of transactions that everyone participating to the network can store to acknowledge a common transaction history:

"a blockchain data structure is an ordered, back-linked list of blocks of transactions. Each block within the blockchain is identified by a hash, generated using the SHA256 cryptographic hash algorithm on the header of the block" [21].

This technical arrangement enables network participants to share a common transaction history among a group of distrusting peers or nodes. In the Bitcoin reference implementation [10], nodes compete to generate the next block and acquire a reward by consuming resources, i.e. electricity, to run the consensus algorithm, in the case of Bitcoin based on a Proof-of-Work mechanism. This mechanism is put in place to avoid that block producers named miners assign to themselves extra coins and engage in double spending. Participants can freely join the network by downloading the client without the need for human identity verification. Consequently, access to the Bitcoin blockchain is public and permission-less.

Following the deployment of the Bitcoin network in 2009, second generation blockchains such as Ethereum [22] added the possibility to execute smart contracts [23] on top of the blockchain layer. Smart contracts are computer programs that enable to perform transactional semantics more powerful than mere monetary exchange either directly on a distributed ledger by requesting all nodes to execute complex business logics or more simply to record their outputs on a distributed ledger. Smart contracts are designed to impersonate the role typically attributed to trusted third parties. As an example, we can consider the typical escrow use case, where some currency funds are managed by a smart contract and sent to the recipient only after specific conditions are met. More in general, smart contracts enable to program business logics on a distributed ledger, ensuring that their execution is not manipulated.

It then followed a plethora of implementations, some detaching from strict Proof-of-Work consensus blockchains and proposing alternative data structures, for instance Directed Acyclic Graphs, e.g. IOTA [24], Hashgraph [25] and Keyless Signature Infrastructure [26]. "Blockchain" has been then reclassified as a special case of DLTs systems as there are many other possible ways to achieve distributed consensus on the transaction history tracking in principle any type of digital data and asset, without relying on a central authority as a single source of truth.

As opposed to public permission-less distributed ledgers such as the Bitcoin or Ethereum blockchains designed for highly distrusting environments, a private, semi-private or permissioned distributed ledger which can be either a blockchain or another type of data structure, leverages on already existing trust and collaboration among stakeholders and processing units belonging to a shared operational environment. This type of DLT systems is shared by the members of either a single company or an industrial consortium. Stakeholders can agree on the type of consensus mechanism to order transactions, the governance of the infrastructure to run nodes participating to consensus rounds and define read/write access permissions for different types of participants tasked to maintain the distributed ledger.

Concluding our genealogical exercise on background knowledge, we adopt this overarching working definition of DLT system:

"A system of electronic records that (i) enables a network of independent participants to establish a consensus around (ii) the authoritative ordering of cryptographically-validated ('signed') transactions. These records are made (iii) persistent by replicating the data across multiple nodes, and (iv) tamper-evident by linking them by cryptographic hashes. (v) The shared result of the reconciliation/ consensus process - the 'ledger' - serves as the authoritative version for these records." [13]

We propose this definition, because it is general enough to include public blockchains while leaving open the opportunity to explore other data structures such as permissioned distributed ledgers.

2.2 Key beneficial properties emerging from DLT systems

The general DLT systems properties that are considered beneficial in the literature referred to in the table below are summarised in Table 1.

2.3 Challenges emerging from DLT systems

By contrast to DLT systems' benefits and desirable features, we identified a set of challenges that currently curb their widespread adoption. Indeed, research efforts are underway in governments, industry and academia to overcome the limits of such a relatively immature technology. As for the benefits elicited above, also with regard to challenges, alternative classifications are possible as a matter

Property	Description
DECENTRALIZATION	The reason why DLT systems, and in particular public blockchains, were designed in the first place is to eliminate the need of either a trusted third party or an intermediary responsible for validating and settling transactions [12]. A decentralized consensus mechanism, instead of an independent and centralized validator, enables all participants to the network to agree on the validity of transactions.
AUDITABILITY	A practically immutable audit trail of all identities comprising a record of related operations and any changes is kept [27]. This quality attribute can be achieved by DLT systems on a per case basis. Either all (e.g. in public blockchains) or some types of participants (e.g. in permissioned contexts) can maintain, store and access the full history of transactions or parts of it, depending on the opacity needs of the system.
AUTOMATION	Smart contracts enable programmable business logics. They are triggered when certain conditions are met. Their data output or a message digest referring to such data can either be stored off-chain in a local database or be written on a distributed ledger either before or after consensus on transaction ordering, execution and validation is reached by the distributed network. Some DLT systems require the installation and execution of the smart contract on each node of the network, while others pre-process the smart contract locally and broadcast to all nodes only the output of the smart contract.
STRONG IDENTITY MANAGEMENT	By design, DLT systems implement strong identity management mechanisms. This ensures that only who is allowed to perform a certain transaction/operation can actually do so. The identity of a user is verified through strong asymmetric cryptography algorithms.
TIMESTAMPING	DLT systems embed timestamping to coordinate nodes in an asynchronous way. This property can be applied to prove that information existed when the timestamp had been created.
RESILIENCE	Because DLT are distributed systems made by a reasonable high number of nodes, they are highly resilient systems: each node stores all the history of transactions solving the single points of trust and failure problems affecting, by definition, any centralised system. This applies also to physically segregated systems as there can always be the possibility for insider threats. For instance, by outsourcing parts of a digital identity management infrastructure to an independent network such as a public blockchain, DLT systems structurally reduce the attack surface available to malicious insiders.
IMMUTABILITY	DLT systems offer by design practically immutable records of their transactions history primarily by employing both cryptographic hashing functions and consensus mechanisms. Indeed, depending on several characteristics of a distributed ledger such as the number of nodes, the type of consensus mechanism and cryptographic hashing functions used, it is considered practically unfeasible also for well-funded adversaries to dispose of the necessary computational resources to hijack a majority of the nodes, corrupt data by changing the whole chain of blocks and rewrite transactions history. Accordingly, DLT systems resistance to quantum computing attacks is currently being researched and developed [28].
NON-REPUDIATION	Non-repudiation is a security service that provides unforgeable evidence that a particular action has occurred [29]. The service provides cryptographic evidence in electronic transactions so that, in case of disputes, it can be used as a confirmation of an action [27].

Table 1: DLT systems main features and quality attributes

Challenge	Public Blockchains	Permissioned DLT
Scalability	Public blockchains cannot process a high number of transactions per second, if compared to centralized systems. The throughput is limited to a few transactions per second. [27]. At the contrary, they have generally no problems in increasing the number of concurrent nodes connected to the network.	Permissioned DLT systems offer better throughput performance in terms of transactions per second. Nevertheless, they suffer of technical constraints in viably increasing the number of nodes above a certain threshold. [30]
Performance	Alongside throughput efficiency, latency in both data transmission and append-only operations can be a limit in some use cases, particularly in the domains of financial services and the Internet of Things.	Permissioned DLT systems usually perform better than Public Blockchain in terms of throughput efficiency and latency. However, they suffer from performance degradation when the number of nodes increases above a certain threshold. [30]
Adaptability	Especially in public blockchains, once the system is operational, it is hard to change configuration parameters such as consensus mechanisms.	This may not be the case for permissioned DLT systems designed to offer pluggable consensus capabilities.
Privacy	Public blockchains are inherently transparent and offer limited privacy usually achieved with pseudonymity. There are however newer public blockchains (i.e. Monero [31]) that are able to keep transactions details private using Zero Knowledge Proof [32] and related cryptographic methods	Some permissioned distributed ledgers are designed to embed a privacy layer to deploy use cases where information must be accessed on need-to-know basis. Nevertheless, there are claims that adding privacy layers on DLT is not straightforward and can add quite a significant amount of complexity [33]
Interoperability	It is still a challenge to have different public blockchain systems to seamlessly communicate with each other efficiently.	It is still a challenge to have different DLT systems to seamlessly communicate with each other efficiently.
Energy efficiency	Public blockchains based on Proof-of-Work are costly to run and burn significant amounts of electricity to secure the network against cyberattacks such as Distributed Denial of Service [27]. More recent public blockchains implementations, however, use different types of consensus mechanisms (e.g. Proof-of-Stake) that do not require high electricity consumption to operate.	Not having a Proof-of-Work consensus mechanism, permissioned DLTs do not have the same amount of energy expenditure as the Public blockchains based on that specific consensus mechanism.
Easiness of use	Interacting with a public blockchain is not usually straightforward for the average user. If we consider also that mistakes are, as well, immutable, we can see how this is still an area that needs improvements.	On a permissioned DLT system, the user interface can be built in a way that it is easier to interact. It should be noted however that also in this case mistakes will remain written on the ledger. Moreover, on permissioned DLT system it should be considered also the complexity of maintaining the network by IT personnel [33]
Transaction cost	Transacting on public blockchains can be expensive as the fees depend on the price of the underlying cryptocurrency or token, which is usually prone to high price volatility and the fee structure of each network, which depends on the incentives conditional on the consensus mechanism (e.g. requiring high transaction speeds results in increased transaction fees).	Many permissioned DLT systems do not rely on an underlying cryptocurrency as an incentive mechanism and, therefore, the cost per transaction is entirely dependent on the use case. However, on permissioned DLT systems, infrastructure setup cost is a fundamental parameter to consider for deployment and maintenance.
Limited storage space	As a consequence of the high number of data replicas (e.g. on a public blockchain network the data is replicated on every full node) and the fact that historical data is not deleted, the amount of data stored on a distributed ledger should be kept to a minimum. This is especially true for public blockchains, because the paid fees are proportional to data volumes.	Also in permissioned DLT systems the stored data on the ledger should be kept to a minimum as the stored data is replicated on different locations and historical data is not deleted, meaning that the storage need will grow over time.

Table 2: DLT systems main challenges

of course. However, we selected the challenges listed below as we maintain that they are mostly relevant in the nuclear sector.

Considering that these challenges have different applicability on public blockchains and permissioned DLT systems, we summarised them in Table 2 with a different description for the two families.

After briefly introducing a series of benefits and challenges of DLT systems, in the next section we will elicit our methodological choices.

3. Methodology – a Proof-of-Concept strategy

Starting from DLT systems' properties, we performed deductive inferences intended to define use cases in the nuclear sector that, in our view, more adequately adapted to such properties. We endorsed this type of methodological approach, because our primary goal was to evaluate in practice the tangible benefits and challenges that would arise by applying DLTs systems' properties to the nuclear sector in view of adding value to nuclear safeguards. In turn, we adopted a Proof-of-Concept [34] strategy for software design to implement use cases' requirements. In fact, both enterprises and institutions commonly use this strategy to test new products and technologies while avoiding putting too much financial effort at stake. Because the technology is new and in continuous evolution, hands-on experience is essential. In this view, the ultimate goal of a Proof-of-Concept strategy is to provide evidence-based recommendations on whether what we are attempting to achieve is actually feasible and could add tangible value to nuclear safeguards business processes.

In both the use cases on containment and surveillance and on the decentralized timestamping of radiation protection's data, we endorsed the MoSCoW method [35]: a categorization method for software design that uses the following modal adverbs to better clarify the requirements' priority: Must, Should, Could and Would. Moreover, considering the nature of the software artefacts to be developed, we are performing design and implementation using the Software Prototyping methodology [36] Short and fast iterations enabled us to quickly test the functionalities that we intended to deploy, and to have a working prototype that can be easily shown to domain experts and other stakeholders involved.

For the digitalization of the radiation passbook, we endorsed LEAN-UX [37], an Agile method for software requirements analysis. Standing for Lean User Experience, LEAN-UX enabled us to define hypothesis statements for each stakeholder type, creating use case scenarios in a bottom-up process and in a language accessible to both business and technical domain experts. In particular, a Radiation Protection Expert colleague at the Joint Research Center and his team members could directly inform use case requirements without leaving much space for our misinterpretation.

After requirements analysis and co-creation, software design and development together with testing and evaluation phases of our approach have been dealt with the endorsement of the software design and implementation methodology named Behaviour Driven Development (BDD) [38] [39]. With BDD we designed and developed sample smart contracts for the digitalization of the radiation passbook, according to the three phases arguments of this methodology: Given (validates the input), When (processes the contents); and Then (prints out the results).

In the next section, we will present three key DLT systems' properties that while they are partly derived from non-strictly safeguards domains of the nuclear sector, they nevertheless add, in our humble view, value to nuclear safeguards.

4. Key DLT systems properties adding value to nuclear safeguards

4.1 Practical immutability for sensors identity management

In nuclear safeguards, several types of equipment and devices such as sensors, cameras and seals are used to ensure that proper containment and surveillance is applied throughout the fuel cycle. Their deployment is crucial to help inspectorates in formulating safeguards conclusions, because their data can provide relevant information on what has happened inside a facility.

Especially in modern times, most of these devices are electronic in nature, can send remotely their data to an inspectorate, in case connectivity is present and the operator agrees to it, and are equipped with hardware security modules capable of performing asymmetric cryptographic operations on the data produced. Asymmetric cryptography [40] is based on the concept of private and public keys: these two keys are mathematically related to each other so that a message encrypted with one key can be decrypted with the other one and vice versa. The private key is secret and stored on a secure memory inside the device, while the public key, as the name suggests, can be shared with anyone. In our case, asymmetric cryptography is used to digitally sign data so that who receives them or retrieves them from the device's memory can verify both data provenance (i.e. the identity of who created the data) and integrity (i.e. the absence of data modification after the signature).

To achieve this outcome, who retrieves the data must know the public key associated to the private key used to sign them. This can be done in two ways: a simple approach prescribes that before installing the device, the inspectorate

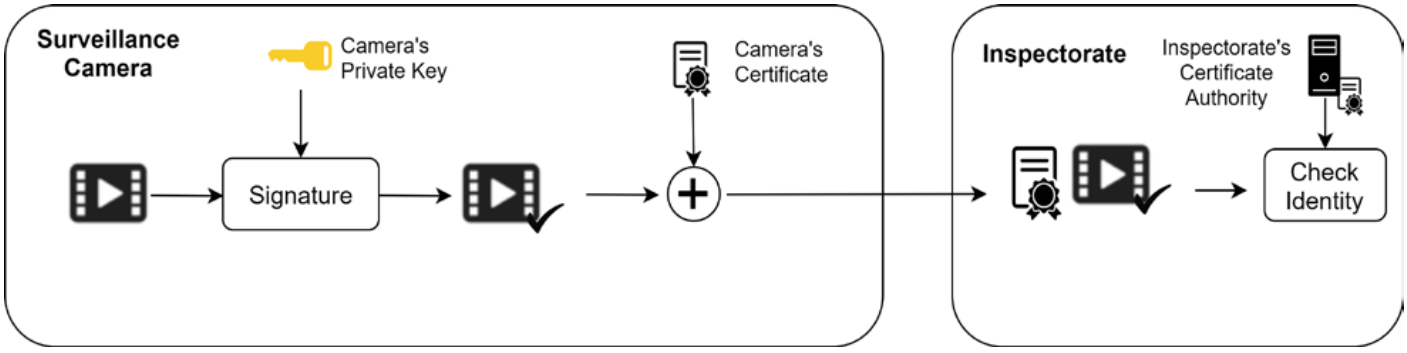

Figure 1: The original video authentication workflow

record on a master list the association between the device's identity and its public key. A more robust approach, currently used, prescribes instead that the public key be inserted into a digital certificate, created and signed by a Certificate Authority, in our case owned and controlled by the inspectorate. This second approach is generally known as a Public Key Infrastructure (henceforth, PKI) [41].

Both these approaches are vulnerable to an insider threat scenario. In fact, if someone is able to modify an entry on the master list, or to issue a valid while non-authorized certificate, s/he can do it so that even a tampered or fake device will have its own entry on the master list or its own valid certificate. If that is the case, data sent from the tampered or forged device will be recognized as authentic, leading to the possibility for a well-funded malicious entity to provide counterfeit data to the inspectorate with the goal of hiding material's diversion or other illicit operations. Moreover, the same person or group of people that has access to the systems used to record relations between a public key and a device's identity (i.e. the master list or the Certificate Authority) could also delete traces of their operations (e.g. log entries). All this could increase the chances that their actions will go indefinitely undetected.

This kind of issue is pervasive to every traditional PKI, having to rely on a Certificate Authority that is trusted by default [42] and consequently it is present in our case as well. In our exploratory research, we initially considered exclusively a specific type of safeguards device, i.e. surveillance cameras. Accordingly, we developed a Proof-of-Concept software implementation to address this specific issue by leveraging on the practical immutability property of data registered on a public blockchain.

More in particular, modern surveillance cameras deployed in nuclear safeguards produce digitally signed video streams. Key pairs are randomly initialized during the camera's setup and the public key is used to create a certificate signing request that, in turn, enables the inspectorate's internal Certificate Authority to generate a certificate. Two different algorithms for asymmetric cryptography are employed: the Digital Signature Algorithm (DSA) is used to digitally sign every single frame, while the Rivest-Shamir-Adleman (RSA) algorithm is used to digitally sign an entire daily video stream. The respective private keys used for the signatures are stored on a secure memory inside the camera, automatically zeroed in case a tampering attempt is detected, whereas the corresponding certificates (containing the public keys also stored within the camera) are embedded in the video stream file itself.

When the inspectorate receives a new video stream, it is therefore able to verify the correctness of each signature and the validity of the certificates (Figure 1). As mentioned above, while very robust, this process is vulnerable to attackers or malicious insiders whom, by having access to the Certificate Authority used to generate the certificates, are enabled to forge new, albeit unauthorized, certificates to be assigned to tampered cameras.

We therefore propose a scenario whereby every certificate (or public key, in case we are referring to the simpler master list approach) is hashed and registered on a public blockchain [43]. In applied cryptography, a hash results from a cryptographic operation that from an input of any size calculates an output of a fixed (usually smaller) size. For each input value there is a single output, but the opposite is not true: from an output, there are multiple (infinite in fact) input values that would lead to it. The hashing function is therefore mathematically irreversible. Thanks to this property of one-way cryptographic hashing functions, a hash therefore is not a sensitive information. Hence, the hash of a certificate can be recorded on a publicly accessible system without the danger to reveal confidential information. Moreover, even a single bit changed on the input causes a huge difference on the output. Such difference, unless the used hashing algorithm has vulnerabilities, is not predictable, so that there is no way other than pure brute forcing to try to obtain a specific output [44].

In other words, if these hashes are recorded somewhere where they cannot be modified (e.g. a blockchain), we can use them to check whether a certificate that we have received is exactly the same one that was initially generated during a surveillance camera's initialisation, by calculating again the hash and comparing it with the registered one.

By registering the hash of issued certificates on a public blockchain, we ensure that such hashes would benefit from the practical immutability that data stored on a public blockchain take on. This in turn ensures that there will always be a trace left of every certificate issuance operation, enabling us to keep this log of information monitored to detect suspicious certificate issuance operations, and leading eventually to flagging the corresponding camera (and its video streams) in order to raise attention.

Indeed, and conversely, if malicious actors could gain control of the inspectorate's internal Certificate Authority to issue a new digital certificate for a tampered camera, they would have to register such operation on the blockchain otherwise the new malicious certificate would not be recognized as valid. By doing so, they leave an undeletable trace of their malicious operation that can be detected.

Also in the simpler master list case, attackers, assuming that they are capable of penetrating and gaining control of the centralized system, could either tamper with or substitute a camera and modify the relative entry on the master list to match the substitution and make it looks like as if the substitution never happened. Storing such information on a blockchain would instead require rewriting part of the transactions history to match a locally stored public key with the one linked to the hash stored on-chain.

For this use case, we are focusing specifically on public blockchains and not on permissioned DLT systems. The rationale behind this decision is based on two considerations: firstly, having underlined that hashes are not sensitive information, from which it is practically unfeasible with current technology to retrieve the original information, we can claim that we do not need confidentiality in this use case. Secondly, the immutability property that data acquires on a blockchain can be considered fully achieved especially on public blockchains. We can argue this because either to alter or to delete stored information, attackers should maliciously operate a majority of the public blockchain's nodes to attempt rewriting transactions history with modified data. This operation requires increasing resources as time passes and blocks accumulate. Notwithstanding how well-funded attackers might be, it is considered practically unfeasible to successfully rewrite the transactions history on public blockchains with a considerably high number of nodes without being detected by the rest of honest nodes. As an example, at the time of writing, on the Bitcoin network nobody has ever been able to perform a successful attack of this sort.

This form of assurance on immutability is generally stronger than the one provided by permissioned distributed ledgers. In the latter case, there is a lower number of nodes and, consequently, data manipulation can occur, in theory, if the participants of the DLT system's network jointly agree to do so [45]. Obviously, such a scenario is hard to image in Nuclear Safeguards, but it could nevertheless happen in principle (e.g. a coalition of malicious states corrupting inspectorates' system administrators). Some permissioned DLT infrastructures partly address this by periodically publishing on a public repository (e.g. on social media, newspapers or websites) a hash that represents an anchor to their private data [26]. In this way, even in the case where all the participants to the permissioned DLT jointly decided to alter data stored in the distributed ledger, there would still be an unambiguously identifiable mismatch with the published hashes. While this solution is certainly valuable, especially in the case of confidential data, where it would be not possible to use a public blockchain, in our specific case it would represent too much of a burden considering that we do not need confidentiality. More importantly, by choosing to adopt a public blockchain, we do not have costs and other organisational issues related to the infrastructure set-up and maintenance, because those public blockchain networks that we analysed are already existing and there are no barriers of entry.

To showcase this approach, and initially focusing on the simpler public keys master list case, we created three implementations using three different public blockchains, i.e. Bitcoin [12], Ethereum [22] and Algorand [46] for managing surveillance cameras' digital identities. Selection criteria considered three facets: (1) overall security of the blockchain network, (2) flexibility in terms of possibility to add features other than merely storing information (e.g. the possibility to authorize only specific accounts to store either certificate or public key's hashes), and (3) cost associated to transactions fees. We therefore identified the following public blockchains according to these rationales: the Bitcoin network has not been disrupted from its inception to the time of writing. This makes it the oldest and most secure public blockchain available for experimentation. Secondly, Ethereum offers one of the most widely used platforms for smart contracts deployment. Thirdly, Algorand has very low transaction fees and it enables to provide signature delegation capabilities for smart contracts. This last property is relevant to be tested for the use case at hand, because it could enable inspectorates from regulatory agencies such as IAEA and EURATOM to share responsibilities when installing common infrastructure.

A generalized architecture of the proofs-of-concept implemented with these three blockchain networks is depicted in Figure 2

The architecture spans across three loci: the inspectorate premises, the nuclear facility and the connection channels

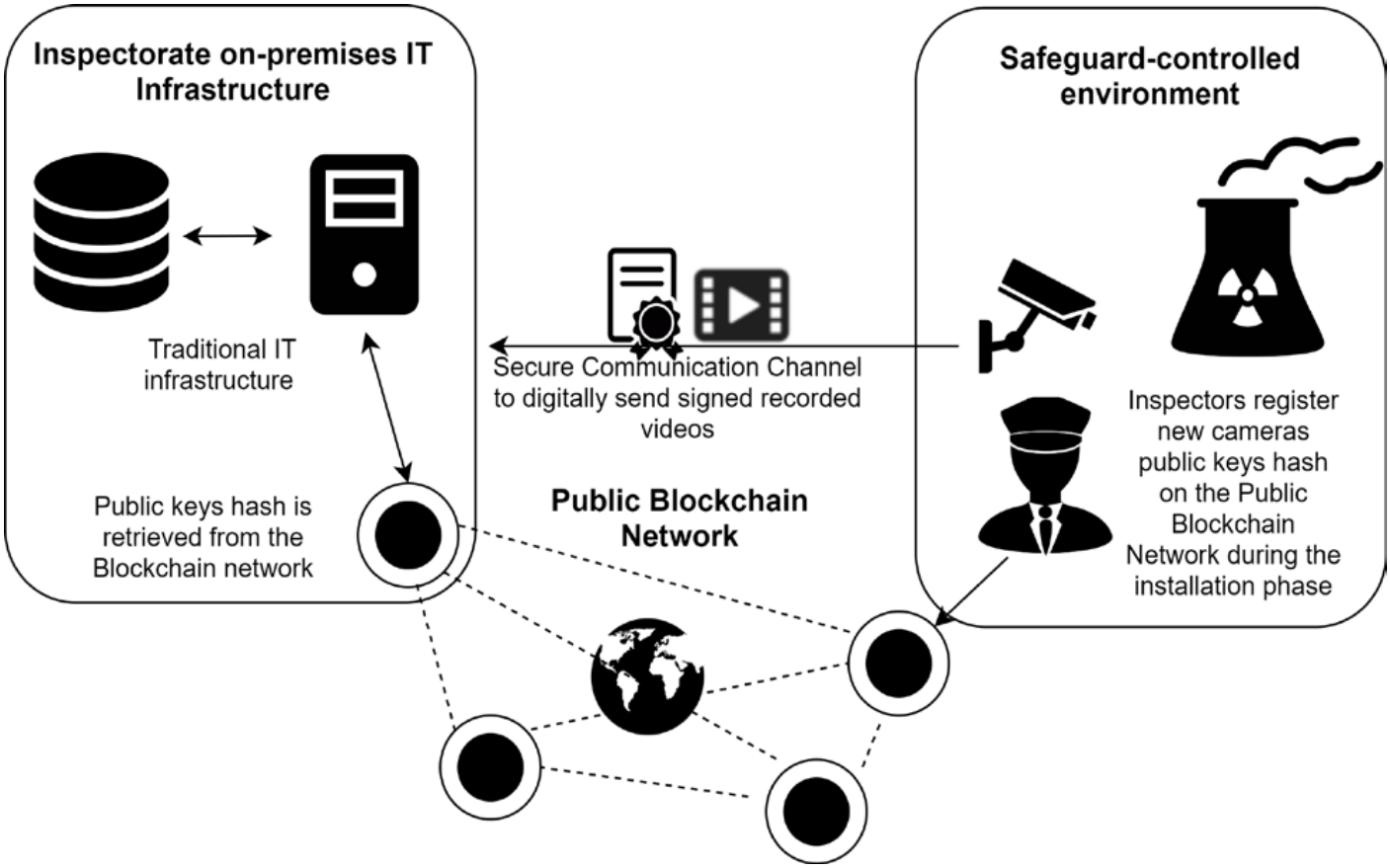

Figure 2: General high-level architecture of the process monitoring use case (source [43])

between the two. The novelty, with respect to the traditional master list approach, lies on the utilization of a public blockchain network to store hashes of a camera's public keys.

First, in the Bitcoin proof-of-concept implementation, we proceeded accounting for the protocol constraint that a maximum of 83 bytes of arbitrary data can be recorded in a Bitcoin transaction. While they are not sufficient for storing DSA and RSA public keys, they are enough for storing the public keys' hashes. The transaction identifier is a pointer to the Bitcoin blockchain where it is possible to locate the camera identifier and the hash of the corresponding public key. The drawback is that this adds the small overhead to set up a local database for managing transaction pointers, because searching the Bitcoin blockchain to retrieve public keys' hashes without a pointer would greatly reduce performance. It is nevertheless important to note that such transaction pointers' database is not a single point of failure, because it can be rebuilt in case of data loss for analysing the blockchain.

Secondly, on Ethereum, it is possible to implement the same model by using smart contracts. Contrary to Bitcoin, there is no need to set up a local database to store transaction pointers, as the smart contract is natively equipped with storage capabilities that enables quick information retrieval. However, compared to a traditional software, the implementation phase needs to put more emphasis on the testing part, as fixing bugs on smart contracts is more complicated. Indeed, once deployed a smart contract cannot be modified but must be deactivated and redeployed. In all cases, by virtue of the remarkable volatility of native cryptocurrencies on both Bitcoin and Ethereum networks, transaction costs can change swiftly. Volatility and transaction costs are thus important elements to take into account when defining added value and business viability of this solution at scale.

Finally, as a response to high volatility and transaction costs to curb the effect of highly volatile cryptocurrencies, Algorand can be an appropriate candidate as it offers a very low transaction cost of 0,0002 USD per transaction with storage capacity of up to 1 Kb of data per transaction. However, Algorand's smart contract semantics is less powerful than Ethereum's, but thanks to it, it also reduces the possibility that bugs are introduced in the system. The main drawback with Algorand is that storage capacity must grow quicker over time, if compared to Bitcoin and Ethereum.

In summary, the simple proof-of-concept implementations that we developed on the Bitcoin, Ethereum and Algorand public blockchain networks enabled us to confirm that the idea of using the immutability property of public blockchains to store hashes related to digital identities of safeguards sensors is correct and implementable. Such result shows that DLT not only can have a role in Nuclear Material Accountancy, as shown by the referenced research on DLT and Safeguards, but also in Containment and Surveillance.

At this stage we are not proposing a specific public blockchain network for further implementations as that choice would be dependent on specific application requirements that are usually formulated on a more advanced implementation stage (i.e. a pilot project). In case of further developments, it is indeed of the utmost importance to clearly identify and detail, together with the relevant stakeholders, what are the requirements and constraints that such a system should consider (e.g. total number of sensors, average number of maintenance operations in a sensor lifetime that require the reissuing of a certificate, advanced features like signature delegation, etc.). The final decision on the specific blockchain network to use shall be derived considering such detailed requirements and constraints.

Potential further applications in the containment and surveillance domain can be summarised as follows:

- Not only surveillance cameras, but all digital sensors embedding strong security features (e.g. fiber-optic seals, laser scanners and in principle all sensors used in safeguards) can benefit from the added security of their identities by applying what has been described in this section.
- Analogue sensors could also benefit from it as long as it is possible to derive a “unique” signature of the sensor via signal analysis. If that is possible, what has been described in this section can be applied by registering a hash of the signature on a public blockchain.
- Ad-hoc scripts/libraries could be developed for custom sensors to offer the identity registration on the blockchain as an additional feature.

4.2 Data anchoring through decentralised timestamping

A second property of DLT systems applied to nuclear safeguards is decentralised timestamping for data anchoring on public blockchains.

Data anchoring [47] refers to the process of taking every piece of meaningful data, calculate its hash and publish it on an immutable timestamped repository (e.g. a public blockchain). By doing so, without disclosing any sensitive information thanks to the nature of the hash (as explained in section 4.1), we have a secure way to check if a specific datum was modified simply by recalculating its hash and comparing it with the registered one. It is important to note that other than the immutability of the hash, also its associated timestamp is relevant in this process as it gives a precise indication on when that hash was registered and therefore from which point in time we can speculate on the integrity of the underlying data.

Applying this process to safeguards enables us to generate proofs of existence for nuclear safeguards data, files or events, i.e. that data existed at the time when the timestamp had been created and was not modified ever since. The added value of this process lies on the possibility to check with certainty if information has been modified. In particular, this feature not only provides an additional internal security measure for an inspectorate (e.g. as a way to check integrity of backups, archives and whatsoever relevant data), but also an increased layer of transparency to prove to external parties that the data used to draw safeguards conclusions have not been tampered (e.g. in case of disputes).

While it could be argued that integrity of digital data can be proved also with digital signatures, it should be noted that the difference in the two approaches (i.e. data anchoring on public blockchain versus digital signature) lies on the timestamp. Timestamping of data per se is not a novelty and can be already implemented by a Time Stamping Authority as it happens within the digital signature context. Considering that the timestamping is coming from a third party, there is however the concrete possibility that a Time Stamping Authority could make a mistake or misbehave, thus providing an incorrect timestamp [48].

On a public blockchain, by contrast, each new block is timestamped when it is created. Such timestamp cannot deviate from real time, because it must be temporally situated strictly after the previous block, but not too far in the future. For instance, on the Bitcoin blockchain a new block is discarded, even where formally valid, if its timestamp points to a time situated more than two hours after the latest block [21]. As a downside however, we need to consider that such timestamps cannot be considered extremely precise (e.g. on Bitcoin we should consider a timeframe of 2 hours uncertainty) and therefore they cannot be used for applications where timestamping precision is fundamental.

To explore the feasibility of the decentralised timestamping to ensure data integrity, in the domain of radiation protection (our first use case in this field) we explored the OpenTimestamps protocol to notarise dosimetry data stored on legacy systems at the Joint Research Center, i.e. the Unified Dosimetry System (henceforth, UDS). The OpenTimestamps protocol was firstly proposed by Peter Tood in 2012 [49]. It is an attempt at standardising and solving the scalability and cost issues of timestamping on a public blockchain. Merely notarising every single data element on the

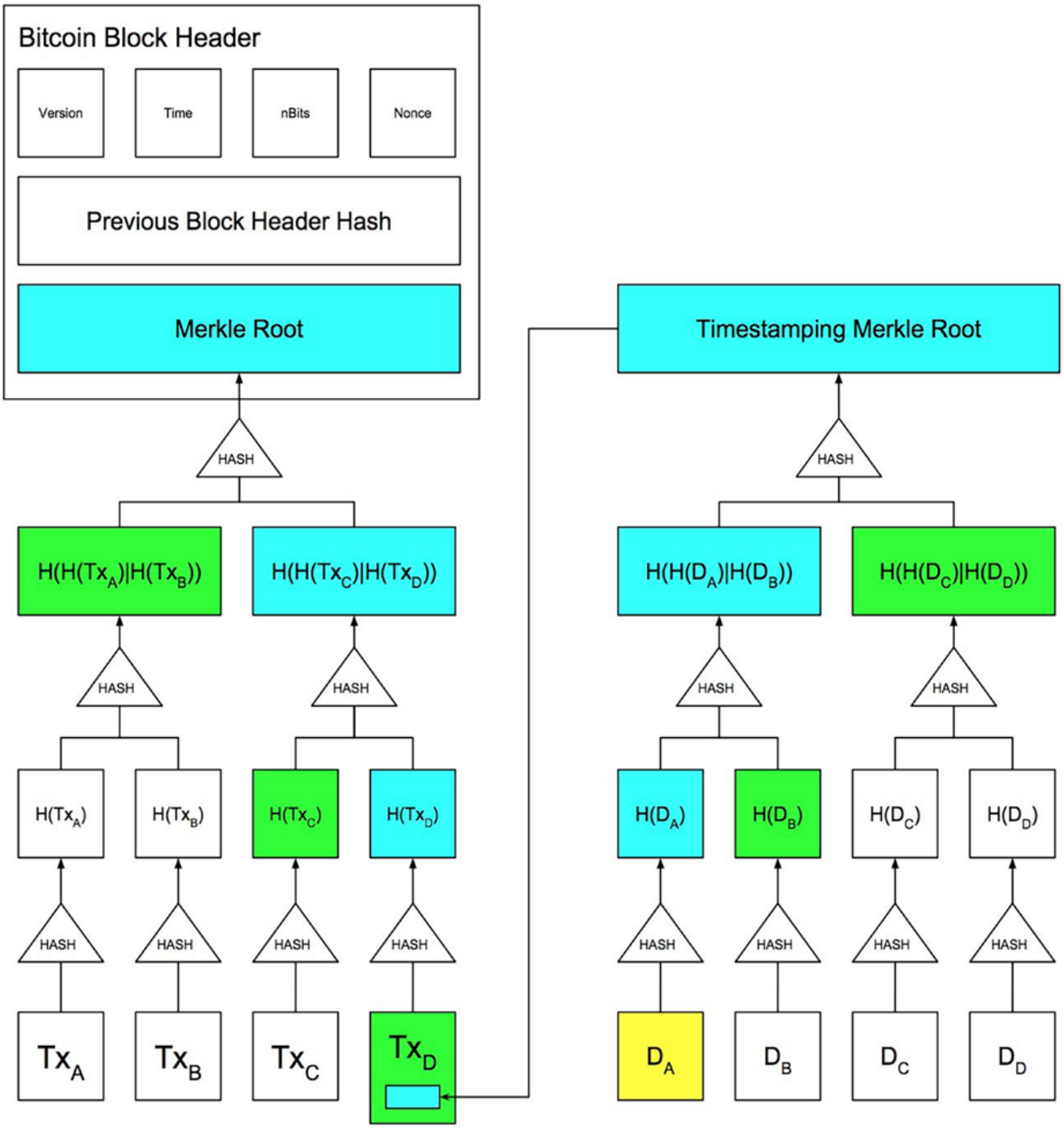

Figure 2: OpenTimestamps protocol: highlighting the path from the Document A (DA) up until the Bitcoin block. In green are highlighted the information contained on the registration proof, which enable to verify mathematically, together with the original data (in yellow) that the information has indeed been timestamped on the Bitcoin blockchain (source: [52])

blockchain, in fact, would lead to the creation of a high number of transactions that are both expensive (taken as a whole) and may clog the blockchain itself by increasing its size too much and by raising the average fee for a transaction to be committed. [50].

The idea proposed by the OpenTimestamps protocol is simple and efficient: instead of timestamping and registering on the blockchain individual hashes, the protocol aims at creating Merkle Trees of data hashes, registering only the root element of the tree on the blockchain as depicted in Figure 3. In cryptography, a Merkle Tree [51] is a data structure used for data verification. It is a binary tree where each leaf node (i.e. all nodes that do not have any child) contains the hash of some data block, and each non-leaf node contains the hash of its child nodes, up to the root element of the tree (i.e. the only element that has no parents).

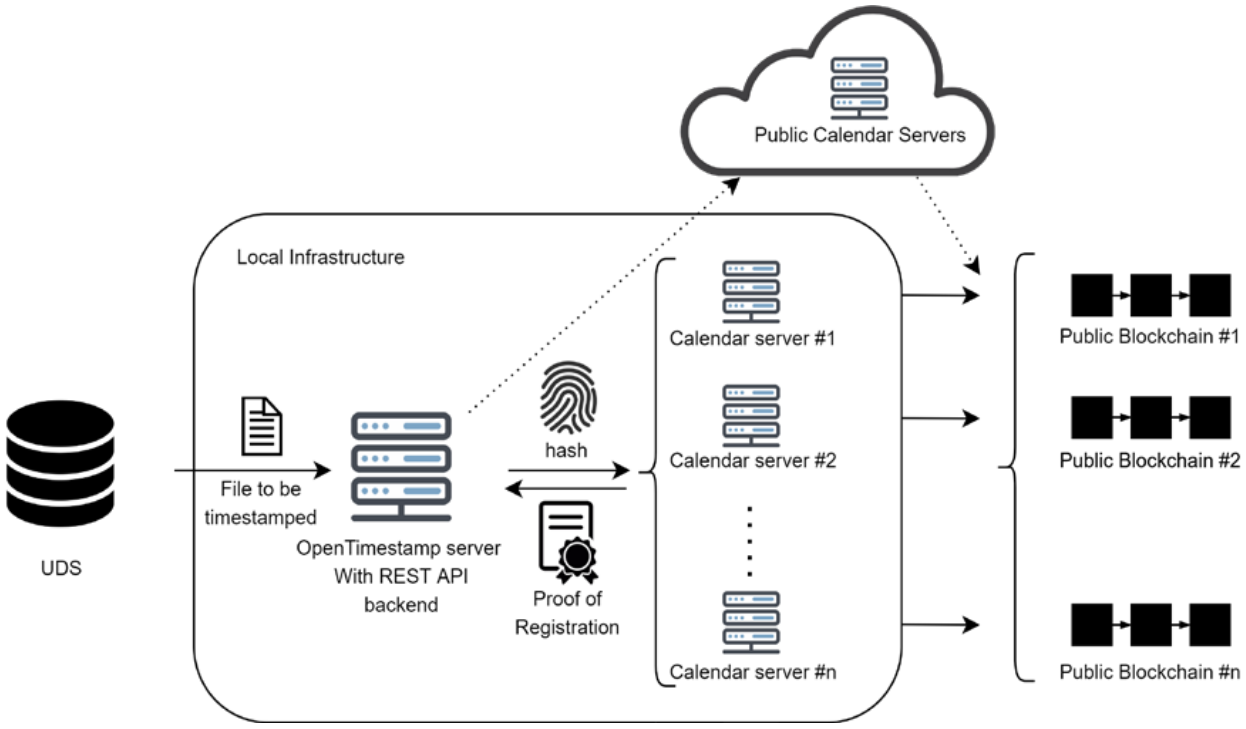

Figure 4: High-level view of how an OpenTimestamps architecture connected to Unified Dosimetry System

The properties of both hashes and Merkle trees enable anyone to verify mathematically that the tree's root element stored on the blockchain has been derived taking into consideration also the hash of a specific datum: to do so it is fundamental to have the list of operations applied starting from the original data to the root element.

To be useful this timestamping process requires that two preconditions be met:

- The original timestamped data must be available over time as is, with absolutely no modifications.
- The proof of registration must be stored together with the original data as the validity of the timestamp is confirmed only by having both of them.

If both requirements are satisfied, who requested the timestamp can mathematically prove the existence of that particular data at the timestamp calendar date.

The required infrastructure is composed at minimum only by a machine to implement the client-side of the OpenTimestamp protocol.

Such client will:

1. Calculate the hash of the data to be timestamped. To be more precise, such hash will be modified by appending a nonce (i.e. a random number) and rehashing the result to avoid involuntary information exposure on the original data, but for simplicity we can consider it as being a simple hash of the data.
2. Send the hash to a calendar server, which is a server responsible of aggregating multiple timestamping requests by generating a Merkle Tree, and of ultimately registering the tree's root element on the blockchain.
3. Receive back from the calendar server the information related to the operations performed starting from the original request that leads to the Merkle Tree root inserted on the blockchain transaction and up until the block header of the blockchain block. This information will be used together with the list of operations performed to generate the data's hash (see 1st step) to generate the proof of registration: a file that lists all operations performed to be stored together with the original data.
4. Independently verify, starting from the original data and the registration proof, if indeed by repeating all the operations we can confirm that there is a block on the blockchain that proves such data existed when the block was created.

As briefly explained, to perform all these operations, the client needs to interface itself with two other servers: a calendar server for the registration operations and a blockchain node (i.e. a machine which has downloaded the complete blockchain and keeps it synced through the consensus algorithm) for the verification.

To be completely secure from any man-in-the-middle attack, it is not recommended to use third party services, but instead to deploy an owned blockchain node. In fact, if the verification phase is performed through an external blockchain monitor (i.e. a webservice provided by a third party that permits to query easily the blockchain without having to download it), nothing can ensure us that the verification itself is not tampered.

The calendar servers instead could still be public (i.e. offered by third parties) considering that (1) they do not receive the original data and (2) the received proofs are independently verified. A private calendar server can nevertheless be deployed in case it is desirable to be completely independent from third party's services (e.g. for business continuity reasons).

The OpenTimestamps protocol, born with the Bitcoin blockchain, nowadays works also with other public blockchains. It is therefore possible to publish the same proof of existence on different blockchains to make it even more tamper resistant. To do so, it is necessary to add additional calendar servers, each one devoted to a particular public blockchain. Obviously, also for the verification part, one node for each blockchain used needs to be locally present to guarantee a better security.

In Figure 4, it is depicted how a high-level architecture of the system would be:

This approach enables the sustainable use of a public blockchain as a reliable while decentralised timestamping authority.

Further potential applications of data anchoring could be:

- All relevant data, declarations, reports, which an operator or the inspectorate might need to be able to prove their existence at a given time and un-alteration ever since, are suitable for this approach.
- Secure software update (e.g. of containment and surveillance devices) by timestamping executables.

Among these possible further applications, we will initially focus on the application of this approach for data integrity in the context of nuclear material accountancy. Indeed, individual nuclear facilities may voluntarily transmit reports or other form of information to EURATOM and IAEA via mailbox. There are cases, however, where this additional information is not sent directly to the inspectorates but must remain on the facility's premises to be retrieved manually by the inspectors. In this case, this type of information on nuclear material accountancy would add value to nuclear safeguards as it could be timestamped following the same steps of the process described above for radiation protection data anchoring to ensure that they are not modified once inserted in the system.

4.3 Structural auditability of dosimetry data

While the previous two properties of DLT systems that can add value to nuclear safeguards emerged from the domain of public blockchains, we inferred a third added value from another property of DLT systems, i.e. structural auditability of data on a permissioned distributed ledger. Also known as consortium blockchains, permissioned DLT systems enable the creation and the broadcasting of transactions only by nodes that have permissions to write new blocks on the ledger. The requirement that only authorised parties can manage certain types of data after permission is granted is normal practice in the use case on radiation protection data management that we will analyse in this section.

As we argued above, if compared to public blockchains, permissioned DLT systems can count on a definition of immutability only in the limited sense that it is difficult for a participant to modify data on all the nodes. There could be, however in principle, a potential collusion risk if all participants jointly decided to modify transactions history recorded on the permissioned distributed ledger.

Contrary to public blockchains designed for environments dominated by high distrust among participants usually operating with pseudonyms, deployment of permissioned distributed ledgers can nevertheless be beneficial in all the cases where higher levels of trust than those characteristic of public blockchains already exist among participating stakeholders (e.g. between nuclear operators and inspectorates). Moreover, permissioned distributed ledgers are recommended when stakeholders also share the requirement to preserve confidentiality of data exclusively accessible by those with permission.

In the use case scenario analyzed in this section, i.e. the digitalization of the radiation passbook on a single shared infrastructure, there is indeed already present a significant level of trust among clearly identifiable stakeholders: an authority issuing a radiation passbook, Radiation Protection Experts at every site, Medical Physics Experts and radiation protection workers. In our scenario, RPEs are the only actors with permission to create new blocks and write digitally signed transactions on the distributed ledger. In this specific use case, confidential data are directly written and shared on the ledger, and this is the reason for the selection of a permissioned DLT system and not a public permission-less one. In other words, in the test for the use case on containment and surveillance, because no confidential information was shared, a public distributed ledger was selected. While in this use case on radiation protection, a permissioned distributed ledger enabling

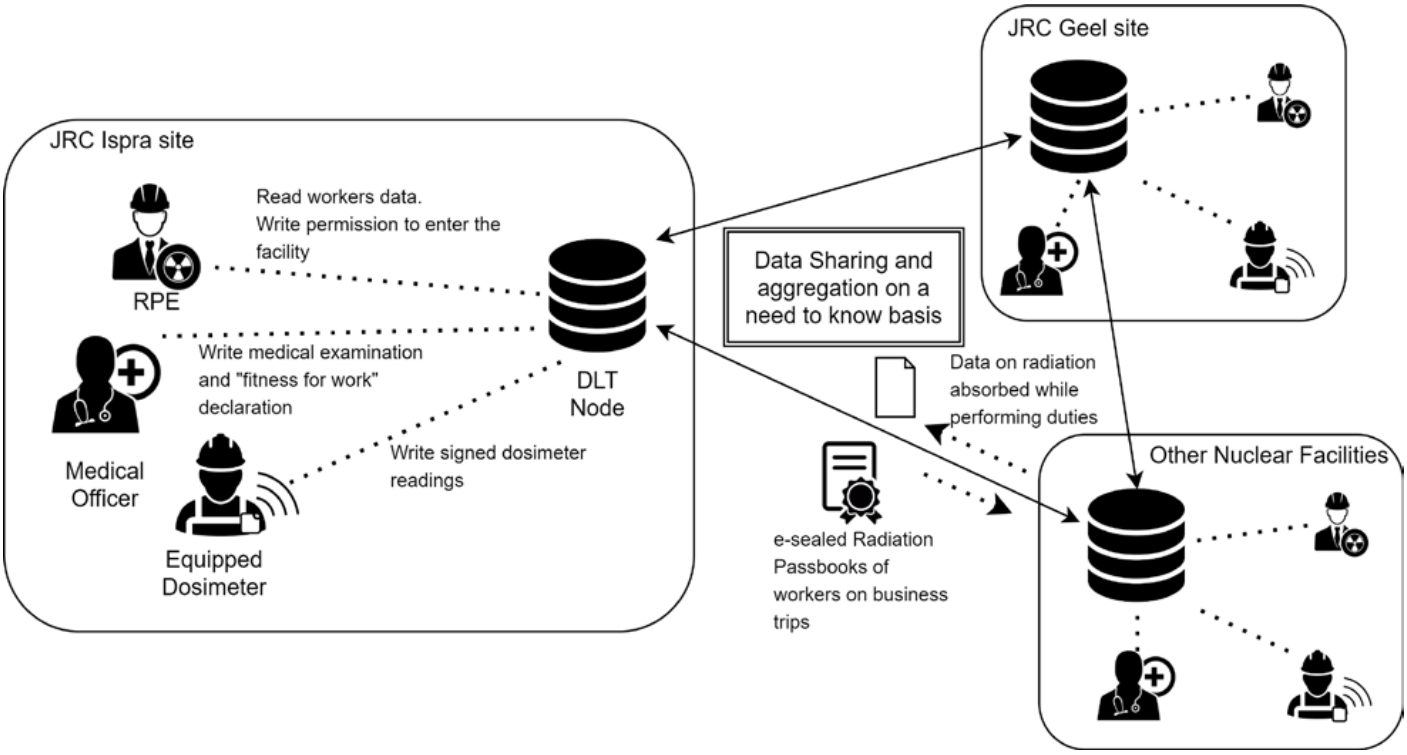

Figure 5: High-level schema of the digitalisation of the radiation passbook

confidentiality (also providing immutability as for every DLT system) by design, was the correct technology selection outcome.

By virtue of their network and data structure, permissioned distributed ledgers embed auditability and non-repudiation properties, because all parties with access permission can write and read information on a need-to-know basis. Structural auditability is a property of DLT systems resulting from ordering and timestamping signed dosimetry data transactions that cannot be repudiated. The added value is threefold: (1) higher efficiency in information sharing; (2) lower number of clerical errors thanks to going paperless through smart contracts' automation; and (3) creation of forensic evidence that can help solve disputes on legal liability. As we will discuss below, these three added values emerged from a use case in the nuclear sector of radiation protection could also be applied to nuclear safeguards, specifically in the domain of nuclear material accountancy.

In particular, the radiation passbook is a paper booklet of the dimension of a conventional passport. It lists fields to record employees and inspectors' personal data, and a list of approved compilers, i.e. Radiation Protection Experts with their signatures. Moreover, the radiation passbook registers an employee's occupational exposure to radiations and any involvement in accidents. In turn, it records the 5-year dose limit, the dose assessment for the calendar year; the estimated doses in mSv in another employer's-controlled area(s); Whole Body Count; Radiotoxicologial monitoring; medical examinations; fitness-for-work in normal and in case of arduous conditions; and radiation protection training. A final section includes important addresses and telephone numbers, specifically Headquarters, Medical Service and Radiation Protection Experts.

The choice to explore DLT systems' applications for the radiation passbook was initiated by acknowledging the fact that nuclear safeguards workers travel to different locations, where they are potentially exposed to radiation. However, data related to absorbed doses during missions are rarely shared between their employer and the nuclear installation. Indeed, workers carry two separate dosimeters: exposure to ionising materials is measured using both their employer's and nuclear installations' dosimeters. Using a permissioned DLT system, it is possible to digitally record and share dosimetry data to track radiation exposure of workers as depicted in Figure 5:

As a hands-on proof-of-concept exercise, we implemented sample smart contracts using Zenroom [53], an output implementation funded by DG CNECT to research distributed applications for compliance with the EU General Data Protection Regulation [54]. Zenroom is a trusted execution environment with no external dependencies. It comprises a tiny library (1Mb) and requires low memory usage (600 Kb – 2 Mb). It runs smart contracts written with Zencode, a

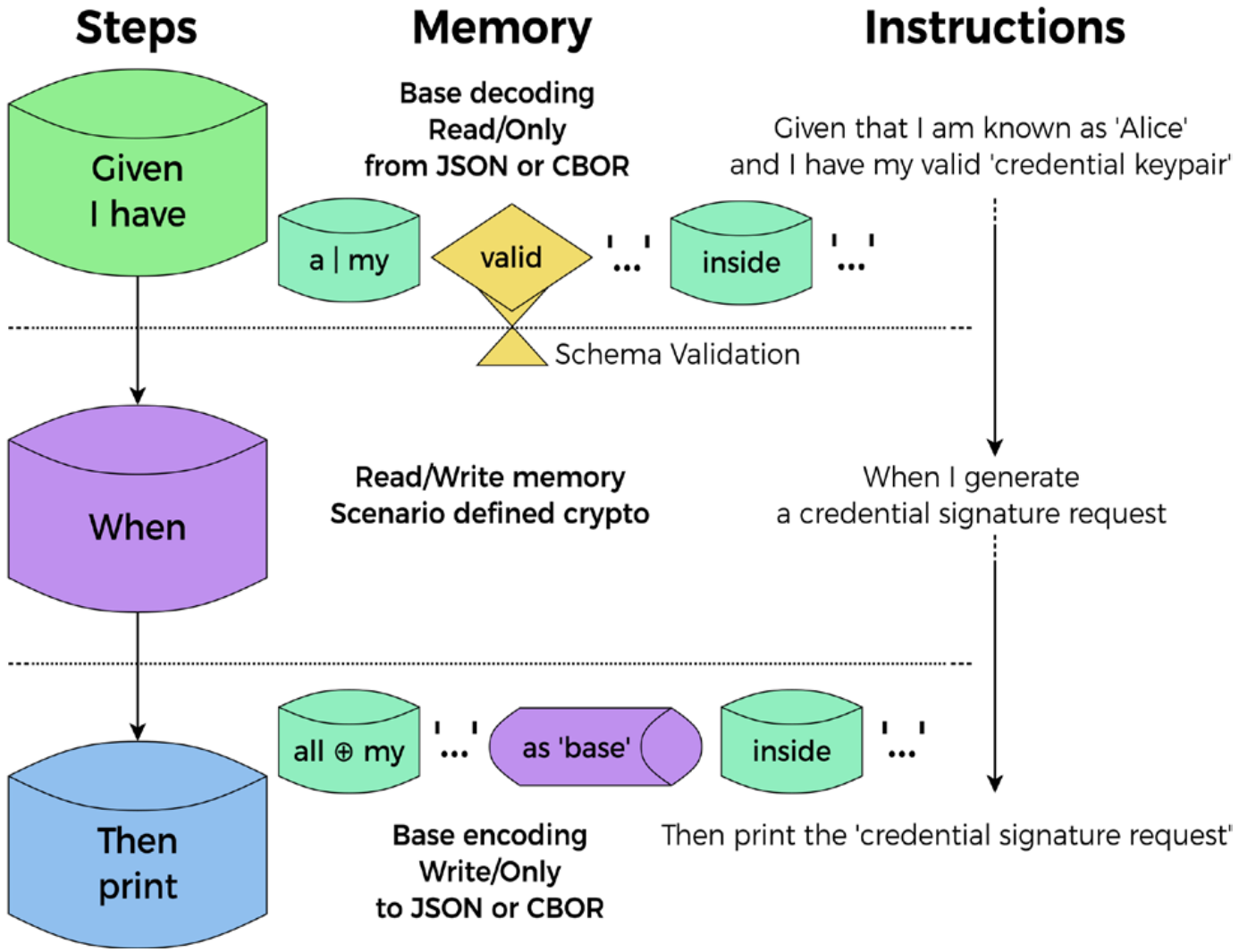

Figure 6: High-level schema of the Zenroom virtual machine's memory model (source [37]).

human readable, English-like Domain Specific Language [29]. Zencode language design followed the principles of language theoretic security [55] formally verifying that smart contracts are free of currently dominant classes of bugs and vulnerabilities.

This design approach implements a memory model based on Behaviour Driven Development that segregates from external calls input (Given), processing (When) and output (Then) phases of a smart contract's encoding and execution. The result is a highly efficient process virtual machine, which provides a powerful smart contracts semantics less prone to unexpected data change and control flow bugs [56], i.e. the classes of bugs that led, for instance, to the 2016 'DAO hack' on the Ethereum blockchain [38]. Figure 6 depicts the Zencode processing memory model:

In our implementation, deterministic smart contracts have been encoded to issue a digitalized version of the radiation passbook authenticated through electronic sealing by means of Elliptic Curve Digital Signature Algorithm (ECSDA) digital signatures. Moreover, we implemented smart contracts to process digital signatures in order to provide RPEs with the means to proof dosimetry data provenance, non-repudiation and ensure confidentiality. Signed dosimetry data can thus be stored on a permissioned distributed ledger.

We ran a test using Zenroom integrated as a transaction processor on the Hyperledger Sawtooth permissioned distributed ledger. Hyperledger Sawtooth offers the flexibility for pluggable consensus and smart contract virtual machines [57]. In particular, we implemented a version of Hyperledger Sawtooth v1.0.1 ordering transactions with Practical Byzantine Fault Tolerance [39] consensus, whereby no more than one third of the nodes (rounded down) can be unreachable or dishonest at any given time. In the future, we will aim to complement confidentiality and non-repudiation with a data aggregation module to update dosimetry data history on the radiation passbook each time a nuclear safeguards worker completes a mission.

As also stated by other research institutes in the nuclear sector [7] [8], we also believe that a system similar to the one described for this use case, based on a permissioned DLT system, could be implemented applied to add value to Nuclear Material Accountancy and Control business processes. For instance, using a permissioned DLT system to process nuclear material accounting records could enable near-real time reporting as data, e.g. an Inventory Change Report is shared to relevant stakeholders (strictly on a need-to-know basis) immediately after it is issued. Moreover, structural auditability would provide early data analysis with the goal of detecting red flags soon enough to promptly address potential criticalities. Secondly, smart contracts could automate data validation and reconciliation operations, i.e. transit matching. Finally, a permissioned DLT system would offer a single source of truth to all stakeholders involved, providing also in this case a source of forensic evidence to help address disputes in nuclear material accountancy.

However, we anticipate that DLT systems applications on nuclear material accountancy must be carefully studied and tested, because there are several constraints that could hinder their applicability. While a complete feasibility study on this specific topic is not within the scope of this paper, we report some examples of constraints, also analysed in related work [7], which should be carefully considered when designing permissioned DLT system applications in the context of nuclear material accountancy at an international level:

— International Regulations: since some regulations, for instance EURATOM Regulation 302/2005, details quite specifically how Nuclear Accountancy Reporting must be performed, new systems must accordingly be compatible with the standard procedure listed on this regulation.
— Data locality: some nation states forbid reliance on safeguards related data other than the official accountancy records (e.g. safeguards sensors data, mailbox declarations) from leaving either the country or the facility premises where they are produced. Consequently, a DLT system shall implement measures to provide data locality on some categories or data, or that such system should be used only to provide proof of existence and non-alteration and not to store the actual data.
— Data transmission format: some nation states forbid the usage of electronic communications media for sending accounting records to inspectorates. As stated in the previous point, this could mean that a DLT system should be used only as an additional integrity layer and not to store the actual data.

5. Conclusion and potential way forward

In this paper, we presented three key properties of DLT systems, whose application has been transversal to the nuclear sector in general with special emphasis on added value to nuclear safeguards: practical immutability, data anchoring through decentralised timestamping for public blockchains and structural auditability for permissioned DLT systems. Practical immutability adds value by increasing the level of cybersecurity, potentially impacting inspections plans thanks to a more efficient automation of safeguards business processes for containment and surveillance, specifically for surveillance cameras' Public Key Infrastructure management.

Moreover, decentralised timestamping and structural auditability, albeit tested in radiation protection, can add value to nuclear safeguards by lowering clerical errors through enhanced automation and consistency of business processes by virtue an additional layer of both data integrity and a real-time audit trail of transactions' history. These two key DLT systems' properties can also be seen as innovative sources of forensic evidence for legal dispute resolution not only in radiation protection but also in the domain nuclear material accountancy.

Future research aims at further testing these findings on the Experimental Infrastructure for Internet Contingencies (EPIC), maintained by JRC-Ispra E.3 Cyber and Digital Citizens' Security Unit. EPIC enables the re-creation of cyber-infrastructures for testing various configurations. It provides special physical equipment, such as a Programmable Logical Controller, enabling cyber-physical testing (max 356 nodes). These characteristics give significant advantages in terms of repeatability, scalability and controllability of experiments and tests.

We plan to run performance experiments on fiber-optic seals for containment and surveillance, and regular mailbox declarations for nuclear material accountancy. We will then plan to emulate the performance of a permissioned DLT system to process the digitalized radiation passbook by Radiation Protection Experts at both JRC sites and from nuclear installations. The goal of these tests is to build robust datasets for performance comparison between DLT-based systems and more traditional approaches. The objective is to generate quantitative metrics to more finely evaluate the benefits and added value of DLT systems applied to nuclear safeguards. The overarching ambition of these experimental exercises within the SLT4SFG exploratory research project is to define a general methodology to select key DLT properties for their applications to nuclear safeguards.

6. Acknowledgements

The authors would like to acknowledge all those who have reviewed previous drafts of this paper and contributed to its completion together with JRC-Ispra Units A.5 (Scientific Development), G.ii.7 (Nuclear Security), E.3 (Cyber and Digital Citizens' Security) and R.I.5 (Ispra site Safety & Security) for enabling, operationalising and supporting the exploratory research project Shared Ledger Technologies for Nuclear Safeguards.

7. References

[1] W. Janseens, "Nuclear Safeguards Challenges from a JRC Perspective," in International Cooperation for Enhancing Nuclear Safety, Security and Non proliferation - 60 Years of IAEA and EURATOM, Rome, 2018.

[2] European Commission, "European countries join Blockchain Partnership," [Online]. Available: https://ec.europa.eu/digital-single-market/en/news/european-countries-join-blockchain-partnership. [Accessed 14 May 2021].

[3] EU Blockchain Observatory and FOrum, "EU Blockchain Observatory and Forum," [Online]. Available: https://www.eublockchainforum.eu/. [Accessed 14 May 2021].

[4] European Commission, "EBSI - Experience the future with the European Blockchain Service Infrastructure (EBSI)," [Online]. Available: https://ec.europa.eu/cefdigital/wiki/display/CEFDIGITAL/ebsi. [Accessed 14 May 2021].

[5] European Commission, "European Blockchain Pre-Commercial Procurement," [Online]. Available: https://ec.europa.eu/digital-single-market/en/news/online-questionnaire-european-blockchain-pre-commercial-procurement-live. [Accessed 14 May 2021].

[6] S. Nonneman, G. Renda, L. Dechamp, M. Isabella, T. Jacobi and I. N. Fovino, "Distributed Ledger Technology in Nuclear non-proliferation Safeguards?," in Symposium on International Safeguards, Stresa, 2018.

[7] C. Vestergaard, G. Green, E. G. Obbard, E. Yu and G. D. Putra, "SLAFKA Demonstrating the Potential for Distributed Ledger Technology for Nuclear Safeguards Information Management," Stimson Center, 2020.

[8] S. Frazar, C. Joslyn, R. Goychayev and A. Randall, "Developing an Electronic Distributed Ledger For Transit Matching," in Proceedings of the INMM 61st Annual Meeting, Baltimore, MD, USA, 2020.

[9] N. Pattengale, "DLT Activities at Sandia National Laboratory (Presentation)," Sandia National Laboratory, 2020.

[10] L. Umayam and C. Vestergaard, "Complementing the Padlock: The prospect of blockchain for strengthening nuclear security," Stimson Center, 2020.

[11] E. Androulaki, A. Barger, V. Bortnikov, C. Cachin, K. Christidis, A. De Caro, D. Enyeart, C. Ferris, G. Laventman, Y. Manevich and S. Muralidharan, "Hyperledger fabric: a distributed operating system for permissioned blockchains," in Euro Sys '18: Proceedings of the Thirtheenth EuroSys Conference, 2018.

[12] S. Nakamoto, "Bitcoin: A Peer-to-Peer Electronic Cash System," 2009. [Online].

[13] M. Rauchs, A. Glidden, B. Gordon, G. Pieters, M. Recanatini, F. Rostand, K. Vagneur and B. Zhang, "Distributed Ledger Technology Systems - a Conceptual Framework," Cambridge Centre for Alternative Finance, University of Cambridge, Judge Business School, 2018.

[14] N. Ferguson, B. Schneier and T. Kohno, Cryptography Engineering Design Principles and Practical Applications, Indianapolis: Wiley Publishing, Inc., 2010.

[15] B. Schneier, Applied Cryptography: Protocols, Algorithms and Source Code in C, John Wiley & Sons, Inc., 1995.

[16] G. J. Simmons, "How to Insure that Data Acquired to Verify Treaty Compliance are Trustworthy," in Proceedings of the IEEE, 1988.

[17] D. Chaum, "Blind signatures for untraceable payments," in Advances in Cryptology Proceedings 82, 1983.

[18] D. Chaum, A. Fiat and M. Naor, "Untraceable electronic cash," in Advances in Cryptology - CRYPTO '88 Proceedings, New York, 1988.

[19] A. Back, "Hashcash - A Denial of Service Counter-Measure," 2002.

[20] C. Dwork and M. Naor, "Pricing via Processing or Combatting Junk Mail," in Advances in Cryptology - Crypto '92, 1992.

[21] A. Antonopoulos, Mastering Bitcoin, O'Really, 2015.

[22] G. Wood, "Ethereum: A Secure Decentralised Generalised Transaction Ledger," 2014. [Online]. Available: gavwood.com/paper.pdf.

[23] L. Luu, D.-H. Chu, H. Olickel, P. Saxena and A. Hobor, "Making Smart Contracts Smarter," in Proceeding of

the 2016 ACM SIGSAC Conference on Computer and Communications Security, 2016.

[24] U. Sarfraz, M. Alam, S. Zeadally and A. Khan, "Privacy aware IOTA ledger: Decentralized mixing and unlinkable IOTA transactions," Computer Networks 148, pp. 361-372, 2019.

[25] L. Baird, M. Harmon and M. Paul, "Hedera: A Public Hashgraph Network & Governing Council," 2019. [Online]. Available: https://hedera.com/hh-whitepaper-v1.5-190219.pdf.

[26] A. Buldas, L. Risto and A. Truu, "Keyless signature infrastructure and PKI: hash-tree signatures in pre- and post-quantum world," International Journal of Services Technology and Management, pp. 117-130, 2017.

[27] I. Bashir, Mastering Blockchain: A deep dive into distributed ledgers, consensus protocols, smart contracts, DApps, cryptocurrencies, Ethereum, and more, Birmingham: Packt Publishing, 2020.

[28] T. M. Fernandes-Camares and P. Fraga-Lamas, "Towards Post-Quantum Blockchain: A Review on Blockchain Cryptography Resistant to Quantum Computing Attacks," IEEE Acess, vol. 8, pp. 21091-21116, 2020.

[29] E. A. Brewer, Towards robust distributed systems (Invited Talk), Portland, Oregon, 2000.

[30] Q. Nasir, I. A. Qasse, M. A. Talib and A. B. Nassif, "Performance Analysis of Hyperledger Fabric Platforms," Security and Communication Networks, vol. 2018, 2018.

[31] The Monero Project, "About Monero," [Online]. Available: https://www.getmonero.org/resources/about/. [Accessed 03 June 2021].

[32] S. Goldwasser, S. Micali and C. Rackoff, "The Knowledge Complexity of Interactive Proof Systems," SIAM Journal on Computing, vol. 18, no. 1, pp. 186-208, 1989.

[33] L. Feagan, "Hyperledger Fabric Myths and Reality," April 2020. [Online]. Available: https://objectcomputing.com/resources/publications/sett/april-2020-hyperledger-fabric-myths-and-reality. [Accessed 3 June 2021].

[34] M. K. Pratt, "proof of concept (POC)," [Online]. Available: https://searchcio.techtarget.com/definition/proof-of-concept-POC. [Accessed 14 May 2021].

[35] Wikipedia, "MoSCoW Method," [Online]. Available: https://en.wikipedia.org/wiki/MoSCoW_method. [Accessed 14 May 2021].

[36] Wikipedia, "Software Prototyping," [Online]. Available: https://en.wikipedia.org/wiki/Software_prototyping. [Accessed 14 May 2021].

[37] D. Roio and A. Dintino, "Smart Contracts for Data Commons integrated with GDPR compliant legal rules and tested in pilots," European Commission DG CNECT, 2019.

[38] K. O'Hara, "Smart Contracts - Dumb Idea," IEEE Internet Computing, vol. 21, no. 2, pp. 97-101, 2017.

[39] M. Castro and B. Liskov, "Practical Byzantine fault tolerance," in OSDI '99: Proceedings of the third symposium on Operating systems design and implementation, 1999.

[40] M. E. Hellman, "An Overview of Public Key Cryptography," IEEE Communications Magazine, 2002.

[41] C. Adams and S. Lloyd, Understanding public-key infrastructure: concepts, standards, and deployment considerations, 1999.

[42] J. A. Berkowsky and T. Havaineh, "Security Issues with Certificate Authorities," in IEEE 8th Annual Ubiquitous Computing Electronics and Mobile Communication Conference (UEMCON), 2017.

[43] R. Spigolon, M. Sachy, S. Nonneman, R. Neisse, I. Maschio and I. Nai Fovino, "Using Public Blockchain for the management of Public Key Infrastructure to strengthen Nuclear Safeguards," in Proceedings of the INMM 61st Annual Meeting, Baltimore, MD, USA, 2020.

[44] R. Sobti and G. Geetha, "Cryptographic hash functions: a review," International Journal of Computer Science Issues (IJCSI), 2012.

[45] B. Putz and G. Pernul, "Trust Factors and Insider Threats in Permissioned Distributed Ledgers," in Transactions on Large-Scale Data and Knowledge-Centered Systems XLII, vol. 11860, Springer, 2019, pp. 25-50.

[46] S. Micali and J. Chen, "Algorand," 26 May 2017. [Online]. Available: https://algorandcom.cdn.prismic.io/algorandcom%2Fece77f38-75b3-44de-bc7f-805f0e53a8d9_theoretical.pdf.

[47] O. Konashevuch and M. Poblet, "Blockchain Anchoring of Public Registries: Options and Challenges," in ICEGOV2019 Proceedings of the 12th International Conference on Theory and Practice of Electronic Governance, 2019.

[48] M. Vigil, D. Cabarcas, J. Buchmann and J. Huang, "Assessing trust in the long-term protection of

socuments," in 2013 IEEE Symposium on Computers and Communications (ISCC), 2013.

[49] P. Tood, "OpenTimestamps: Scalable, Trust-Minimized, Distributed Timestamping with Bitcoin," 15 September 2016. [Online]. Available: https://petertodd.org/2016/opentimestamps-announcement. [Accessed 6 November 2020].

[50] E. Strehle and F. Steinmetz, "Dominating OP Returns: The Impact of Omni and Veriblock on Bitcoin," Journal of Grid Computing, pp. 575-592, 2020.

[51] R. Merkle, Secrecy, authentication and public key systems/ A certified digital signature, Dept. of Electrical Engineering, Stanford University, 1979.

[52] R. Casatta, "Scalable and Accountable Timestamping (presentation)," [Online]. Available: https://bit.ly/321YcNy.

[53] Zenroom, "Zenroom," [Online]. Available: https://dev.zenroom.org/. [Accessed 14 May 2021].

[54] European Commission, "Decentralised Citizens Owned Data Ecosystem," [Online]. Available: https://cordis.europa.eu/project/id/732546. [Accessed 14 May 2021].

[55] F. Momot, S. Bratus, S. Hallberg and M. Patterson, "The Seven Turrets of Babel: A Taxonomy of LangSec Errors and How to Expunge Them," IEEE Cybersecurity Development, SecDev 2016, pp. 45-52, 3-4 November 2016.

[56] D. Roio and M. Sachy, "Initial Definition of Smart Rules and Taconomy," European Commission H2020 DECODE Project Deliverable, 2018.

[57] Bitwise IO, Inc , "Sawtooth PBFT," [Online]. Available: https://sawtooth.hyperledger.org/docs/pbft/releases/1.0.1/. [Accessed 14 May 2021].

esarda.jrc.ec.europa.eu